

1 Testing for ancient selection using cross-population allele 2 frequency differentiation

3 Fernando Racimo^{1,*}

4 **1 Department of Integrative Biology, University of California, Berkeley, CA, USA**

5 * **E-mail: fernandoracimo@gmail.com**

6 **1 Abstract**

7 A powerful way to detect selection in a population is by modeling local allele frequency changes in a
8 particular region of the genome under scenarios of selection and neutrality, and finding which model is
9 most compatible with the data. Chen et al. [2010] developed a composite likelihood method called XP-
10 CLR that uses an outgroup population to detect departures from neutrality which could be compatible
11 with hard or soft sweeps, at linked sites near a beneficial allele. However, this method is most sensitive
12 to recent selection and may miss selective events that happened a long time ago. To overcome this,
13 we developed an extension of XP-CLR that jointly models the behavior of a selected allele in a three-
14 population tree. Our method - called 3P-CLR - outperforms XP-CLR when testing for selection that
15 occurred before two populations split from each other, and can distinguish between those events and
16 events that occurred specifically in each of the populations after the split. We applied our new test to
17 population genomic data from the 1000 Genomes Project, to search for selective sweeps that occurred
18 before the split of Yoruba and Eurasians, but after their split from Neanderthals, and that could have
19 led to the spread of modern-human-specific phenotypes. We also searched for sweep events that occurred
20 in East Asians, Europeans and the ancestors of both populations, after their split from Yoruba. In both
21 cases, we are able to confirm a number of regions identified by previous methods, and find several new
22 candidates for selection in recent and ancient times. For some of these, we also find suggestive functional
23 mutations that may have driven the selective events.

24 **2 Introduction**

25 Genetic hitchhiking will distort allele frequency patterns at regions of the genome linked to a beneficial
26 allele that is rising in frequency [Smith and Haigh, 1974]. This is known as a selective sweep. If the

27 sweep is restricted to a particular population and does not affect other closely related populations, one
28 can detect such an event by looking for extreme patterns of localized population differentiation, like high
29 values of F_{st} at a specific locus [Lewontin and Krakauer, 1973]. This and other related statistics have
30 been used to scan the genomes of present-day humans from different populations, so as to detect signals
31 of recent positive selection [Akey et al., 2002, Oleksyk et al., 2008, Weir et al., 2005, Yi et al., 2010].

32 Once it became possible to sequence entire genomes of archaic humans (like Neanderthals) [Green
33 et al., 2010, Meyer et al., 2012, Prüfer et al., 2014], researchers also began to search for selective sweeps
34 that occurred in the ancestral population of all present-day humans. For example, Green et al. [2010]
35 searched for genomic regions with a depletion of derived alleles in a low-coverage Neanderthal genome,
36 relative to what would be expected given the derived allele frequency in present-day humans. This is
37 a pattern that would be consistent with a sweep in present-day humans. Later on, Prüfer et al. [2014]
38 developed a hidden Markov model (HMM) that could identify regions where Neanderthals fall outside
39 of all present-day human variation (also called "external regions"), and are therefore likely to have been
40 affected by ancient sweeps in early modern humans. They applied their method to a high-coverage
41 Neanderthal genome. Then, they ranked these regions by their genetic length, to find segments that
42 were extremely long, and therefore highly compatible with a selective sweep. Finally, Racimo et al.
43 [2014] used summary statistics calculated in the neighborhood of sites that were ancestral in archaic
44 humans but fixed derived in all or almost all present-day humans, to test if any of these sites could be
45 compatible with a selective sweep model. While these methods harnessed different summaries of the
46 patterns of differentiation left by sweeps, they did not attempt to explicitly model the process by which
47 these patterns are generated over time.

48 Chen et al. [2010] developed a method called XP-CLR, which is designed to test for selection in
49 one population after its split from a second, outgroup, population t_{AB} generations ago. It does so by
50 modeling the evolutionary trajectory of an allele under linked selection and under neutrality, and then
51 comparing the likelihood of the data for each of the two models. The method detects local allele frequency
52 differences that are compatible with the linked selection model [Smith and Haigh, 1974], along windows
53 of the genome.

54 XP-CLR is a powerful test for detecting selective events restricted to one population. However, it
55 provides little information about when these events happened, as it models all sweeps as if they had
56 immediately occurred in the present generation. Additionally, if one is interested in selective sweeps

57 that took place before two populations a and b split from each other, one would have to run XP-CLR
58 separately on each population, with a third outgroup population c that split from the ancestor of a and
59 b t_{ABC} generations ago (with $t_{ABC} > t_{AB}$). Then, one would need to check that the signal of selection
60 appears in both tests. This may miss important information about correlated allele frequency changes
61 shared by a and b , but not by c , limiting the power to detect ancient events.

62 To overcome this, we developed an extension of XP-CLR that jointly models the behavior of an allele
63 in all 3 populations, to detect selective events that occurred before or after the closest two populations
64 split from each other. Below we briefly review the modeling framework of XP-CLR and describe our new
65 test, which we call 3P-CLR. In the Results, we show this method outperforms XP-CLR when testing for
66 selection that occurred before the split of two populations, and can distinguish between those events and
67 events that occurred after the split, unlike XP-CLR. We then apply the method to population genomic
68 data from the 1000 Genomes Project [Abecasis et al., 2012], to search for selective sweep events that
69 occurred before the split of Yoruba and Eurasians, but after their split from Neanderthals. We also use
70 it to search for selective sweeps that occurred in the Eurasian ancestral population, and to distinguish
71 those from events that occurred specifically in East Asians or specifically in Europeans.

72 3 Materials and Methods

73 3.1 XP-CLR

74 First, we review the procedure used by XP-CLR to model the evolution of allele frequency changes of
75 two populations a and b that split from each other t_{AB} generations ago (Figure 1.A). For neutral SNPs,
76 Chen et al. [2010] use an approximation to the Wright-Fisher diffusion dynamics [Nicholson et al., 2002].
77 Namely, the frequency of a SNP in a population a (p_A) in the present is treated as a random variable
78 governed by a normal distribution with mean equal to the frequency in the ancestral population (β) and
79 variance proportional to the drift time ω from the ancestral to the present population:

$$p_A|\beta \sim N(\beta, \omega\beta(1-\beta)) \quad (1)$$

80 where $\omega = t_{AB}/(2N_e)$ and N_e is the effective size of population A.

81 This is a Brownian motion approximation to the Wright-Fisher model, as the drift increment to

82 variance is constant across generations. If a SNP is segregating in both populations - i.e. has not hit the
 83 boundaries of fixation or extinction - this process is time-reversible. Thus, one can model the frequency
 84 of the SNP in population a with a normal distribution having mean equal to the frequency in population
 85 b and variance proportional to the sum of the drift time (ω) between a and the ancestral population, and
 86 the drift time between b and the ancestral population (ψ):

$$p_A|p_B \sim N(p_B, (\omega + \psi)p_B(1 - p_B)) \quad (2)$$

87 For SNPs that are linked to a beneficial allele that has produced a sweep in population a only, Chen
 88 et al. [2010] model the allele as evolving neutrally until the present and then apply a transformation to
 89 the normal distribution that depends on the distance to the selected allele r and the strength of selection
 90 s [Durrett and Schweinsberg, 2004, Fay and Wu, 2000]. Let $c = 1 - q_0^{r/s}$ where q_0 is the frequency of the
 91 beneficial allele in population a before the sweep begins. The frequency of a neutral allele is expected to
 92 increase from p to $1 - c + cp$ if the allele is linked to the beneficial allele, and this occurs with probability
 93 equal to the frequency of the neutral allele (p) before the sweep begins. Otherwise, the frequency of the
 94 neutral allele is expected to decrease from p to cp . This leads to the following transformation of the
 95 normal distribution:

$$f(p_A|p_B, r, s, \omega, \psi) = \frac{1}{\sqrt{2\pi}\sigma} \frac{p_A + c - 1}{c^2} e^{-\frac{(p_A + c - 1 - cp_B)^2}{2c^2\sigma^2}} I_{[1-c, 1]}(p_A) + \frac{1}{\sqrt{2\pi}\sigma} \frac{c - p_A}{c^2} e^{-\frac{(p_A - cp_B)^2}{2c^2\sigma^2}} I_{[0, c]}(p_A) \quad (3)$$

96 where $\sigma^2 = (\omega + \psi)p_B(1 - p_B)$ and $I_{[x, y]}(z)$ is 1 on the interval $[x, y]$ and 0 otherwise.

97 For $s \rightarrow 0$ or $r \gg s$, this distribution converges to the neutral case. Let \mathbf{v} be the vector of all drift
 98 times that are relevant to the scenario we are studying. In this case, it will be equal to (ω, ψ) but in
 99 more complex cases below, it may include additional drift times. Let \mathbf{r} be the vector of recombination
 100 fractions between the beneficial alleles and each of the SNPs within a window of arbitrary size. We can
 101 then calculate the product of likelihoods over all k SNPs in that window for either the neutral or the
 102 linked selection model, after binomial sampling of alleles from the population frequency, and conditioning
 103 on the event that the allele is segregating in the population:

$$CL_{XP-CLR}(\mathbf{r}, \mathbf{v}, s) = \prod_{j=1}^k \frac{\int_0^1 f(p_A^j | p_B^j, \mathbf{v}, s, r^j) \binom{n}{m_j} (p_A^j)^{m_j} (1 - p_A^j)^{n - m_j} dp_A^j}{\int_0^1 f(p_A^j | p_B^j, \mathbf{v}, s, r^j) dp_A^j} \quad (4)$$

104 This is a composite likelihood [Lindsay, 1988, Varin et al., 2011], because we are ignoring the correla-
 105 tion in frequencies produced by linkage among SNPs that is not strictly due to proximity to the beneficial
 106 SNP. We note that the denominator in the above equation is not explicitly stated in Chen et al. [2010]
 107 for ease of notation, but appears in the published online implementation of the method.

108 Finally, we obtain a composite likelihood ratio statistic S_{XP-CLR} of the hypothesis of linked selection
 109 over the hypothesis of neutrality:

$$S_{XP-CLR} = 2[\sup_{\mathbf{r}, \mathbf{v}, s} \log(CL_{XP-CLR}(\mathbf{r}, \mathbf{v}, s)) - \sup_{\mathbf{v}} \log(CL_{XP-CLR}(\mathbf{r}, \mathbf{v}, s = 0))] \quad (5)$$

110 For ease of computation, Chen et al. [2010] assume that \mathbf{r} is given (via a recombination map) instead of
 111 maximizing the likelihood with respect to it, and we will do so too. Furthermore, they empirically estimate
 112 \mathbf{v} using F_2 statistics [Patterson et al., 2012] calculated over the whole genome, and assume selection is
 113 not strong or frequent enough to affect their genome-wide values. Therefore, the likelihoods in the above
 114 equation are only maximized with respect to the selection coefficient, using a grid of coefficients on a
 115 logarithmic scale.

116 3.2 3P-CLR

117 We are interested in the case where a selective event occurred more anciently than the split of two
 118 populations (a and b) from each other, but more recently than their split from a third population c (Figure
 119 1.B). We begin by modeling p_A and p_B as evolving from an unknown common ancestral frequency β :

$$p_A | \beta, \omega \sim N(\beta, \omega\beta(1 - \beta)) \quad (6)$$

120

$$p_B | \beta, \psi \sim N(\beta, \psi\beta(1 - \beta)) \quad (7)$$

121 Let χ be the drift time separating the most recent common ancestor of a and b from the most recent
 122 common ancestor of a , b and c . Additionally, let ν be the drift time separating population c in the
 123 present from the most recent common ancestor of a , b and c . Given these parameters, we can treat β
 124 as an additional random variable that either evolves neutrally or is linked to a selected allele that swept

125 immediately more anciently than the split of a and b . In both cases, the distribution of β will depend on
 126 the frequency of the allele in population c (p_C) in the present. In the neutral case:

$$f_{neut}(\beta|p_C, \nu, \chi) = N(p_C, (\nu + \chi)p_C(1 - p_C)) \quad (8)$$

127 In the linked selection case:

$$f_{sel}(\beta|p_C, \nu, \chi, r, s) = \frac{1}{\sqrt{2\pi\kappa}} \frac{\beta + c - 1}{c^2} e^{-\frac{(\beta+c-1-cp_C)^2}{2c^2\kappa^2}} I_{[1-c,1]}(\beta) + \frac{1}{\sqrt{2\pi\kappa}} \frac{c - \beta}{c^2} e^{-\frac{(\beta-cp_C)^2}{2c^2\kappa^2}} I_{[0,c]}(\beta) \quad (9)$$

128 where $\kappa^2 = (\nu + \chi)p_C(1 - p_C)$

129 The frequencies in a and b given the frequency in c can be obtained by integrating β out. This leads
 130 to a density function that models selection in the ancestral population of a and b .

$$f(p_A, p_B|p_C, \mathbf{v}, r, s) = \int_0^1 f_{neut}(p_A|\beta, \omega) f_{neut}(p_B|\beta, \psi) f_{sel}(\beta|p_C, \nu, \chi, r, s) d\beta \quad (10)$$

131 Additionally, formula 10 can be modified to test for selection that occurred specifically in one of the
 132 terminal branches that lead to a or b (Figures 1.C and 1.D), rather than in the ancestral population of a
 133 and b . For example, the density of frequencies for a scenario of selection in the branch leading to a can
 134 be written as:

$$f(p_A, p_B|p_C, \mathbf{v}, r, s) = \int_0^1 f_{sel}(p_A|\beta, \omega, r, s) f_{neut}(p_B|\beta, \psi) f_{neut}(\beta|p_C, \nu, \chi) d\beta \quad (11)$$

135 We will henceforth refer to the version of 3P-CLR that is tailored to detect selection in the internal
 136 branch that is ancestral to a and b as 3P-CLR(Int). In turn, the versions of 3P-CLR that are designed
 137 to detect selection in each of the daughter populations a and b will be designated as 3P-CLR(A) and
 138 3P-CLR(B), respectively.

139 We can now calculate the probability density of specific allele frequencies in populations a and b , given
 140 that we observe m_C derived alleles in a sample of size n_C from population c :

$$f(p_A, p_B|m_C, \mathbf{v}, r, s) = \int_0^1 f(p_A, p_B|p_C, \mathbf{v}, r, s) f(p_C|m_C) dp_C \quad (12)$$

141 and

$$f(p_C|m_C) = \frac{1}{B(m_C, n_C - m_C + 1)} p_C^{m_C-1} (1 - p_C)^{n_C - m_C} \quad (13)$$

142 where $B(x,y)$ is the Beta function. We note that formula 13 assumes that the unconditioned density
 143 function for the population derived allele frequency $f(p_C)$ comes from the neutral infinite-sites model at
 144 equilibrium and is therefore equal to the product of a constant and $1/p_C$ [Ewens, 2012].

145 Conditioning on the event that the site is segregating in the population, we can then calculate the
 146 probability of observing m_A and m_B derived alleles in a sample of size n_A from population a and a sample
 147 of size n_B from population b , respectively, given that we observe m_C derived alleles in a sample of size
 148 n_C from population c , using binomial sampling:

$$P(m_A, m_B|m_C, \mathbf{v}, r, s) = \frac{\int_0^1 \int_0^1 P(m_A|p_A)P(m_B|p_B)f(p_A, p_B|m_C, \mathbf{v}, r, s)dp_A dp_B}{\int_0^1 \int_0^1 f(p_A, p_B|m_C, \mathbf{v}, r, s)dp_A dp_B} \quad (14)$$

149 where

$$P(m_A|p_A) = \binom{n_A}{m_A} p_A^{m_A} (1 - p_A)^{n_A - m_A} \quad (15)$$

150 and

$$P(m_B|p_B) = \binom{n_B}{m_B} p_B^{m_B} (1 - p_B)^{n_B - m_B} \quad (16)$$

151 This allows us to calculate a composite likelihood of the derived allele counts in a and b given the
 152 derived allele counts in c :

$$CL_{3P-CLR}(\mathbf{r}, \mathbf{v}, s) = \prod_{j=1}^k P(m_A^j, m_B^j|m_C^j, \mathbf{v}, r^j, s) \quad (17)$$

153 As before, we can use this composite likelihood to produce a composite likelihood ratio statistic
 154 that can be calculated over regions of the genome to test the hypothesis of linked selection centered on a
 155 particular locus against the hypothesis of neutrality. Due to computational costs in numerical integration,
 156 we skip the sampling step for population c (formula 13) in our implementation of 3P-CLR. In other
 157 words, we assume $p_C = m_C/n_C$, but this is also assumed in XP-CLR when computing its corresponding

158 outgroup frequency. To perform the numerical integrations, we used the package Cubature (v.1.0.2). We
159 implemented our method in a freely available C++ program that can be downloaded from here:

160 <https://github.com/ferracimo>

161 The program requires the neutral drift parameters α , β and $(\nu + \chi)$ to be specified as input. These
162 can be obtained using F_3 statistics [Felsenstein, 1981, Patterson et al., 2012], which have previously been
163 implemented in programs like MixMapper [Lipson et al., 2013]. For example, α can be obtained via
164 $F_3(A; B, C)$, while $(\nu + \chi)$ can be obtained via $F_3(C; A, B)$. When computing F_3 statistics, we use only
165 sites where population C is polymorphic, and so we correct for this ascertainment in the calculation.
166 Another way of calculating these drift times is via $\partial a \partial i$ [Gutenkunst et al., 2009]. Focusing on two
167 populations at a time, we can fix one population's size and allow the split time and the other population's
168 size to be estimated by the program, in this case using all polymorphic sites, regardless of which population
169 they are segregating in. We then obtain the two drift times by scaling the inferred split time by the two
170 different population sizes. We provide scripts in our github page for the user to obtain these drift
171 parameters using both of the above ways.

172 4 Results

173 4.1 Simulations

174 We generated simulations in SLiM [Messer, 2013] to test the performance of XP-CLR and 3P-CLR in
175 a three-population scenario. We first focused on the performance of 3P-CLR(Int) in detecting ancient
176 selective events that occurred in the ancestral branch of two sister populations. We assumed that the
177 population history had been correctly estimated (i.e. the drift parameters and population topology were
178 known). First, we simulated scenarios in which a beneficial mutation arose in the ancestor of populations
179 a and b , before their split from each other but after their split from c (Table 1). Although both XP-CLR
180 and 3P-CLR are sensitive to partial or soft sweeps (as they do not rely on extended patterns of haplotype
181 homozygosity [Chen et al., 2010]), we required the beneficial allele to have fixed before the split (at time
182 t_{ab}) to ensure that the allele had not been lost by then, and also to ensure that the sweep was restricted to
183 the internal branch of the tree. We fixed the effective size of all three populations at $N_e = 10,000$. Each
184 simulation consisted in a 5 cM region and the beneficial mutation occurred in the center of this region.
185 The mutation rate was set at $2.5 * 10^{-8}$ per generation and the recombination rate between adjacent

186 nucleotides was set at 10^{-8} per generation.

187 To make a fair comparison to 3P-CLR(Int), and given that XP-CLR is a two-population test, we
188 applied XP-CLR in two ways. First, we pretended population b was not sampled, and so the "test"
189 panel consisted of individuals from a only, while the "outgroup" consisted of individuals from c . In the
190 second implementation (which we call "XP-CLR-avg"), we used the same outgroup panel, but pooled
191 the individuals from a and b into a single panel, and this pooled panel was the "test". The window
192 size was set at 0.5 cM and the number of SNPs sampled between each window's central SNP was set
193 at 600 (this number is large because it includes SNPs that are not segregating in the outgroup, which
194 are later discarded). To speed up computation, and because we are largely interested in comparing the
195 relative performance of the three tests under different scenarios, we used only 20 randomly chosen SNPs
196 per window in all tests. We note, however, that the performance of all of these tests can be improved by
197 using more SNPs per window.

198 Figure 2 shows receiver operating characteristic (ROC) curves comparing the sensitivity and specificity
199 of 3P-CLR(Int), 3P-CLR(A), XP-CLR and XP-CLR-avg in the first six demographic scenarios described
200 in Table 1. Each ROC curve was made from 100 simulations under selection (with $s = 0.1$ for the central
201 mutation) and 100 simulations under neutrality (with $s = 0$ and no fixation required). In each simulation,
202 100 haploid individuals (or 50 diploids) were sampled from population a , 100 individuals from population
203 b and 100 individuals from the outgroup population c . For each simulation, we took the maximum value
204 at a region in the neighborhood of the central mutation (± 0.5 cM) and used those values to compute
205 ROC curves under the two models.

206 When the split times are recent or moderately ancient (models A to D), 3P-CLR(Int) outperforms
207 the two versions of XP-CLR. Furthermore, 3P-CLR(A) is the test that is least sensitive to selection in
208 the internal branch as it is only meant to detect selection in the terminal branch leading to population
209 a . When the split times are very ancient (models E and F), none of the tests perform well. The root
210 mean squared error (RMSE) of the genetic distance between the true selected site and the highest scored
211 window is comparable across tests in all six scenarios (Figure S5). 3P-CLR(Int) is the best test at finding
212 the true location of the selected site in almost all demographic scenarios. We observe that we lose almost
213 all power if we simulate demographic scenarios where the population size is 10 times smaller ($N_e = 1,000$)
214 (Figure S1). Additionally, we observe that the power and specificity of 3P-CLR decrease as the selection
215 coefficient decreases (Figure S2).

216 We also simulated a situation in which only a few individuals are sequenced from the outgroup, while
217 large numbers of sequences are available from the tests. Figures S3 and S6 show the ROC curves and
218 RMSE plots, respectively, for a scenario in which 100 individuals were sampled from the test populations
219 but only 10 individuals (5 diploids) were sampled from the outgroup. Unsurprisingly, all tests have less
220 power to detect selection when the split times and the selection events are recent to moderately ancient
221 (models A-D). Interestingly though, when the split times and the selective events are very ancient (models
222 E-F), both 3P-CLR and XP-CLR perform better when using a small outgroup panel (Figure S3) than
223 when using a large outgroup panel (Figure 2). This is due to the Brownian motion approximation that
224 these methods utilize. Under the Wright-Fisher model, the drift increment at generation t is proportional
225 to $p(t)^*(1-p(t))$, where $p(t)$ is the derived allele frequency. The derivative of this function gets smaller
226 the closer $p(t)$ is to 0.5 (and is exactly 0 at that point). Small outgroup panels serve to filter out loci
227 with allele frequencies far from 0.5, and so small changes in allele frequency will not affect the drift
228 increment much, making Brownian motion a good approximation to the Wright-Fisher model. Indeed,
229 when running 3P-CLR(Int) in a demographic scenario with very ancient split times (Model E) and a large
230 outgroup panel (100 sequences) but only restricting to sites that are at intermediate frequencies in the
231 outgroup ($25\% \leq m_C/n_C \leq 75\%$), we find that performance is much improved relative to the case when
232 we use all sites that are segregating in the outgroup (Figure S4).

233 Importantly, the usefulness of 3P-CLR(Int) resides not just in its performance at detecting selective
234 sweeps in the ancestral population, but in its specific sensitivity to that particular type of events. Because
235 the test relies on correlated allele frequency differences in both population a and population b (relative
236 to the outgroup), selective sweeps that are specific to only one of the populations will not lead to high
237 3P-CLR(Int) scores, but will instead lead to high 3P-CLR(A) scores or 3P-CLR(B) scores, depending
238 on where selection took place. Figure 3 shows ROC curves in two scenarios in which a selective sweep
239 occurred only in population a (models I and J in Table 1), using 100 sampled individuals from each of
240 the 3 populations. Here, XP-CLR performs well, but is outperformed by 3P-CLR(A). Furthermore, 3P-
241 CLR(Int) shows almost no sensitivity to the recent sweep. For example, in Model I, at a specificity of 90%,
242 3P-CLR(A) and XP-CLR(A) have 86% and 80% sensitivity, respectively, while at the same specificity,
243 3P-CLR(Int) only has 18% sensitivity. One can compare this to the same demographic scenario but with
244 selection occurring in the ancestral population of a and b (model C, Figure 2), where at 90% specificity,
245 3P-CLR(A) and XP-CLR(A) have 72% and 84% sensitivity, respectively, while 3P-CLR(Int) has 90%

246 sensitivity. We also observe that 3P-CLR(A) is the best test at finding the true location of the selected
247 site when selection occurs in the terminal branch leading to population *a* (Figure S7).

248 Finally, we tested the behavior of 3P-CLR under selective scenarios that we did not explicitly model.
249 First, we simulated a selective sweep in the outgroup population. We find that all three types of 3P-CLR
250 statistics (3P-CLR(Int), 3P-CLR(A) and 3P-CLR(B)) are largely insensitive to this type of event, though
251 3P-CLR(Int) is relatively more sensitive than the other two. Second, we simulated two independent
252 selective sweeps in populations *a* and *b* (convergent evolution). This results in elevated 3P-CLR(A) and
253 3P-CLR(B) statistics, but 3P-CLR(Int) remains largely insensitive (Figure S8). We note that 3P-CLR
254 should not be used to detect selective events that occurred before the split of all three populations (i.e.
255 before the split of *c* and the ancestor of *a* and *b*), as it relies on allele frequency differences between the
256 populations.

257 4.2 Selection in Eurasians

258 We first applied 3P-CLR to modern human data from phase 1 of the 1000 Genomes Project [Abecasis
259 et al., 2012]. We used the African-American recombination map [Hinch et al., 2011] to convert physical
260 distances into genetic distances. We focused on Europeans (CEU, FIN, GBR, IBS, TSI) and East Asians
261 (CHB, CHS, JPT) as the two sister populations, using Yoruba (YRI) as the outgroup population (Figure
262 S9.A). We randomly sampled 100 individuals from each population and obtained sample derived allele
263 frequencies every 10 SNPs in the genome. We then calculated likelihood ratio statistics by a sliding
264 window approach, where we sampled a "central SNP" once every 10 SNPs. The central SNP in each
265 window was the candidate beneficial SNP for that window. We set the window size to 0.25 cM, and
266 randomly sampled 100 SNPs from each window, centered around the candidate beneficial SNP. In each
267 window, we calculated 3P-CLR to test for selection at three different branches of the population tree:
268 the terminal branch leading to Europeans (3P-CLR Europe), the terminal branch leading to East Asians
269 (3P-CLR East Asia) and the ancestral branch of Europeans and East Asians (3P-CLR Eurasia). Results
270 are shown in Figure S10. For each scan, we selected the windows in the top 99.9% quantile of scores
271 and merged them together if their corresponding central SNPs were contiguous, effectively resulting in
272 overlapping windows being merged. Tables S1, S2 and S3 show the top hits for Europeans, East Asians
273 and the ancestral Eurasian branch, respectively

274 We observe several genes that were identified in previous selection scans. In the East Asian branch,

275 one of the top hits is *EDAR*. Figure 4.A shows that this gene appears to be under selection exclusively
276 in this population branch. It codes for a protein involved in hair thickness and incisor tooth morphology
277 [Fujimoto et al., 2008, Kimura et al., 2009], and has been repeatedly identified as a candidate for a sweep
278 in East Asians [Grossman et al., 2010, Sabeti et al., 2007].

279 Furthermore, 3P-CLR allows us to narrow down on the specific time at which selection for previously
280 found candidates occurred in the history of particular populations. For example, Chen et al. [2010]
281 performed a scan of the genomes of East Asians using XP-CLR with Yoruba as the outgroup, and
282 identified a number of candidate genes [Chen et al., 2010]. 3P-CLR confirms recovers several of their
283 loci when looking specifically at the East Asian branch: *OR56A1*, *OR56B4*, *OR52B2*, *SLC30A9*, *BBX*,
284 *EPHB1*, *ACTN1* and *XKR6*. However, when applied to the ancestral Eurasian branch, 3P-CLR finds
285 some genes that were previously found in the XP-CLR analysis of East Asians, but that are not among
286 the top hits in 3P-CLR applied to the East Asian branch: *COMMD3*, *BMI1*, *SPAG6*, *NGLY1*, *OXSM*,
287 *CD226*, *ABCC12*, *ABCC11*, *LONP2*, *SIAH1*, *PPARA*, *PKDREJ*, *GTSE1*, *TRMU* and *CELSR1*. This
288 suggests selection in these regions occurred earlier, i.e. before the European-East Asian split. Figure 4.B
289 shows a comparison between the 3P-CLR scores for the three branches in the region containing genes
290 *BMI1* (a proto-oncogene [Siddique and Saleem, 2012]) and *SPAG6* (involved in sperm motility [Sapiro
291 et al., 2002]). Here, the signal of Eurasia-specific selection is evidently stronger than the other two signals.
292 Finally, we also find some candidates from Chen et al. [2010] that appear to be under selection in both
293 the ancestral Eurasian branch and the East Asian daughter branch: *SFXN5*, *EMX1*, *SPR* and *CYP26B1*.
294 Interestingly, both *CYP26B1* and *CYP26A1* are very strong candidates for selection in the East Asian
295 branch. These two genes lie in two different chromosomes, so they are not part of a gene cluster, but
296 they both code for proteins that hydrolyze retinoic acid, an important signaling molecule [Topletz et al.,
297 2012, White et al., 2000].

298 Other selective events that 3P-CLR infers to have occurred in Eurasians include the region containing
299 *HERC2* and *OCA2*, which are major determinants of eye color [Branicki et al., 2009, Eiberg et al.,
300 2008, Han et al., 2008]. There is also evidence that these genes underwent selection more recently in
301 the history of Europeans [Mathieson et al., 2015], which could suggest an extended period of selection
302 - perhaps influenced by migrations between Asia and Europe - or repeated selective events at the same
303 locus.

304 When running 3P-CLR to look for selection specific to Europe, we find that *TYRP1*, which plays a

305 role in human skin pigmentation [Halaban and Moellmann, 1990], is among the top hits. This gene has
306 been previously found to be under strong selection in Europe [Voight et al., 2006], using a statistic called
307 *iHS*, which measures extended patterns of haplotype homozygosity that are characteristic of selective
308 sweeps. Interestingly, a change in the gene *TYRP1* has also been found to cause a blonde hair phenotype
309 in Melanesians [Kenny et al., 2012]. Another of our top hits is the region containing *SH2B3*, which was
310 identified previously as a candidate for selection in Europe based on both *iHS* and F_{st} [Pickrell et al.,
311 2009]. This gene contains a nonsynonymous SNP (rs3184504) segregating in Europeans. One of its alleles
312 (the one in the selected haplotype) has been associated with celiac disease and type 1 diabetes [Hunt
313 et al., 2008, Todd et al., 2007] but is also protective against bacterial infection [Zhernakova et al., 2010].

314 We used Gowinda (v1.12) [Kofler and Schlötterer, 2012] to find enriched Gene Ontology (GO) cate-
315 gories among the regions in the 99.5% highest quantile for each branch score, relative to the rest of the
316 genome ($P < 0.05$, FDR < 0.3). The significantly enriched categories are listed in Table S4. In the East
317 Asian branch, we find categories related to alcohol catabolism, retinol binding, vitamin metabolism and
318 epidermis development, among others. In the European branch, we find cuticle development and hydro-
319 gen peroxide metabolic process as enriched categories. We find no enriched categories in the Eurasian
320 branch that pass the above cutoffs.

321 4.3 Selection in ancestral modern humans

322 We applied 3P-CLR to modern human data combined with recently sequenced archaic human data. We
323 sought to find selective events that occurred in modern humans after their split from archaic groups. We
324 used the combined Neanderthal and Denisovan high-coverage genomes [Meyer et al., 2012, Prüfer et al.,
325 2014] as the outgroup population, and, for our two test populations, we used Eurasians (CEU, FIN,
326 GBR, IBS, TSI, CHB, CHS, JPT) and Yoruba (YRI), again from phase 1 of the 1000 Genomes Project
327 Abecasis et al. [2012] (Figure S9.B). As before, we randomly sampled 100 genomes for each of the two
328 daughter populations at each site, and tested for selective events that occurred more anciently than the
329 split of Yoruba and Eurasians, but more recently than the split from Neanderthals. Figure S11 shows
330 an ROC curve for a simulated scenario under these conditions, based on the history of population size
331 changes inferred by PSMC [Li and Durbin, 2011, Prüfer et al., 2014], suggesting we should have power
332 to detect strong ($s=0.1$) selective events in the ancestral branch of present-day humans. We observe that
333 3P-CLR(Int) has similar power as XP-CLR and XP-CLR-avg at these time-scales, but is less prone to

334 also detect recent (post-split) events, making it more specific to ancestral sweeps.

335 We ran 3P-CLR using 0.25 cM windows as above (Figure S13). As before, we selected the top 99.9%
336 windows and merged them together if their corresponding central SNPs were contiguous (Table S5). The
337 top 20 regions are in Table 3. Figure S13 shows that the outliers in the genome-wide distribution of
338 scores are not strong. We wanted to verify that the density of scores was robust to the choice of window
339 size. By using a larger window size (1 cM), we obtained a distribution with slightly more extreme outliers
340 (Figures S12 S13). For that reason, we also show the top hits from this large-window run (Tables S6,
341 3), using a smaller density of SNPs (200/1cM rather than 100/0.25cM), due to costs in speed. To find
342 putative candidates for the beneficial variants in each region, we queried the catalogs of modern human-
343 specific high-frequency or fixed derived changes that are ancestral in the Neanderthal and/or the Denisova
344 genomes [Castellano et al., 2014, Prüfer et al., 2014] and overlapped them with our regions.

345 We found several genes that were identified in previous studies that looked for selection in modern
346 humans after their split from archaic groups [Green et al., 2010, Prüfer et al., 2014], including *SIPA1L1*,
347 *ANAPC10*, *ABCE1*, *RASA1*, *CCNH*, *KCNJ3*, *HBP1*, *COG5*, *CADPS2*, *FAM172A*, *POU5F2*, *FGF7*,
348 *RABGAP1*, *SMURF1*, *GABRA2*, *ALMS1*, *PVRL3*, *EHBP1*, *VPS54*, *OTX1*, *UGP2*, *GTDC1*, *ZEB2*
349 and *OIT3*. One of our strongest candidate genes among these is *SIPA1L1* (Figure 5.A), which is in the
350 first and the fourth highest-ranking region, when using 1 cM and 0.25 cM windows, respectively. The
351 protein encoded by this gene (E6TP1) is involved in actin cytoskeleton organization and controls neural
352 morphology (UniProt by similarity). Interestingly, it is also a target of degradation of the oncoproteins
353 of high-risk papillomaviruses [Gao et al., 1999].

354 Another candidate gene is *ANAPC10* (Figure 5.B). This gene codes for a core subunit of the cyclosome,
355 which is involved in progression through the cell cycle [Pravtcheva and Wise, 2001], and may play a role
356 in oocyte maturation and human T-lymphotropic virus infection (KEGG pathway [Kanehisa and Goto,
357 2000]). *ANAPC10* is noteworthy because it was found to be significantly differentially expressed in
358 humans compared to other great apes and macaques: it is up-regulated in the testes [Brawand et al.,
359 2011]. The gene also contains two intronic changes that are fixed derived in modern humans, ancestral
360 in both Neanderthals and Denisovans and that have evidence for being highly disruptive, based on a
361 composite score that combines conservation and regulatory data (PHRED-scaled C-scores > 11 [Kircher
362 et al., 2014, Prüfer et al., 2014]). The changes, however, appear not to lie in any obvious regulatory
363 region [Dunham et al., 2012, Rosenbloom et al., 2011].

364 We also find *ADSL* among the list of candidates. This gene is known to contain a nonsynonymous
365 change that is fixed in all present-day humans but homozygous ancestral in the Neanderthal genome, the
366 Denisova genome and two Neanderthal exomes [Castellano et al., 2014] (Figure 6.A). It was previously
367 identified as lying in a region with strong support for positive selection in modern humans, using summary
368 statistics implemented in an ABC method [Racimo et al., 2014]. The gene is interesting because it is
369 one of the members of the Human Phenotype ontology category "aggression / hyperactivity" which is
370 enriched for nonsynonymous changes that occurred in the modern human lineage after the split from
371 archaic humans [Castellano et al., 2014, Robinson et al., 2008]. *ADSL* codes for adenylosuccinase, an
372 enzyme involved in purine metabolism [Van Keuren et al., 1987]. A deficiency of adenylosuccinase can lead
373 to apraxia, speech deficits, delays in development and abnormal behavioral features, like hyperactivity
374 and excessive laughter [Gitiaux et al., 2009]. The nonsynonymous mutation (A429V) is in the C-terminal
375 domain of the protein (Figure 6.B) and lies in a highly conserved position (primate PhastCons = 0.953;
376 GERP score = 5.67 [Cooper et al., 2010, Kircher et al., 2014, Siepel et al., 2005]). The ancestral amino
377 acid is conserved across the tetrapod phylogeny, and the mutation is only three residues away from the
378 most common causative SNP for severe adenylosuccinase deficiency [Edery et al., 2003, Kmoch et al.,
379 2000, Maaswinkel-Mooij et al., 1997, Marie et al., 1999, Race et al., 2000]. The change has the highest
380 probability of being disruptive to protein function, out of all the nonsynonymous modern-human-specific
381 changes that lie in the top-scoring regions (C-score = 17.69). While *ADSL* is an interesting candidate
382 and lies in the center of the inferred selected region (Figure 6.A), there are other genes in the region too,
383 including *TNRC6B* and *MKLI*. *TNRC6B* may be involved in miRNA-guided gene silencing [Meister
384 et al., 2005], while *MKLI* may play a role in smooth muscle differentiation [Du et al., 2004], and has
385 been associated with acute megakaryocytic leukemia [Mercher et al., 2001].

386 *RASA1* was also a top hit in a previous scan for selection [Green et al., 2010], and was additionally
387 inferred to have evidence in favor of selection in Racimo et al. [2014]. The gene codes for a protein involved
388 in the control of cellular differentiation [Trahey et al., 1988], and has a modern human-specific fixed
389 nonsynonymous change (G70E). Human diseases associated with *RASA1* include basal cell carcinoma
390 [Friedman et al., 1993] and arteriovenous malformation [Eerola et al., 2003, Hershkovitz et al., 2008].

391 The *GABA_A* gene cluster in chromosome 4p12 is also among the top regions. The gene within the
392 putatively selected region codes for a subunit (*GABRA2*) of the *GABA_A* receptor, which is a ligand-
393 gated ion channel that plays a key role in synaptic inhibition in the central nervous system (see review by

394 Whiting et al. [1999]). *GABRA2* is significantly associated with risk of alcohol dependence in humans
395 [Edenberg et al., 2004], perception of pain [Knabl et al., 2008] and asthma [Xiang et al., 2007].

396 Two other candidate genes that may be involved in brain development are *FOXP1* and *CADPS2*.
397 *FOXP1* was not identified in any of the previous selection scans, and codes for a protein called forkhead
398 box G1, which plays an important role during brain development. Mutations in this gene are associated
399 with a slow-down in brain growth during childhood resulting in microcephaly, which in turn causes various
400 intellectual disabilities [Ariani et al., 2008, Mencarelli et al., 2010]. *CADPS2* was identified in Green et al.
401 [2010] as a candidate for selection, and has been associated with autism [Sadakata and Furuichi, 2010].
402 The gene has been suggested to be specifically important in the evolution of all modern humans, as it
403 was not found to be selected earlier in great apes or later in particular modern human populations [Crisci
404 et al., 2011].

405 Finally, we find a signal of selection in a region containing the gene *EHBP1* and *OTX1*. This region
406 was identified in both of the two previous scans for modern human selection [Green et al., 2010, Prüfer
407 et al., 2014]. *EHBP1* codes for a protein involved in endocytic trafficking [Guilherme et al., 2004] and
408 has been associated with prostate cancer [Gudmundsson et al., 2008]. *OTX1* is a homeobox family gene
409 that may play a role in brain development [Gong et al., 2003]. Interestingly, *EHBP1* contains a single-
410 nucleotide intronic change (chr2:63206488) that is almost fixed in all present-day humans and homozygous
411 ancestral in Neanderthal and Denisova [Prüfer et al., 2014]. This change is also predicted to be highly
412 disruptive (C-score = 13.1) and lies in a position that is extremely conserved across primates (PhastCons
413 = 0.942), mammals (PhastCons = 1) and vertebrates (PhastCons = 1). The change is 18 bp away from
414 the nearest splice site and overlaps a VISTA conserved enhancer region (element 1874) [Pennacchio et al.,
415 2006], suggesting a putative regulatory role for the change.

416 We again used Gowinda [Kofler and Schlötterer, 2012] to find enriched GO categories among the
417 regions with high 3P-CLR scores in the Modern Human branch. The significantly enriched categories (P
418 < 0.05 , FDR < 0.3) are listed in Table S4. We find several GO terms related to the regulation of the cell
419 cycle, T cell migration and intracellular transport.

420 We overlapped the genome-wide association studies (GWAS) database [Li et al., 2011, Welter et al.,
421 2014] with the list of fixed or high-frequency modern human-specific changes that are ancestral in archaic
422 humans [Prüfer et al., 2014] and that are located within our top putatively selected regions in modern
423 humans (Tables S7 and S8 for the 0.25 cM and 1 cM scans, respectively). None of the resulting SNPs

424 are completely fixed derived, because GWAS can only yield associations from sites that are segregating.
425 We find several SNPs in the *RAB28* gene [Dunham et al., 2012, Rosenbloom et al., 2011], which are
426 significantly associated with obesity [Paternoster et al., 2011]. We also find a SNP with a high C-score
427 (rs10171434) associated with urinary metabolites [Suhre et al., 2011] and suicidal behavior in patients with
428 mood disorders [Perlis et al., 2010]. The SNP is located in an enhancer regulatory feature [Dunham et al.,
429 2012, Rosenbloom et al., 2011] located between genes *PELI1* and *VPS54*, in the same putatively selected
430 region as genes *EHBP1* and *OTX1* (see above). Finally, there is a highly C-scoring SNP (rs731108) that
431 is associated with renal cell carcinoma [Henrion et al., 2013]. This SNP is also located in an enhancer
432 regulatory feature [Dunham et al., 2012, Rosenbloom et al., 2011], in an intron of *ZEB2*. In this last
433 case, though, only the Neanderthal genome has the ancestral state, while the Denisova genome carries
434 the modern human variant.

435 5 Discussion

436 We have developed a new method called 3P-CLR, which allows us to detect positive selection along the
437 genome. The method is based on an earlier test (XP-CLR [Chen et al., 2010]) that uses linked allele
438 frequency differences between two populations to detect population-specific selection. However, unlike
439 XP-CLR, 3P-CLR can allow us to distinguish between selective events that occurred before and after the
440 split of two populations. Our method has some similarities to an earlier method developed by Schlebusch
441 et al. [2012], which used an F_{st} -like score to detect selection ancestral to two populations. In that case,
442 though, the authors used summary statistics and did not explicitly model the process leading to allele
443 frequency differentiation. It is also similar to a more recent method [Fariello et al., 2013] that models
444 differences in haplotype frequencies between populations, while accounting for population structure.

445 We used our method to confirm previously found candidate genes in particular human populations,
446 like *EDAR*, *TYRP1* and *CYP26B1*, and find some novel candidates too (Tables S1, S2, S3). Additionally,
447 we can infer that certain genes, which were previously known to have been under selection in East Asians
448 (like *SPAG6*), are more likely to have undergone a sweep in the population ancestral to both Europeans
449 and East Asians than in East Asians only. We find that genes involved in epidermis development and
450 alcohol catabolism are particularly enriched among the East Asian candidate regions, while genes involved
451 in peroxide catabolism and cuticle development are enriched in the European branch. This suggests these

452 biological functions may have been subject to positive selection in recent times.

453 We also used 3P-CLR to detect selective events that occurred in the ancestors of modern humans,
454 after their split from Neanderthals and Denisovans (Table S5). These events could perhaps have led to
455 the spread of phenotypes that set modern humans apart from other hominin groups. We find several
456 interesting candidates, like *SIPA1L1*, *ADSL*, *RASA1*, *OTX1*, *EHBP1*, *FOXP1*, *RAB28* and *ANAPC10*,
457 some of which were previously detected using other types of methods [Green et al., 2010, Prüfer et al.,
458 2014, Racimo et al., 2014]. We also find an enrichment for GO categories related to cell cycle regulation
459 and T cell migration among the candidate regions, suggesting that these biological processes might have
460 been affected by positive selection after the split from archaic humans.

461 An advantage of differentiation-based tests like XP-CLR and 3P-CLR is that, unlike other patterns
462 detected by tests of neutrality (like extended haplotype homozygosity, [Sabeti et al., 2002]) that are
463 exclusive to hard sweeps, the patterns that both XP-CLR and 3P-CLR are tailored to find are based on
464 regional allele frequency differences between populations. These patterns can also be produced by soft
465 sweeps from standing variation or by partial sweeps [Chen et al., 2010], and there is some evidence that
466 the latter phenomena may have been more important than classic sweeps during human evolutionary
467 history [Hernandez et al., 2011].

468 Another advantage of both XP-CLR and 3P-CLR is that they do not rely on an arbitrary division of
469 genomic space. Unlike other methods which require the partition of the genome into small windows of
470 fixed size, our composite likelihood ratios can theoretically be computed over windows that are as big as
471 each chromosome, while only switching the central candidate site at each window. This is because the
472 likelihood ratios use the genetic distance to the central SNP as input. SNPs that are very far away from
473 the central SNP will not contribute much to the likelihood function of both the neutral and the selection
474 models, while those that are close to it will. In the interest of speed, we heuristically limit the window size
475 in our implementation, and use less SNPs when calculating likelihoods over larger windows. Nevertheless,
476 these parameters can be arbitrarily adjusted by the user as needed, and if enough computing resources
477 are available. The use of genetic distance in the likelihood function also allows us to take advantage of the
478 spatial distribution of SNPs as an additional source of information, rather than only relying on patterns
479 of population differentiation restricted to tightly linked SNPs.

480 3P-CLR also has an advantage over HMM-based selection methods, like the one implemented in Prüfer
481 et al. [2014]. The likelihood ratio scores obtained from 3P-CLR can provide an idea of how credible a

482 selection model is for a particular region, relative to the rest of the genome. The HMM-based method
483 previously used to scan for selection in modern humans [Prüfer et al., 2014] can only rank putatively
484 selected regions by genetic distance, but cannot output a statistical measure that may indicate how likely
485 each region is to have been under selection in ancient times. In contrast, 3P-CLR provides a composite
486 likelihood ratio score, which allows for a statistically rigorous way to compare the neutral model and a
487 specific selection model (for example, recent or ancient selection).

488 The outliers from Figure S10 have much higher scores (relative to the rest of the genome) than the
489 outliers from Figure S13. This may be due to both the difference in time scales in the two sets of tests
490 and to the uncertainty that comes from estimating outgroup allele frequencies using only two archaic
491 genomes. This pattern can also be observed in Figure S14, where the densities of the scores looking for
492 patterns of ancient selection (3P-CLR Modern Human and 3P-CLR Eurasia) have much shorter tails
493 than the densities of scores looking for patterns of recent selection (3P-CLR Europe and 3P-CLR East
494 Asia). Simulations show that 3P-CLR(Int) score distributions are naturally shorter than 3P-CLR(A)
495 scores (Figure S15), which could explain the short tail of the 3P-CLR Eurasia distribution. Additionally,
496 the even shorter tail in the distribution of 3P-CLR Modern Human scores may be a consequence of the
497 fact that the split times of the demographic history in that case are older than the split times in the
498 Eurasian tree, as simulations show that ancient split times tend to further shorten the tail of the 3P-CLR
499 score distribution (Figure S15). We note, though, that using a larger window size produces a larger
500 number of strong outliers (Figure S12).

501 A limitation of composite likelihood ratio tests is that the composite likelihood calculated for each
502 model under comparison is obtained from a product of individual likelihoods at each site, and so it
503 underestimates the correlation that exists between SNPs due to linkage effects [Chen et al., 2010, Lindsay,
504 1988, Pace et al., 2011, Varin et al., 2011]. One way to partially mitigate this problem is by using corrective
505 weights based on linkage disequilibrium (LD) statistics calculated on the outgroup population [Chen et al.,
506 2010]. Our implementation of 3P-CLR allows the user to incorporate such weights, if appropriate LD
507 statistics are available from the outgroup. However, in cases where these are unreliable, it may not be
508 possible to correct for this (for example, when only a few unphased genomes are available, as in the case
509 of the Neanderthal and Denisova genomes).

510 While 3P-CLR relies on integrating over the possible allele frequencies in the ancestors of populations
511 a and b (formula 10), one could envision using ancient DNA to avoid this step. Thus, if enough genomes

512 could be sampled from that ancestral population that existed in the past, one could use the sample
513 frequency in the ancient set of genomes as a proxy for the ancestral population frequency. This may soon
514 be possible, as several early modern human genomes have already been sequenced in recent years [Fu
515 et al., 2014, Lazaridis et al., 2014, Seguin-Orlando et al., 2014].

516 Though we have focused on a three-population model in this manuscript, it should be straightforward
517 to expand our method to a larger number of populations, albeit with additional costs in terms of speed
518 and memory. 3P-CLR relies on a similar framework to the demographic inference method implemented
519 in TreeMix [Pickrell and Pritchard, 2012], which can estimate population trees that include migration
520 events, using genome-wide data. With a more complex modeling framework, it may be possible to
521 estimate the time and strength of selective events with better resolution and using more populations,
522 and also to incorporate additional demographic forces, like continuous migration between populations or
523 pulses of admixture.

524 Acknowledgments

525 We thank Montgomery Slatkin, Rasmus Nielsen, Joshua Schraiber, Nicolas Duforet-Frebourg, Emilia
526 Huerta-Sánchez, Hua Chen, Benjamin Peter, Nick Patterson, David Reich, Joachim Hermisson, Graham
527 Coop and members of the Slatkin and Nielsen labs for helpful advice and discussions. We also thank two
528 anonymous reviewers for their helpful comments. This work was supported by NIH grant R01-GM40282
529 to Montgomery Slatkin.

530 Literature Cited

531 Goncalo R Abecasis, Adam Auton, Lisa D Brooks, Mark A DePristo, Richard M Durbin, Robert E
532 Handsaker, Hyun Min Kang, Gabor T Marth, Gil A McVean, Hans Lehrach, et al. An integrated map
533 of genetic variation from 1,092 human genomes. *Nature*, 491(7422):56–65, 2012.

534 Joshua M Akey, Ge Zhang, Kun Zhang, Li Jin, and Mark D Shriver. Interrogating a high-density snp
535 map for signatures of natural selection. *Genome research*, 12(12):1805–1814, 2002.

536 Francesca Ariani, Giuseppe Hayek, Dalila Rondinella, Rosangela Artuso, Maria Antonietta Mencarelli,
537 Ariele Spanhol-Rosseto, Marzia Pollazzon, Sabrina Buoni, Ottavia Spiga, Sara Ricciardi, et al. Foxg1

- 538 is responsible for the congenital variant of rett syndrome. *The American Journal of Human Genetics*,
539 83(1):89–93, 2008.
- 540 Wojciech Branicki, Urszula Brudnik, and Anna Wojas-Pelc. Interactions between *herc2*, *oca2* and *mc1r*
541 may influence human pigmentation phenotype. *Annals of human genetics*, 73(2):160–170, 2009.
- 542 David Brawand, Magali Soumillon, Anamaria Necseulea, Philippe Julien, Gábor Csárdi, Patrick Harrigan,
543 Manuela Weier, Angélica Liechti, Ayinuer Aximu-Petri, Martin Kircher, et al. The evolution of gene
544 expression levels in mammalian organs. *Nature*, 478(7369):343–348, 2011.
- 545 Sergi Castellano, Genís Parra, Federico A Sánchez-Quinto, Fernando Racimo, Martin Kuhlwilm, Martin
546 Kircher, Susanna Sawyer, Qiaomei Fu, Anja Heinze, Birgit Nickel, et al. Patterns of coding variation
547 in the complete exomes of three neandertals. *Proceedings of the National Academy of Sciences*, 111
548 (18):6666–6671, 2014.
- 549 Hua Chen, Nick Patterson, and David Reich. Population differentiation as a test for selective sweeps.
550 *Genome research*, 20(3):393–402, 2010.
- 551 Gregory M Cooper, David L Goode, Sarah B Ng, Arend Sidow, Michael J Bamshad, Jay Shendure,
552 and Deborah A Nickerson. Single-nucleotide evolutionary constraint scores highlight disease-causing
553 mutations. *Nature methods*, 7(4):250–251, 2010.
- 554 Jessica L Crisci, Alex Wong, Jeffrey M Good, and Jeffrey D Jensen. On characterizing adaptive events
555 unique to modern humans. *Genome biology and evolution*, 3:791–798, 2011.
- 556 Kevin L Du, Mary Chen, Jian Li, John J Lepore, Patricia Mericko, and Michael S Parmacek. Megakary-
557 oblastic leukemia factor-1 transduces cytoskeletal signals and induces smooth muscle cell differentia-
558 tion from undifferentiated embryonic stem cells. *Journal of Biological Chemistry*, 279(17):17578–17586,
559 2004.
- 560 I Dunham, A Kundaje, SF Aldred, PJ Collins, C Davis, F Doyle, CB Epstein, S Fretze, J Harrow,
561 R Kaul, et al. An integrated encyclopedia of dna elements in the human genome. *Nature*, 489(7414):
562 57–74, 2012.
- 563 Richard Durrett and Jason Schweinsberg. Approximating selective sweeps. *Theoretical population biology*,
564 66(2):129–138, 2004.

- 565 Howard J Edenberg, Danielle M Dick, Xiaoling Xuei, Huijun Tian, Laura Almasy, Lance O Bauer,
566 Raymond R Crowe, Alison Goate, Victor Hesselbrock, Kevin Jones, et al. Variations in *gabra2*, en-
567 coding the $\alpha 2$ subunit of the gaba a receptor, are associated with alcohol dependence and with brain
568 oscillations. *The American Journal of Human Genetics*, 74(4):705–714, 2004.
- 569 Patrick Edery, Stéphane Chabrier, Irène Ceballos-Picot, Sandrine Marie, Marie-Françoise Vincent, and
570 Marc Tardieu. Intrafamilial variability in the phenotypic expression of adenylosuccinate lyase deficiency:
571 a report on three patients. *American Journal of Medical Genetics Part A*, 120(2):185–190, 2003.
- 572 Iiro Eerola, Laurence M Boon, John B Mulliken, Patricia E Burrows, Anne Dompmartin, Shoji Watanabe,
573 Romain Vanwijck, and Miikka Vikkula. Capillary malformation–arteriovenous malformation, a new
574 clinical and genetic disorder caused by *rasa1* mutations. *The American Journal of Human Genetics*,
575 73(6):1240–1249, 2003.
- 576 Hans Eiberg, Jesper Troelsen, Mette Nielsen, Annemette Mikkelsen, Jonas Mengel-From, Klaus W Kjaer,
577 and Lars Hansen. Blue eye color in humans may be caused by a perfectly associated founder mutation
578 in a regulatory element located within the *herc2* gene inhibiting *oca2* expression. *Human genetics*, 123
579 (2):177–187, 2008.
- 580 Warren J Ewens. *Mathematical Population Genetics 1: Theoretical Introduction*, volume 27. Springer
581 Science & Business Media, 2012.
- 582 María Inés Fariello, Simon Boitard, Hugo Naya, Magali SanCristobal, and Bertrand Servin. Detecting
583 signatures of selection through haplotype differentiation among hierarchically structured populations.
584 *Genetics*, 193(3):929–941, 2013.
- 585 Justin C Fay and Chung-I Wu. Hitchhiking under positive darwinian selection. *Genetics*, 155(3):1405–
586 1413, 2000.
- 587 Joseph Felsenstein. Evolutionary trees from gene frequencies and quantitative characters: finding maxi-
588 mum likelihood estimates. *Evolution*, pages 1229–1242, 1981.
- 589 Eitan Friedman, Pablo V Gejman, George A Martin, and Frank McCormick. Nonsense mutations in the
590 c-terminal sh2 region of the gtpase activating protein (*gap*) gene in human tumours. *Nature genetics*,
591 5(3):242–247, 1993.

- 592 Qiaomei Fu, Heng Li, Priya Moorjani, Flora Jay, Sergey M Slepchenko, Aleksei A Bondarev, Philip LF
593 Johnson, Ayinuer Aximu-Petri, Kay Prüfer, Cesare de Filippo, et al. Genome sequence of a 45,000-
594 year-old modern human from western siberia. *Nature*, 514(7523):445–449, 2014.
- 595 Akihiro Fujimoto, Ryosuke Kimura, Jun Ohashi, Kazuya Omi, Rika Yuliwulandari, Lilian Batubara,
596 Mohammad Syamsul Mustofa, Urai Samakkarn, Wannapa Settheetham-Ishida, Takafumi Ishida, et al.
597 A scan for genetic determinants of human hair morphology: Edar is associated with asian hair thickness.
598 *Human Molecular Genetics*, 17(6):835–843, 2008.
- 599 Qingshen Gao, Seetha Srinivasan, Sarah N Boyer, David E Wazer, and Vimla Band. The e6 oncoproteins
600 of high-risk papillomaviruses bind to a novel putative gap protein, e6tp1, and target it for degradation.
601 *Molecular and cellular biology*, 19(1):733–744, 1999.
- 602 Cyril Gitiaux, Irène Ceballos-Picot, Sandrine Marie, Vassili Valayannopoulos, Marlène Rio, Séverine
603 Verrieres, Jean François Benoist, Marie Françoise Vincent, Isabelle Desguerre, and Nadia Bahi-Buisson.
604 Misleading behavioural phenotype with adenylosuccinate lyase deficiency. *European Journal of Human*
605 *Genetics*, 17(1):133–136, 2009.
- 606 Shiaoqing Gong, Chen Zheng, Martin L Doughty, Kasia Losos, Nicholas Didkovsky, Uta B Schambra,
607 Norma J Nowak, Alexandra Joyner, Gabrielle Leblanc, Mary E Hatten, et al. A gene expression atlas
608 of the central nervous system based on bacterial artificial chromosomes. *Nature*, 425(6961):917–925,
609 2003.
- 610 Richard E Green, Johannes Krause, Adrian W Briggs, Tomislav Maricic, Udo Stenzel, Martin Kircher,
611 Nick Patterson, Heng Li, Weiwei Zhai, Markus Hsi-Yang Fritz, et al. A draft sequence of the neandertal
612 genome. *science*, 328(5979):710–722, 2010.
- 613 Sharon R Grossman, Ilya Shylakhter, Elinor K Karlsson, Elizabeth H Byrne, Shannon Morales, Gabriel
614 Frieden, Elizabeth Hostetter, Elaine Angelino, Manuel Garber, Or Zuk, et al. A composite of multiple
615 signals distinguishes causal variants in regions of positive selection. *Science*, 327(5967):883–886, 2010.
- 616 Julius Gudmundsson, Patrick Sulem, Thorunn Rafnar, Jon T Bergthorsson, Andrei Manolescu, Daniel
617 Gudbjartsson, Bjarni A Agnarsson, Asgeir Sigurdsson, Kristrun R Benediktsdottir, Thorarinn Blondal,
618 et al. Common sequence variants on 2p15 and xp11. 22 confer susceptibility to prostate cancer. *Nature*
619 *genetics*, 40(3):281–283, 2008.

- 620 Adilson Guilherme, Neil A Soriano, Paul S Furcinitti, and Michael P Czech. Role of ehdl and ehbp1
621 in perinuclear sorting and insulin-regulated glut4 recycling in 3t3-l1 adipocytes. *Journal of Biological*
622 *Chemistry*, 279(38):40062–40075, 2004.
- 623 Ryan N Gutenkunst, Ryan D Hernandez, Scott H Williamson, and Carlos D Bustamante. Inferring the
624 joint demographic history of multiple populations from multidimensional snp frequency data. *PLoS*
625 *genetics*, 5(10):e1000695, 2009.
- 626 Ruth Halaban and Gisela Moellmann. Murine and human b locus pigmentation genes encode a glycopro-
627 tein (gp75) with catalase activity. *Proceedings of the National Academy of Sciences*, 87(12):4809–4813,
628 1990.
- 629 Jiali Han, Peter Kraft, Hongmei Nan, Qun Guo, Constance Chen, Abrar Qureshi, Susan E Hankinson,
630 Frank B Hu, David L Duffy, Zhen Zhen Zhao, et al. A genome-wide association study identifies novel
631 alleles associated with hair color and skin pigmentation. *PLoS genetics*, 4(5):e1000074, 2008.
- 632 Marc Henrion, Matthew Frampton, Ghislaine Scelo, Mark Purdue, Yuanqing Ye, Peter Broderick, Alastair
633 Ritchie, Richard Kaplan, Angela Meade, James McKay, et al. Common variation at 2q22. 3 (zeb2)
634 influences the risk of renal cancer. *Human molecular genetics*, 22(4):825–831, 2013.
- 635 Ryan D Hernandez, Joanna L Kelley, Eyal Elyashiv, S Cord Melton, Adam Auton, Gilean McVean, Guy
636 Sella, Molly Przeworski, et al. Classic selective sweeps were rare in recent human evolution. *science*,
637 331(6019):920–924, 2011.
- 638 D Hershkovitz, D Bercovich, E Sprecher, and M Lapidot. Rasa1 mutations may cause hereditary capillary
639 malformations without arteriovenous malformations. *British Journal of Dermatology*, 158(5):1035–
640 1040, 2008.
- 641 Anjali G Hinch, Arti Tandon, Nick Patterson, Yunli Song, Nadin Rohland, Cameron D Palmer, Gary K
642 Chen, Kai Wang, Sarah G Buxbaum, Ermeg L Akyzbekova, et al. The landscape of recombination in
643 african americans. *Nature*, 476(7359):170–175, 2011.
- 644 Karen A Hunt, Alexandra Zhernakova, Graham Turner, Graham AR Heap, Lude Franke, Marcel Bruinen-
645 berg, Jihane Romanos, Lotte C Dinesen, Anthony W Ryan, Davinder Panesar, et al. Newly identified

- 646 genetic risk variants for celiac disease related to the immune response. *Nature genetics*, 40(4):395–402,
647 2008.
- 648 Minoru Kanehisa and Susumu Goto. Kegg: kyoto encyclopedia of genes and genomes. *Nucleic acids*
649 *research*, 28(1):27–30, 2000.
- 650 Eimear E Kenny, Nicholas J Timpson, Martin Sikora, Muh-Ching Yee, Andrés Moreno-Estrada, Celeste
651 Eng, Scott Huntsman, Esteban González Burchard, Mark Stoneking, Carlos D Bustamante, et al.
652 Melanesian blond hair is caused by an amino acid change in tyrp1. *Science*, 336(6081):554–554, 2012.
- 653 Ryosuke Kimura, Tetsutaro Yamaguchi, Mayako Takeda, Osamu Kondo, Takashi Toma, Kuniaki Haneji,
654 Tsunehiko Hanihara, Hirotaka Matsukusa, Shoji Kawamura, Koutaro Maki, et al. A common variation
655 in edar is a genetic determinant of shovel-shaped incisors. *The American Journal of Human Genetics*,
656 85(4):528–535, 2009.
- 657 Martin Kircher, Daniela M Witten, Preti Jain, Brian J O’Roak, Gregory M Cooper, and Jay Shendure. A
658 general framework for estimating the relative pathogenicity of human genetic variants. *Nature genetics*,
659 46(3):310–315, 2014.
- 660 Stanislav Knoch, Hana Hartmannová, Blanka Stibůrková, Jakub Krijt, Marie Zikánová, and Ivan
661 Šebesta. Human adenylosuccinate lyase (adsl), cloning and characterization of full-length cDNA and
662 its isoform, gene structure and molecular basis for adsl deficiency in six patients. *Human molecular*
663 *genetics*, 9(10):1501–1513, 2000.
- 664 Julia Knabl, Robert Witschi, Katharina Hösl, Heiko Reinold, Ulrike B Zeilhofer, Seifollah Ahmadi,
665 Johannes Brockhaus, Marina Sergejeva, Andreas Hess, Kay Brune, et al. Reversal of pathological pain
666 through specific spinal gabaa receptor subtypes. *Nature*, 451(7176):330–334, 2008.
- 667 Robert Kofler and Christian Schlotterer. Gowinda: unbiased analysis of gene set enrichment for genome-
668 wide association studies. *Bioinformatics*, 28(15):2084–2085, 2012.
- 669 Iosif Lazaridis, Nick Patterson, Alissa Mittnik, Gabriel Renaud, Swapan Mallick, Karola Kiryanow, Pe-
670 ter H Sudmant, Joshua G Schraiber, Sergi Castellano, Mark Lipson, et al. Ancient human genomes
671 suggest three ancestral populations for present-day europeans. *Nature*, 513(7518):409–413, 2014.

- 672 RC Lewontin and Jesse Krakauer. Distribution of gene frequency as a test of the theory of the selective
673 neutrality of polymorphisms. *Genetics*, 74(1):175–195, 1973.
- 674 Heng Li and Richard Durbin. Inference of human population history from individual whole-genome
675 sequences. *Nature*, 475(7357):493–496, 2011.
- 676 Mulin Jun Li, Panwen Wang, Xiaorong Liu, Ee Lyn Lim, Zhangyong Wang, Meredith Yeager, Maria P
677 Wong, Pak Chung Sham, Stephen J Chanock, and Junwen Wang. Gwasdb: a database for human
678 genetic variants identified by genome-wide association studies. *Nucleic acids research*, page gkr1182,
679 2011.
- 680 Bruce G Lindsay. Composite likelihood methods. *Contemporary Mathematics*, 80(1):221–39, 1988.
- 681 Mark Lipson, Po-Ru Loh, Alex Levin, David Reich, Nick Patterson, and Bonnie Berger. Efficient moment-
682 based inference of admixture parameters and sources of gene flow. *Molecular biology and evolution*, 30
683 (8):1788–1802, 2013.
- 684 PD Maaswinkel-Mooij, LAEM Laan, W Onkenhout, OF Brouwer, J Jaeken, and BJHM Poorthuis.
685 Adenylosuccinase deficiency presenting with epilepsy in early infancy. *Journal of inherited metabolic*
686 *disease*, 20(4):606–607, 1997.
- 687 Sandrine Marie, Harry Cuppens, Michel Heuterspreute, Martine Jaspers, Eduardo Zambrano Tola,
688 Xiao Xiao Gu, Eric Legius, M Vincent, Jaak Jaeken, Jean-Jacques Cassiman, et al. Mutation anal-
689 ysis in adenylosuccinate lyase deficiency: Eight novel mutations in the re-evaluated full adsl coding
690 sequence. *Human mutation*, 13(3):197–202, 1999.
- 691 Iain Mathieson, Iosif Lazaridis, Nadin Rohland, Swapan Mallick, Bastien Llamas, Joseph Pickrell, Harald
692 Meller, Manuel A Rojo Guerra, Johannes Krause, David Anthony, et al. Eight thousand years of natural
693 selection in europe. *bioRxiv*, page 016477, 2015.
- 694 Gunter Meister, Markus Landthaler, Lasse Peters, Po Yu Chen, Henning Urlaub, Reinhard Lüthmann,
695 and Thomas Tuschl. Identification of novel argonaute-associated proteins. *Current biology*, 15(23):
696 2149–2155, 2005.
- 697 MA Mencarelli, A Spanhol-Rosseto, R Artuso, D Rondinella, R De Filippis, N Bahi-Buisson, J Nectoux,

- 698 R Rubinsztajn, T Bienvenu, A Moncla, et al. Novel foxg1 mutations associated with the congenital
699 variant of rett syndrome. *Journal of medical genetics*, 47(1):49–53, 2010.
- 700 Thomas Mercher, Maryvonne Busson-Le Coniat, Richard Monni, Martine Mauchauffé, Florence Nguyen
701 Khac, Lætitia Gressin, Francine Mugneret, Thierry Leblanc, Nicole Dastugue, Roland Berger, et al.
702 Involvement of a human gene related to the drosophila spen gene in the recurrent t (1; 22) translocation
703 of acute megakaryocytic leukemia. *Proceedings of the National Academy of Sciences*, 98(10):5776–5779,
704 2001.
- 705 Philipp W Messer. Slim: simulating evolution with selection and linkage. *Genetics*, 194(4):1037–1039,
706 2013.
- 707 Matthias Meyer, Martin Kircher, Marie-Theres Gansauge, Heng Li, Fernando Racimo, Swapan Mallick,
708 Joshua G Schraiber, Flora Jay, Kay Prüfer, Cesare de Filippo, et al. A high-coverage genome sequence
709 from an archaic denisovan individual. *Science*, 338(6104):222–226, 2012.
- 710 George Nicholson, Albert V Smith, Frosti Jónsson, Ómar Gústafsson, Kári Stefánsson, and Peter Don-
711 nelly. Assessing population differentiation and isolation from single-nucleotide polymorphism data.
712 *Journal of the Royal Statistical Society: Series B (Statistical Methodology)*, 64(4):695–715, 2002.
- 713 Taras K Oleksyk, Kai Zhao, M Francisco, Dennis A Gilbert, Stephen J O’Brien, and Michael W Smith.
714 Identifying selected regions from heterozygosity and divergence using a light-coverage genomic dataset
715 from two human populations. *PLoS One*, 3(3):e1712, 2008.
- 716 Luigi Pace, Alessandra Salvan, and Nicola Sartori. Adjusting composite likelihood ratio statistics. *Sta-*
717 *tistica Sinica*, 21(1):129, 2011.
- 718 Lavinia Paternoster, David M Evans, Ellen Aagaard Nohr, Claus Holst, Valerie Gaborieau, Paul Brennan,
719 Anette Prior Gjesing, Niels Grarup, Daniel R Witte, Torben Jørgensen, et al. Genome-wide population-
720 based association study of extremely overweight young adults—the goya study. *PLoS One*, 6(9):e24303,
721 2011.
- 722 Nick Patterson, Priya Moorjani, Yontao Luo, Swapan Mallick, Nadin Rohland, Yiping Zhan, Teri Gen-
723 schoreck, Teresa Webster, and David Reich. Ancient admixture in human history. *Genetics*, 192(3):
724 1065–1093, 2012.

- 725 Len A Pennacchio, Nadav Ahituv, Alan M Moses, Shyam Prabhakar, Marcelo A Nobrega, Malak Shoukry,
726 Simon Minovitsky, Inna Dubchak, Amy Holt, Keith D Lewis, et al. In vivo enhancer analysis of human
727 conserved non-coding sequences. *Nature*, 444(7118):499–502, 2006.
- 728 Roy H Perlis, Jie Huang, Shaun Purcell, Maurizio Fava, A John Rush, Patrick F Sullivan, Steven P
729 Hamilton, Francis J McMahon, Thomas Schulze, James B Potash, et al. Genome-wide association
730 study of suicide attempts in mood disorder patients. *Genome*, 167(12), 2010.
- 731 Joseph K Pickrell and Jonathan K Pritchard. Inference of population splits and mixtures from genome-
732 wide allele frequency data. *PLoS genetics*, 8(11):e1002967, 2012.
- 733 Joseph K Pickrell, Graham Coop, John Novembre, Sridhar Kudaravalli, Jun Z Li, Devin Absher, Balaji S
734 Srinivasan, Gregory S Barsh, Richard M Myers, Marcus W Feldman, et al. Signals of recent positive
735 selection in a worldwide sample of human populations. *Genome research*, 19(5):826–837, 2009.
- 736 Dimitrina D Pravtcheva and Thomas L Wise. Disruption of *apc10/doc1* in three alleles of oligosyn-
737 dactylism. *Genomics*, 72(1):78–87, 2001.
- 738 Kay Prüfer, Fernando Racimo, Nick Patterson, Flora Jay, Sriram Sankararaman, Susanna Sawyer, Anja
739 Heinze, Gabriel Renaud, Peter H Sudmant, Cesare de Filippo, et al. The complete genome sequence
740 of a neanderthal from the altai mountains. *Nature*, 505(7481):43–49, 2014.
- 741 Valérie Race, Sandrine Marie, Marie-Françoise Vincent, and Georges Van den Berghe. Clinical, biochem-
742 ical and molecular genetic correlations in adenylosuccinate lyase deficiency. *Human molecular genetics*,
743 9(14):2159–2165, 2000.
- 744 Fernando Racimo, Martin Kuhlwilm, and Montgomery Slatkin. A test for ancient selective sweeps and an
745 application to candidate sites in modern humans. *Molecular biology and evolution*, 31(12):3344–3358,
746 2014.
- 747 Peter N Robinson, Sebastian Köhler, Sebastian Bauer, Dominik Seelow, Denise Horn, and Stefan Mund-
748 los. The human phenotype ontology: a tool for annotating and analyzing human hereditary disease.
749 *The American Journal of Human Genetics*, 83(5):610–615, 2008.
- 750 Kate R Rosenbloom, Timothy R Dreszer, Jeffrey C Long, Venkat S Malladi, Cricket A Sloan, Brian J

- 751 Raney, Melissa S Cline, Donna Karolchik, Galt P Barber, Hiram Clawson, et al. Encode whole-genome
752 data in the ucsc genome browser: update 2012. *Nucleic acids research*, page gkr1012, 2011.
- 753 Pardis C Sabeti, David E Reich, John M Higgins, Haninah ZP Levine, Daniel J Richter, Stephen F
754 Schaffner, Stacey B Gabriel, Jill V Platko, Nick J Patterson, Gavin J McDonald, et al. Detecting
755 recent positive selection in the human genome from haplotype structure. *Nature*, 419(6909):832–837,
756 2002.
- 757 Pardis C Sabeti, Patrick Varilly, Ben Fry, Jason Lohmueller, Elizabeth Hostetter, Chris Cotsapas, Xiaohui
758 Xie, Elizabeth H Byrne, Steven A McCarroll, Rachelle Gaudet, et al. Genome-wide detection and
759 characterization of positive selection in human populations. *Nature*, 449(7164):913–918, 2007.
- 760 Tetsushi Sadakata and Teiichi Furuichi. Ca²⁺-dependent activator protein for secretion 2 and autistic-
761 like phenotypes. *Neuroscience research*, 67(3):197–202, 2010.
- 762 Rossana Sapiro, Igor Kostetskii, Patricia Olds-Clarke, George L Gerton, Glenn L Radice, and Jerome F
763 Strauss III. Male infertility, impaired sperm motility, and hydrocephalus in mice deficient in sperm-
764 associated antigen 6. *Molecular and cellular biology*, 22(17):6298–6305, 2002.
- 765 Carina M Schlebusch, Pontus Skoglund, Per Sjödin, Lucie M Gattepaille, Dena Hernandez, Flora Jay,
766 Sen Li, Michael De Jongh, Andrew Singleton, Michael GB Blum, et al. Genomic variation in seven
767 khoe-san groups reveals adaptation and complex african history. *Science*, 338(6105):374–379, 2012.
- 768 Andaine Seguin-Orlando, Thorfinn S Korneliussen, Martin Sikora, Anna-Sapfo Malaspinas, Andrea Man-
769 ica, Ida Moltke, Anders Albrechtsen, Amy Ko, Ashot Margaryan, Vyacheslav Moiseyev, et al. Genomic
770 structure in europeans dating back at least 36,200 years. *Science*, 346(6213):1113–1118, 2014.
- 771 Hifzur Rahman Siddique and Mohammad Saleem. Role of bmi1, a stem cell factor, in cancer recurrence
772 and chemoresistance: preclinical and clinical evidences. *Stem Cells*, 30(3):372–378, 2012.
- 773 Adam Siepel, Gill Bejerano, Jakob S Pedersen, Angie S Hinrichs, Minmei Hou, Kate Rosenbloom, Hiram
774 Clawson, John Spieth, LaDeana W Hillier, Stephen Richards, et al. Evolutionarily conserved elements
775 in vertebrate, insect, worm, and yeast genomes. *Genome research*, 15(8):1034–1050, 2005.
- 776 John Maynard Smith and John Haigh. The hitch-hiking effect of a favourable gene. *Genetical research*,
777 23(01):23–35, 1974.

- 778 Karsten Suhre, Henri Wallaschofski, Johannes Raffler, Nele Friedrich, Robin Haring, Kathrin Michael,
779 Christina Wasner, Alexander Krebs, Florian Kronenberg, David Chang, et al. A genome-wide associ-
780 ation study of metabolic traits in human urine. *Nature genetics*, 43(6):565–569, 2011.
- 781 John A Todd, Neil M Walker, Jason D Cooper, Deborah J Smyth, Kate Downes, Vincent Plagnol,
782 Rebecca Bailey, Sergey Nejentsev, Sarah F Field, Felicity Payne, et al. Robust associations of four new
783 chromosome regions from genome-wide analyses of type 1 diabetes. *Nature genetics*, 39(7):857–864,
784 2007.
- 785 Ariel R Topletz, Jayne E Thatcher, Alex Zelter, Justin D Lutz, Suzanne Tay, Wendel L Nelson, and Nina
786 Isoherranen. Comparison of the function and expression of cyp26a1 and cyp26b1, the two retinoic acid
787 hydroxylases. *Biochemical pharmacology*, 83(1):149–163, 2012.
- 788 Meg Trahey, Gail Wong, Robert Halenbeck, Bonnee Rubinfeld, George A Martin, Martha Ladner,
789 Christopher M Long, Walter J Crosier, Ken Watt, Kirston Koths, et al. Molecular cloning of two
790 types of gap complementary dna from human placenta. *Science*, 242(4886):1697–1700, 1988.
- 791 ML Van Keuren, IM Hart, F-T Kao, RL Neve, GAP Bruns, DM Kurnit, and D Patterson. A somatic
792 cell hybrid with a single human chromosome 22 corrects the defect in the cho mutant (ade-i) lacking
793 adenylosuccinase activity. *Cytogenetic and Genome Research*, 44(2-3):142–147, 1987.
- 794 Cristiano Varin, Nancy Reid, and David Firth. An overview of composite likelihood methods. *Statistica*
795 *Sinica*, 21(1):5–42, 2011.
- 796 Benjamin F Voight, Sridhar Kudaravalli, Xiaoquan Wen, and Jonathan K Pritchard. A map of recent
797 positive selection in the human genome. *PLoS biology*, 4(3):e72, 2006.
- 798 Bruce S Weir, Lon R Cardon, Amy D Anderson, Dahlia M Nielsen, and William G Hill. Measures of
799 human population structure show heterogeneity among genomic regions. *Genome research*, 15(11):
800 1468–1476, 2005.
- 801 Danielle Welter, Jacqueline MacArthur, Joannella Morales, Tony Burdett, Peggy Hall, Heather Junkins,
802 Alan Klemm, Paul Flicek, Teri Manolio, Lucia Hindorff, et al. The nhgri gwas catalog, a curated
803 resource of snp-trait associations. *Nucleic acids research*, 42(D1):D1001–D1006, 2014.

804 Jay A White, Heather Ramshaw, Mohammed Taimi, Wayne Stangle, Anqi Zhang, Stephanie Evering-
805 ham, Shelly Creighton, Shui-Pang Tam, Glenville Jones, and Martin Petkovich. Identification of the
806 human cytochrome p450, p450rai-2, which is predominantly expressed in the adult cerebellum and is
807 responsible for all-trans-retinoic acid metabolism. *Proceedings of the National Academy of Sciences*, 97
808 (12):6403–6408, 2000.

809 Paul J Whiting, Timothy P Bonnert, Ruth M McKernan, Sophie Farrar, Beatrice Le Bourdelles, Robert P
810 Heavens, David W Smith, Louise Hewson, Michael R Rigby, Dalip JS Sirinathsinghji, et al. Molecular
811 and functional diversity of the expanding gaba-a receptor gene family. *Annals of the New York Academy
812 of Sciences*, 868(1):645–653, 1999.

813 Yun-Yan Xiang, Shuhe Wang, Mingyao Liu, Jeremy A Hirota, Jingxin Li, William Ju, Yijun Fan, Mar-
814 garet M Kelly, Bin Ye, Beverley Orser, et al. A gabaergic system in airway epithelium is essential for
815 mucus overproduction in asthma. *Nature medicine*, 13(7):862–867, 2007.

816 Xin Yi, Yu Liang, Emilia Huerta-Sanchez, Xin Jin, Zha Xi Ping Cuo, John E Pool, Xun Xu, Hui Jiang,
817 Nicolas Vinckenbosch, Thorfinn Sand Korneliussen, et al. Sequencing of 50 human exomes reveals
818 adaptation to high altitude. *Science*, 329(5987):75–78, 2010.

819 Alexandra Zhernakova, Clara C Elbers, Bart Ferwerda, Jihane Romanos, Gosia Trynka, Patrick C Dubois,
820 Carolien GF De Kovel, Lude Franke, Marije Oosting, Donatella Barisani, et al. Evolutionary and
821 functional analysis of celiac risk loci reveals sh2b3 as a protective factor against bacterial infection.
822 *The American Journal of Human Genetics*, 86(6):970–977, 2010.

823 Tables

Table 1. Description of models tested. All times are in generations. Selection in the "ancestral population" refers to a selective sweep where the beneficial mutation and fixation occurred before the split time of the two most closely related populations. Selection in "daughter population *a*" refers to a selective sweep that occurred in one of the two most closely related populations (*a*), after their split from each other. t_{AB} : split time (in generations ago) of populations *a* and *b*. t_{ABC} : split time of population *c* and the ancestral population of *a* and *b*. t_M : time at which the selected mutation is introduced. *s*: selection coefficient. N_e : effective population size.

Model	Population where selection occurred	t_{AB}	t_{ABC}	t_M	<i>s</i>	N_e
A	Ancestral population	500	2,000	1,800	0.1	10,000
B	Ancestral population	1,000	4,000	2,500	0.1	10,000
C	Ancestral population	2,000	4,000	3,500	0.1	10,000
D	Ancestral population	3,000	8,000	5,000	0.1	10,000
E	Ancestral population	2,000	16,000	8,000	0.1	10,000
F	Ancestral population	4,000	16,000	8,000	0.1	10,000
I	Daughter population <i>a</i>	2,000	4,000	1,000	0.1	10,000
J	Daughter population <i>a</i>	3,000	8,000	2,000	0.1	10,000

Table 2. Genes from top 10 candidate regions for each of the branches on which 3P-CLR was run for the Eurasian population tree. All positions were rounded to the nearest 100 bp. Windows were merged together if the central SNPs that define them were contiguous.

Window size	Position (hg19)	Genes
European	chr9:125424000-126089000	ZBTB26,RABGAP1,GPR21,STRBP,OR1L1,OR1L3,OR1L4,OR1L6,OR5C1,PDCL,OR1K1,RC3H2,ZBTB6
	chr22:35528100-35754100	HMGXB4,TOM1
	chr8:52361800-52932100	PXDNL,PCMTD1
	chr2:74450100-74972700	INO80B,WBP1,MOGS,MRPL53,CCDC142,TTC31,LBX2,PCGF1,TLX2,DQX1,AUP1,HTRA2,LOXL3,DOK1,M1AP,SEMA4F,SLC4A5,DCTN1,WDR54,RTKN
	chr1:35382000-36592200	DLGAP3,ZMYM6NB,ZMYM6,ZMYM1,SFPQ,ZMYM4,KIAA0319L,NCDN,TFAP2E,PSMB2,C1orf216,CLSPN,AGO4,AGO1,AGO3,TEKT2,ADPRHL2,COL8A2
	chr15:29248000-29338300	APBA2
chr12:111747000-113030000	BRAP,ACAD10,ALDH2,MAPKAPK5,TMEM116,ERP29,NAA25,TRAFD1,RPL6,PTPN11,RPH3A,CUX2,FAM109A,SH2B3,ATXN2	
chr9:90909300-91210000	SPIN1,NXNL2	
chr19:33504200-33705700	RHPN2,GPATCH1,WDR88,LRP3,SLC7A10	
chr9:30085400-31031600	-	
East Asian	chr15:63693900-64188300	USP3,FBXL22,HERC1
	chr10:94830500-95093900	CYP26A1,MYOF
	chr2:72353500-73170800	CYP26B1,EXOC6B,SPR,EMX1,SFXN5
	chr2:72353500-73170800	PCDH15
	chr1:234209000-234396000	SLC35F3
	chr5:117344000-117714000	-
	chr17:60907300-61547900	TANC2,CYB561
	chr2:44101400-44315200	ABCG8,LRPPRC
chr11:6028090-6191240	OR56A1,OR56B4,OR52B2	
chr2:108905000-109629000	LIMS1,RANBP2,CCDC138,EDAR,SULT1C2,SULT1C4,GCC2	
Eurasian	chr2:72353500-73170800	CYP26B1,EXOC6B,SPR,EMX1,SFXN5
	chr20:53876700-54056200	-
	chr10:22309300-22799200	EBLN1,COMMD3,COMMD3-BMI1,BMI1,SPAG6
	chr3:25726300-26012000	NGLY1,OXSM
	chr18:67523300-67910500	CD226,RTTN
	chr10:65794400-66339100	-
	chr11:39587400-39934300	-
	chr7:138806000-139141000	TTC26,UBN2,C7orf55,C7orf55-LUC7L2,LUC7L2,KLRG2
chr9:90909300-91202200	SPIN1,NXNL2	
chr4:41454200-42195300	LIMCH1,PHOX2B,TMEM33,DCAF4L1,SLC30A9,BEND4	

Table 3. Genes from top 20 candidate regions for the modern human ancestral branch. All positions were rounded to the nearest 100 bp. Windows were merged together if the central SNPs that define them were contiguous.

Window size	Position (hg19)	Genes
0.25 cM (100 SNPs)	chr2:95561200-96793700	ZNF514,ZNF2,PROM2,KCNIP3,FAHD2A,TRIM43,GPAT2,ADRA2B,ASTL,MAL,MRPS5
	chr5:86463700-87101400	RASA1,CCNH
	chr17:60910700-61557700	TANC2,CYB561,ACE
	chr14:71649200-72283600	SIPA1L1
	chr18:15012100-19548600	ROCK1,GREB1L,ESCO1,SNRPD1,ABHD3,MIB1
	chr3:110513000-110932000	PVRL3
	chr2:37917900-38024200	CDC42EP3
	chr3:36836900-37517500	TRANK1,EPM2AIP1,MLH1,LRRFIP2,GOLGA4,C3orf35,ITGA9
	chr7:106642000-107310000	PRKAR2B,HBP1,COG5,GPR22,DUS4L,BCAP29,SLC26A4
	chr12:96823000-97411500	NEDD1
	chr2:200639000-201340000	C2orf69,TYW5,C2orf47,SPATS2L
	chr1:66772600-66952600	PDE4B
	chr10:37165100-38978800	ANKRD30A,MTRNR2L7,ZNF248,ZNF25,ZNF33A,ZNF37A
	chr2:155639000-156767000	KCNJ3
	chr17:56379200-57404800	BZRAP1,SUPT4H1,RNF43,HSF5,MTMR4,SEPT4,C17orf47,TEX14,RAD51C,PPM1E,TRIM37,SKA2,PRR11,SMG8,GDPD1
	chr5:18493900-18793500	-
	chr2:61050900-61891900	REL,PUS10,PEX13,KIAA1841,AHSA2,USP34,XPO1
chr22:40360300-41213400	GRAP2,FAM83F,TNRC6B,ADSL,SGSM3,MKL1,MCHR1,SLC25A17	
chr2:98996400-99383400	CNGA3,INPP4A,COA5,UNC50,MGAT4A	
chr4:13137000-13533100	RAB28	
1 cM (200 SNPs)	chr14:71349200-72490300	PCNX,SIPA1L1,RGS6
	chr4:145023000-146522000	GYPB,GYPB,HHIP,ANAPC10,ABCE1,OTUD4,SMAD1
	chr2:155391000-156992000	KCNJ3
	chr5:92415600-94128600	NR2F1,FAM172A,POU5F2,KIAA0825,ANKRD32,MCTP1
	chr7:106401000-107461000	PIK3CG,PRKAR2B,HBP1,COG5,GPR22,DUS4L,BCAP29,SLC26A4,CBL1,SLC26A3
	chr7:151651000-152286000	GALNTL5,GALNT11,KMT2C
	chr2:144393000-145305000	ARHGAP15,GTDC1,ZEB2
	chr19:16387600-16994000	KLF2,EPS15L1,CALR3,C19orf44,CHERP,SLC35E1,MED26,SMIM7,TMEM38A,NWD1,SIN3B
	chr2:37730400-38054600	CDC42EP3
	chr2:62639800-64698300	TMEM17,EHBP1,OTX1,WDPCCP,MDH1,UGP2,VPS54,PELI1,LGALS
	chr10:36651400-44014800	ANKRD30A,MTRNR2L7,ZNF248,ZNF25,ZNF33A,ZNF37A,ZNF33B,BMS1,RET,CSGALNACT2,RASGEF1A,FXJD4,HNRNPF
	chr1:26703800-27886000	LIN28A,DHDDS,HMG2,RPS6KA1,ARID1A,PIGV,ZDHHC18,SFN,GPN2,GPATCH3,NUDC,NR0B2,C1orf172,TRNP1,FAM46B,SLC9A1,WDT1, TMEM222,SYTL1,MAP3K6,FCN3,CD164L2,GPR3,WASF2,AHDC1
	chr12:102308000-103125000	DRAM1,CCDC53,NUP37,PARBP,PMCH,IGF1
	chr2:132628000-133270000	GPR39
	chr15:42284300-45101400	PLA2G4E,PLA2G4D,PLA2G4F,VPS39,TMEM87A,GANC,CAPN3,ZNF106,SNAP23,LRRRC57,HAUS2,STARD9,CDAN1,TTBK2,UBR1,EPB42,TMEM62,CCNDBP1,TGM5,TGM7,LCMT2,ADAL,ZSCAN29,TUBGCP4,TP53BP1,MAP1A, PPIP5K1,CKMT1B,STRC,CATSPER2,CKMT1A,PDIA3,ELL3,SERF2,SERINC4
	chr2:73178500-74194400	HYPK,MFAP1,WDR76,FRMD5,CASC4,CTDSP2,EIF3J,SPG11,PATL2,B2M,TRIM69
	chr5:54193000-55422100	SFXN5,RAB11FIP5,NOTO,SMYD5,PRADC1,CCT7,FBXO41,EGR4,ALMS1,NAT8,TPRKB,DUSP11,C2orf78,STAMBP,ACTG2,DGUOK
chr3:50184000-53602300	ESM1,GZMK,GZMA,CDC20B,GPX8,MCIDAS,CCNO,DHX29,SKIV2L2,PPAP2A,SLC38A9,DDX4,IL31RA,IL6ST,ANKRD55	
chr13:96038900-97500100	SEMA3F,GNAT1,GNAI2,LSMEM2,IFRD2,HYAL3,NAT6,HYAL1,HYAL2,TUSC2,RASSF1,ZMYND10,NPRL2,CYB561D2,TMEM115,CACNA2D2,C3orf18,HEMK1,CISH,MAPKAPK3,DOCK3,MANF,RBM15B,RAD54L2,TEX264,GRM2,IQCF6,IQCF3,IQCF2,IQCF5,IQCF1,RRP9,PARP3,GPR62,PCBP4,ABHD14B,ABHD14A,ACY1,RPL29,DUSP7,POC1A,ALAS1,TLR9,TWF2,PPM1M,WDR82,GLYCTK,DNAH1,BAP1,PHF7,SEMA3G,TNNC1,NISCH,STAB1,NT5DC2,SMIM4,PBRM1,GNL3,GLT8D1,SPCS1,NEK4,ITIH1,ITIH3,ITIH4,MUSTN1,TMEM110-MUSTN1, TMEM110,SFMBT1,RFT1,PRKCD,TKT,CACNA1D	
chr18:14517500-19962400	CLDN10,DZIP1,DNAJC3,UGGT2,HS6ST3	
	POTEC,ANKRD30B,ROCK1,GREB1L,ESCO1,SNRPD1,ABHD3,MIB1,GATA6	

824 **Figures**

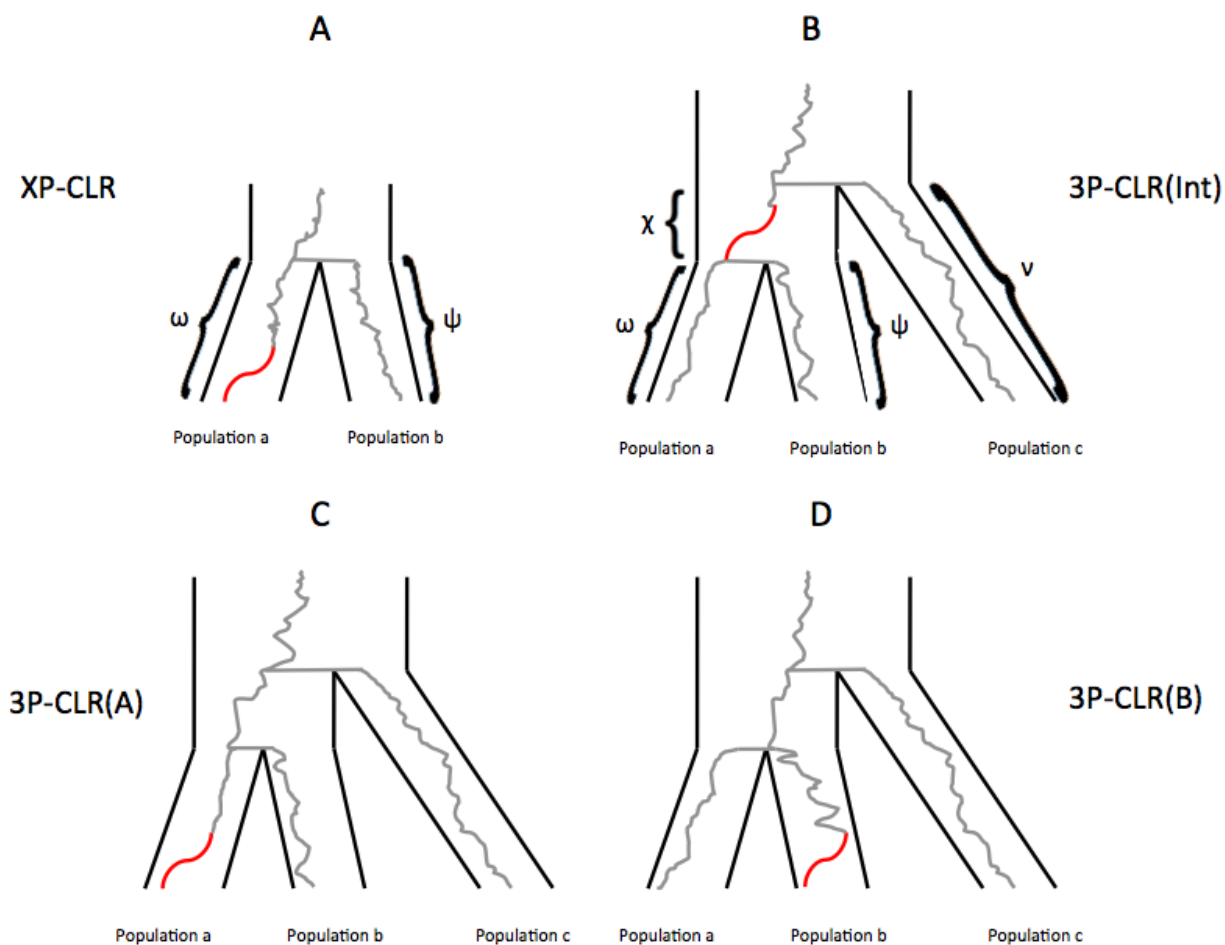


Figure 1. Schematic tree of selective sweeps detected by XP-CLR and 3P-CLR. While XP-CLR can only use two populations (an outgroup and a test) to detect selection (panel A), 3P-CLR can detect selection in the ancestral branch of two populations (3P-CLR(Int), panel B) or on the branches specific to each population (3P-CLR(A) and 3P-CLR(B), panels C and D, respectively). The greek letters denote the known drift times for each branch of the population tree.

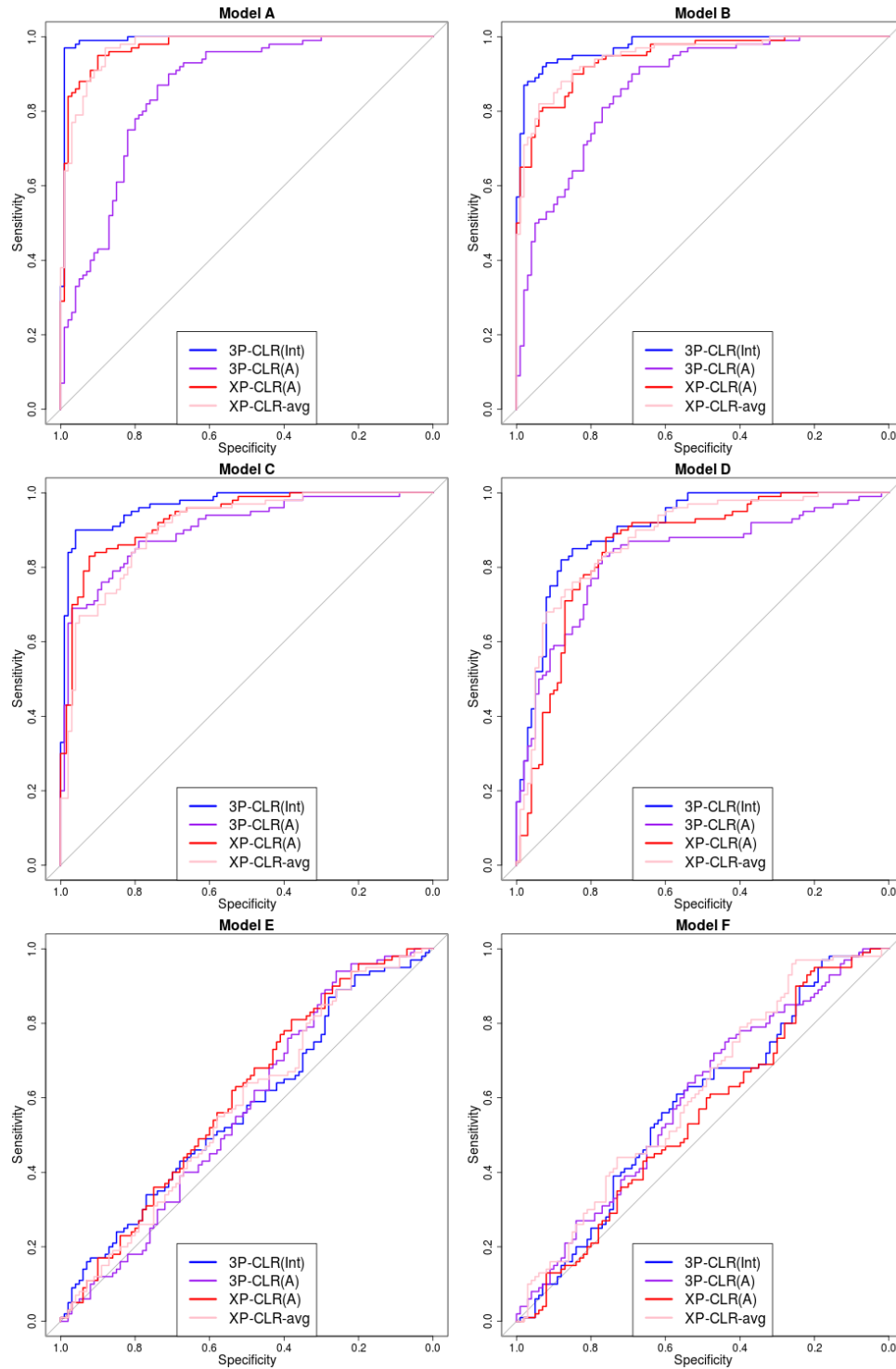


Figure 2. ROC curves for performance of 3P-CLR(Int), 3P-CLR(A) and two variants of XP-CLR in detecting selective sweeps that occurred before the split of two populations *a* and *b*, under different demographic models. In this case, the outgroup panel from population *c* contained 100 haploid genomes. The two sister population panels (from *a* and *b*) also have 100 haploid genomes each.

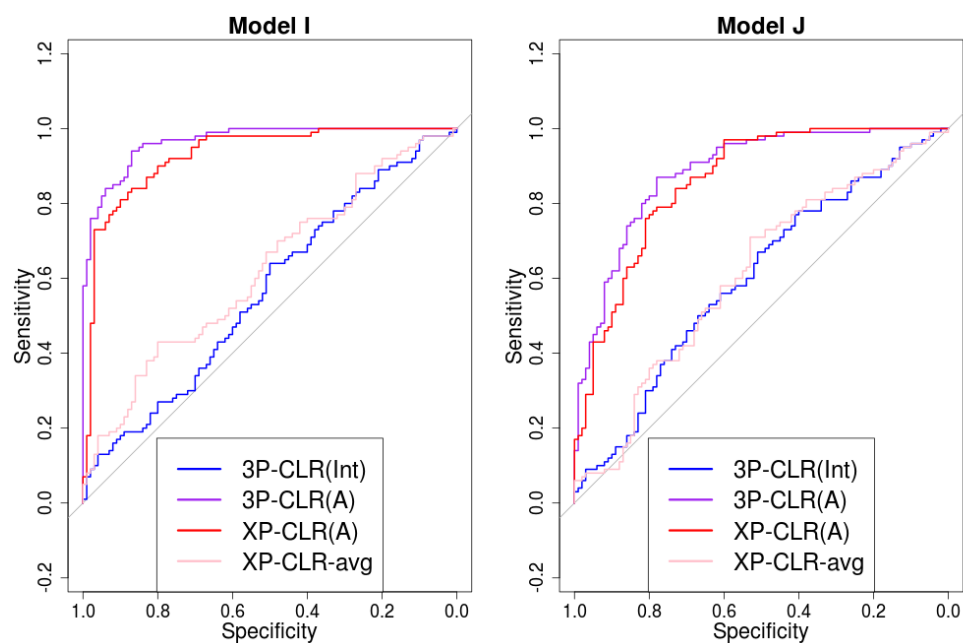


Figure 3. 3P-CLR(Int) is tailored to detect selective events that happened before the split t_{ab} , so it is largely insensitive to sweeps that occurred after the split. ROC curves show performance of 3P-CLR(Int) and two variants of XP-CLR for models where selection occurred in population a after its split from b .

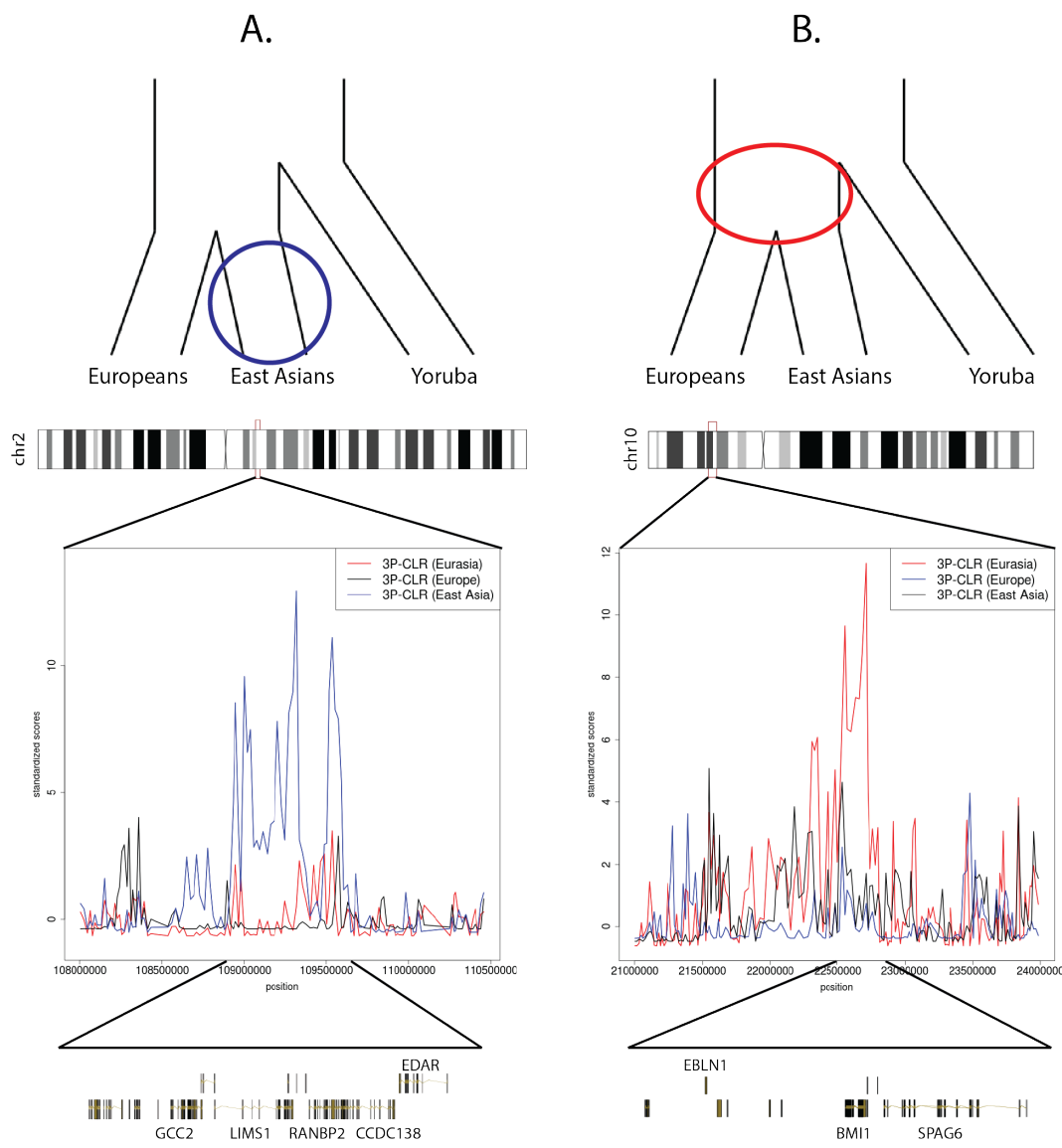


Figure 4. 3P-CLR scan of Europeans (black), East Asians (blue) and the ancestral Eurasian population (red) reveals regions under selection in different branches of the population tree. To make a fair comparison, all 3P-CLR scores were standardized by subtracting the chromosome-wide mean from each window and dividing the resulting score by the chromosome-wide standard deviation. A) The region containing *EDAR* is a candidate for selection in the East Asian population. B) The region containing genes *SPAG6* and *BMI1* is a candidate for selection in the ancestral population of Europeans and East Asians. The image was built using the GenomeGraphs package in Bioconductor.

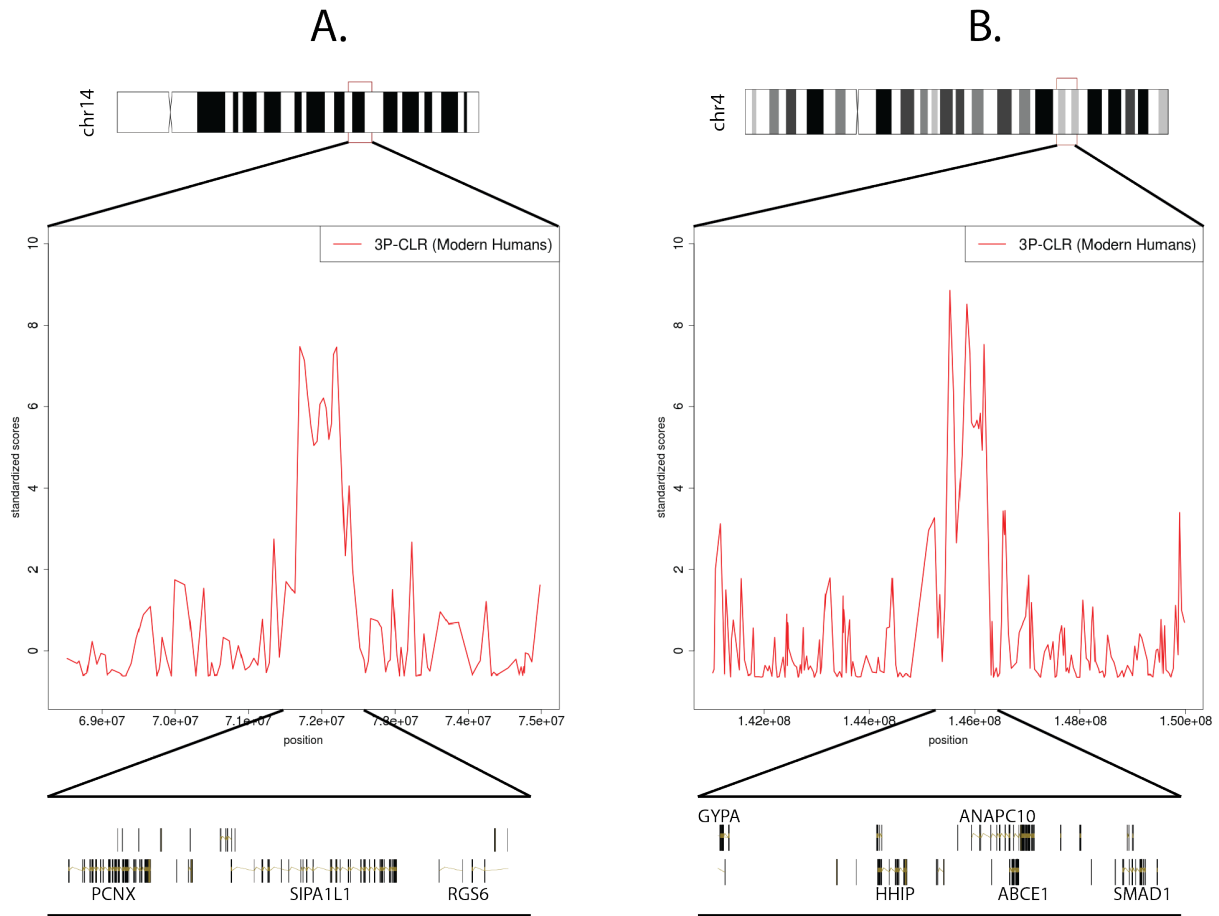


Figure 5. Two of the strongest candidates for selection in the modern human lineage, after the split from Neanderthal and Denisova. We show scores from the 1 cM scan, but the signals persist in the 0.25 cM scan. To make a fair comparison, all 3P-CLR scores were standardized by subtracting the chromosome-wide mean from each window and dividing the resulting score by the chromosome-wide standard deviation. A) The region containing *SIPA1L1*. B) The region containing *ANAPC10*. The image was built using the GenomeGraphs package in Bioconductor.

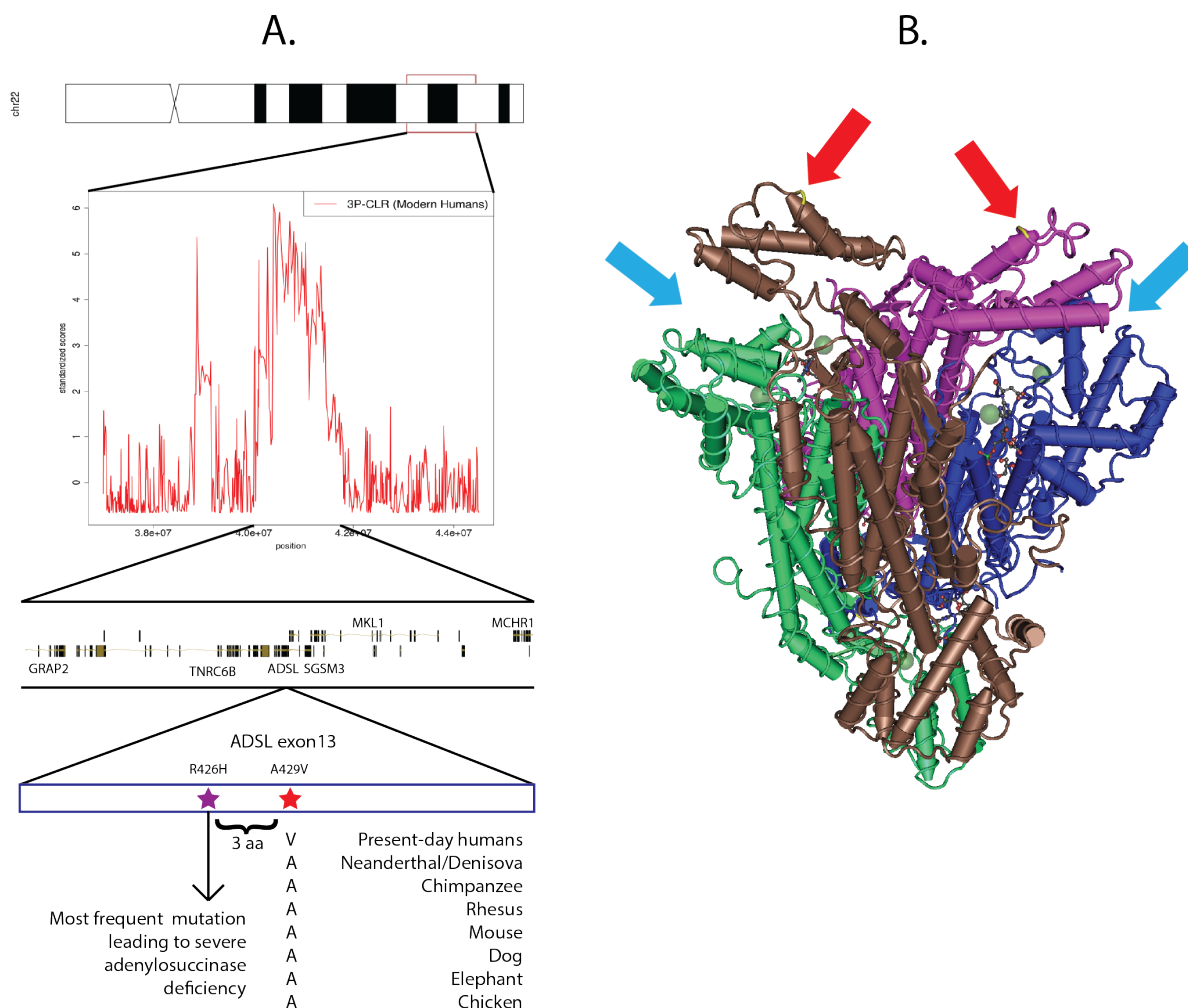


Figure 6. ADSL is a candidate for selection in the modern human lineage, after the split from Neanderthal and Denisova. A) One of the top-scoring regions when running 3P-CLR (0.25 cM windows) on the modern human lineage contains genes *TNRC6B*, *ADSL*, *MKL1*, *MCHR1*, *SGSM3* and *GRAP2*. The most disruptive nonsynonymous modern-human-specific change in the entire list of top regions is in an exon of *ADSL* and is fixed derived in all present-day humans but ancestral in archaic humans. It is highly conserved across tetrapods and lies only 3 residues away from the most common mutation leading to severe adenylosuccinase deficiency. B) The *ADSL* gene codes for a tetrameric protein. The mutation is in the C-terminal domain of each tetrameric unit (red arrows), which are near the active sites (light blue arrows). Scores in panel A were standardized using the chromosome-wide mean and standard deviation. Vertebrate alignments were obtained from the UCSC genome browser (Vertebrate Multiz Alignment and Conservation track) and the image was built using the GenomeGraphs package in Bioconductor and Cn3D.

825 **Supplementary Tables**

Table S1. Top hits for 3P-CLR run on the European terminal branch, using Yoruba as the outgroup. We show the windows in the top 99.9% quantile of scores. Windows were merged together if the central SNPs that define them were contiguous. Win max = Location of window with maximum score. Win start = left-most end of left-most window for each region. Win end = right-most end of right-most window for each region. All positions were rounded to the nearest 100 bp. Score max = maximum score within region.

chr	Win max	Win start	Win end	Score max	Genes within region
9	125585000	125424000	126089000	362.273	ZBTB26,RABGAP1,GPR21,STRBP,OR1L1,OR1L3,OR1L4,OR1L6,OR5C1,PDCL,OR1K1,RC3H2,ZBTB6
22	35631900	35528100	35754100	309.488	HMGXB4,TOM1
8	52698800	52361800	52932100	289.921	PXDNL,PCMTD1
2	74967500	74450100	74972700	289.019	INO80B,WBP1,MOGS,MRPL53,CCDC142,TTC31,LBX2,PCGF1,TLX2,DQX1,AUP1,HTRA2,LOXL3,DOK1,M1AP,SEMA4F,SLC4A5,DCTN1,WDR54,RTKN
1	35634700	35382000	36592200	263.83	DL-GAP3,ZMYM6NB,ZMYM6,ZMYM1,SFPQ,ZMYM4,KIAA0319L,NCDN,TFAP2E,PSMB2,C1orf216,CLSPN,AGO4,AGO1,AGO3,TEKT2,ADPRHL2,COL8A2
15	29279800	29248000	29338300	251.944	APBA2
12	112950000	111747000	113030000	242.067	BRAP,ACAD10,ALDH2,MAPKAP5,TMEM116,ERP29,NAA25,TRAFD1,RPL6,PTPN11,RPH3A,CUX2,FAM109A,SH2B3,ATXN2
9	90947700	90909300	91210000	219.285	SPIN1,NXNL2
19	33644300	33504200	33705700	213.189	RHPN2,GPATCH1,WDR88,LRP3,SLC7A10
9	30546800	30085400	31031600	207.378	-
4	33865300	33604700	34355600	204.96	-
1	198035000	197943000	198308000	197.96	NEK7
1	204868000	204681000	204873000	194.594	NFASC
10	74613800	73802300	75407100	191.864	SPOCK2,ASCC1,ANAPC16,DDIT4,DNAJB12,MICU1,MCU,OIT3,PLA2G12B,P4HA1,NUDT13,ECD,FAM149B1,DNAJC9,MRPS16,TTC18,ANXA7,MSS51,PPP3CB,USP54,MYOZ1,SYNPO2L
7	138809000	138798000	139136000	180.75	TTC26,UBN2,C7orf55,C7orf55-LUC7L2,LUC7L2
6	95678500	95351800	95831000	180.676	-
2	104752000	104592000	104951000	177.053	-
16	7602450	7528820	7612510	171.615	RBFOX1
10	30568100	30361300	30629500	170.714	KIAA1462,MTPAP
3	137183000	136873000	137250000	166.559	-
1	116731000	116709000	116919000	165.137	ATP1A1
9	135136000	135132000	135298000	165.004	SETX,TTF1,C9orf171
13	89882200	89262100	90103800	158.112	-
2	17094600	16977500	17173100	156.531	-
4	82050400	81981400	82125100	154.54	PRKG2
2	69245100	69147300	69342700	149.948	GKN2,GKN1,ANTXR1
17	46949100	46821000	47137900	147.537	ATP5G1,UBE2Z,SNF8,GIP,IGF2BP1,TTL6,CALCOCO2
10	83993700	83977100	84328100	147.072	NRG3
14	63893800	63780300	64044700	142.831	PPP2R5E
1	244070000	243645000	244107000	142.335	SDCCAG8,AKT3
14	66636800	66417700	67889500	140.97	GPHN,FAM71D,MPP5,ATP6V1D,EIF2S1,PLEK2
11	38611200	38349600	39004500	138.731	-
3	123368000	123196000	123418000	136.651	PTPLB,MYLK
6	112298000	111392000	112346000	135.167	SLC16A10,KIAA1919,REV3L,TRAF3IP2,FYN
5	109496000	109419000	109608000	132.766	-
5	142160000	142070000	142522000	132.436	FGF1,ARHGAP26
12	39050200	33590600	39618900	130.832	SYT10,ALG10,ALG10B,CPNE8
9	108423000	108410000	108674000	129.893	TAL2,TMEM38B
3	159453000	159263000	159486000	126.462	IQCJ-SCHIP1
2	70182800	70020100	70563900	126.092	FAM136A,ANXA4,GMCL1,SNRNP27,MXD1,ASPRV1,PCBP1,C2orf42,TIA1,PCYOX1,SNRPG
3	177605000	177536000	177745000	123.927	-
8	18534300	18515900	18656800	123.593	PSD3
5	123555000	123371000	123603000	122.973	-
17	19287500	18887800	19443300	122.35	SLC5A10,FAM83G,GRAP,GRAPL,EPN2,B9D1,MAPK7,MFAP4,RNF112,SLC47A1
11	42236100	41807600	42311500	122.131	-
13	41623700	41119400	41801600	121.214	FOXO1,MRPS31,SLC25A15,ELF1,WBP4,KBTBD6,KBTBD7,MTRF1
5	10311500	10284000	10481500	118.766	CMBL,MARCH6,ROPN1L
14	65288500	65222500	65472700	118.576	SPTB,CHURC1,FNTB,GPX2,RAB15
1	47651700	47396900	47938300	118.241	CYP4A11,CYP4X1,CYP4Z1,CYP4A22,PDZK1IP1,TAL1,STIL,CMPK1,FOXE3,FOXD2
2	138527000	138428000	138694000	116.881	-
17	42294300	42056700	42351800	115.466	PYY,NAGS,TMEM101,LSM12,G6PC3,HDAC5,C17orf53,ASB16,TMUB2,ATXN7L3,UBTF,SLC4A1
9	12480000	12439900	12776500	115.209	TYRP1,LURAP1L
7	78743000	78688400	78897900	114.946	MAGI2
2	216626000	216556000	216751000	114.901	-
1	65511700	65377500	65611400	114.699	JAK1
5	115391000	115369000	115784000	113.862	ARL14EPL,COMMD10,SEMA6A
15	45402300	45096000	45490700	113.69	C15orf43,SORD,DUOX2,DUOXA2,DUOXA1,DUOX1,SHF
3	25840300	25705200	25934000	113.326	TOP2B,NGLY1,OXSM
2	73086900	72373800	73148200	110.523	CYP26B1,EXOC6B,SPR,EMX1

Table S2. Top hits for 3P-CLR run on the East Asian terminal branch, using Yoruba as the outgroup. We show the windows in the top 99.9% quantile of scores. Windows were merged together if the central SNPs that define them were contiguous. Win max = Location of window with maximum score. Win start = left-most end of left-most window for each region. Win end = right-most end of right-most window for each region. All positions were rounded to the nearest 100 bp. Score max = maximum score within region.

chr	Win max	Win start	Win end	Score max	Genes within region
15	64151100	63693900	64188300	266.459	USP3,FBXL22,HERC1
10	94962900	94830500	95093900	241.875	CYP26A1,MYOF
2	73086900	72353500	73170800	218.482	CYP26B1,EXOC6B,SPR,EMX1,SFXN5
10	55988000	55869200	56263600	215.051	PCDH15
1	234359000	234209000	234396000	189.946	SLC35F3
5	117350000	117344000	117714000	189.051	-
17	60964400	60907300	61547900	186.63	TANC2,CYB561
2	44268900	44101400	44315200	185.629	ABCG8,LRPPRC
11	6126830	6028090	6191240	184	OR56A1,OR56B4,OR52B2
2	109318000	108905000	109629000	183.859	LIMS1,RANBP2,CCDC138,EDAR,SULT1C2,SULT1C4,GCC2
4	41882900	41456100	42196500	183.481	LIMCH1,PHOX2B,TMEM33,DCAF4L1,SLC30A9,BEND4
18	5304160	5201440	5314680	183.476	ZBTB14
9	105040000	104779000	105042000	181.781	-
7	105097000	104526000	105128000	181.358	KMT2E,SRPK2,PUS7
3	107609000	107149000	107725000	178.27	BBX
7	101729000	101511000	101942000	169.558	CUX1
6	159274000	159087000	159319000	169.058	SYTL3,EZR,C6orf99
9	90947700	90909300	91202200	163.828	SPIN1,NXNL2
9	92311400	92294400	92495100	162.821	-
15	26885200	26723700	26911100	160.496	GABRB3
5	109197000	108988000	109240000	156.271	MAN2A1
3	12506200	12476600	12819300	151.978	TSEN2,C3orf83,MKRN2,RAF1,TMEM40
2	125998000	125740000	126335000	148.576	-
3	139052000	139033000	139351000	148.572	MRPS22,COPB2,RBP2,RBP1,NMNAT3
3	134739000	134629000	135618000	146.833	EPHB1
2	9766680	9354260	9774110	145.998	ASAP2,ITGB1BP1,CPSF3,IAH1,ADAM17,YWHAQ
3	17873800	17189600	18009400	145.345	TBC1D5
14	69592000	69423900	69791100	144.488	ACTN1,DCAF5,EXD2,GALNT16
22	39747800	39574300	39845300	144.477	PDGFB,RPL3,SYNGR1,TAB1
8	10875300	10731100	11094000	143.754	XKR6
4	99985900	99712200	100322000	143.554	EIF4E,METAP1,ADH5,ADH4,ADH6,ADH1A,ADH1B
4	144235000	143610000	144412000	143.124	INPP4B,USP38,GAB1
2	17596700	16574500	17994400	142.084	FAM49A,RAD51AP2,VSNL1,SMC6,GEN1
2	211707000	211652000	211873000	141.706	-
1	103763000	103353000	103785000	141.473	COL11A1
3	71482600	71372800	71685500	140.75	FOXP1
17	10519000	10280200	10564000	140.243	MYH8,MYH4,MYH1,MYH2,MYH3
4	13283100	13126100	13537100	139.729	RAB28
8	73836900	73815300	73953100	139.423	KCNB2,TERF1
14	50226700	49952500	50426100	139.052	RPS29,LRR1,RPL36AL,MGAT2,DNAAF2,POLE2,KLHDC1,KLHDC2,NEMF,ARF6
2	26167200	25895300	26238100	138.585	KIF3C,DTNB
6	47369600	47312800	47708400	138.112	CD2AF,GPR115
3	102005000	101899000	102361000	137.862	ZPLD1
1	65943500	65891700	66168800	137.68	LEPR,LEPROT
11	25169300	24892400	25274500	137.191	LUZP2
1	28846900	28430000	29177900	136.458	PATFR,DNAJCS,ATPIF1,SESN2,MED18,PHACTR4,RCC1,TRNAU1AP,TAF12,RAB42,GMEB1,YTHDF2,OPRD1
2	154054000	154009000	154319000	136.247	-
7	108874000	108718000	109226000	135.996	-
1	75471000	75277400	75941000	133.055	LHX8,SLC44A5
1	154824000	154802000	155113000	131.45	KCNN3,PMVK,PBXIP1,PYGO2,SHC1,CKS1B,FLAD1,LENEP,ZBTB7B,DCST2,DCST1,ADAM15,EFNA4,EFNA3,EFNA1,SLC50A1,DPM3
3	58413700	58096400	58550500	130.828	FLNB,DNAASEL3,ABHD6,RFP14,PXK,PDHB,KCTD6,ACOX2,FAM107A
1	36170500	35690600	36592200	130.701	ZMYM4,KIAA0319L,NCDN,TFAP2E,PSMB2,C1orf216,CLSPN,AGO4,AGO1,AGO3,TEKT2,ADPRHL2,COL8A2
17	39768900	39673200	39865400	130.04	KRT15,KRT19,KRT9,KRT14,KRT16,KRT17,JUP,EIF1
15	82804000	81842500	82171400	129.682	-
17	30842700	30613600	30868000	128.36	RHBDL3,C1orf75,ZNF207,PSMD11,CDK5R1,MYO1D
2	107933000	107782000	108041000	128.04	-
3	44917100	44138200	45133100	127.824	TOPAZ1,TCAIM,ZNF445,ZKSCAN7,ZNF660,ZNF197,ZNF35,ZNF502,ZNF501,KIAA1143,KIF15,TMEM42,TGM4,ZDHC3,EXOSC7,CLEC3B,CDCP1
4	153009000	152902000	153101000	126.503	-
22	43190000	43148300	43455100	126.326	ARFGAP3,PACIN2,TTL1
4	168849000	168619000	168995000	126.125	-
5	42286000	41478600	42623200	125.831	PLCXD3,OXCT1,C5orf51,FBXO4,GHR
7	136345000	135788000	136570000	125.551	CHRM2
3	60305100	60226500	60349500	125.16	FHIT
10	59763900	59572200	59825500	124.643	-
3	114438000	114363000	115146000	124.535	ZBTB20
4	160142000	159944000	160359000	123.391	C4orf45,RAPGEF2
2	177717000	177613000	177889000	123.094	-
5	119672000	119639000	119868000	122.93	PRR1
20	43771800	43592200	43969300	122.421	STK4,KCNS1,WFDC5,WFDC12,PI3,SEMG1,SEMG2,SLPI,MATN4,RBPJL,SDC4
1	172928000	172668000	172942000	121.532	-
7	112273000	112126000	112622000	121.336	LSMEM1,TMEM168,C7orf60
1	169523000	169103000	169525000	119.533	NME7,BLZF1,CCDC181,SLC19A2,F5
3	26265100	25931700	26512400	119.052	-

Table S3. Top hits for 3P-CLR run on the Eurasian ancestral branch, using Yoruba as the outgroup. We show the windows in the top 99.9% quantile of scores. Windows were merged together if the central SNPs that define them were contiguous. Win max = Location of window with maximum score. Win start = left-most end of left-most window for each region. Win end = right-most end of right-most window for each region. All positions were rounded to the nearest 100 bp. Score max = maximum score within region.

chr	Win max	Win start	Win end	Score max	Genes within region
2	72379700	72353500	73170800	617.695	CYP26B1,EXOC6B,SPR,EMX1,SFXN5
20	53879500	53876700	54056200	605.789	-
10	22712400	22309300	22799200	566.463	EBLN1,COMMD3,COMMD3-BM11,BM11,SPAG6
3	25856600	25726300	26012000	557.376	NGLY1,OXSM
18	67725100	67523300	67910500	535.743	CD226,RTTN
10	66262400	65794400	66339100	532.732	-
11	39695600	39587400	39934300	518.72	-
7	138927000	138806000	139141000	508.385	TTC26,UBN2,C7orf55,C7orf55-LUC7L2,LUC7L2,KLRG2
9	90934600	90909300	91202200	498.898	SPIN1,NXNL2
4	41554200	41454200	42195300	487.476	LIMCH1,PHOX2B,TMEM33,DCAF4L1,SLC30A9,BEND4
16	61271700	61121600	61458700	485.291	-
17	58509300	58113700	59307700	477.117	HEATR6,CA4,USP32,C17orf64,APPBP2,PPM1D,BCAS3
1	230132000	229910000	230208000	468.258	GALNT2
8	35540400	35533900	35913800	454.601	UNC5D
17	60964400	60907300	61547900	449.203	TANC2,CYB561
16	47972300	33707000	48480500	448.504	SHCBP1,VPS35,ORC6,MYLK3,C16orf87,GPT2,DNAJA2,NETO2,ITFG1,PHKB,ABCC12,ABCC11,LONP2,SLAH1
1	90393900	90329700	90521600	436.002	LRRCSL,ZNF326
8	52698800	52238900	52932100	423.865	PXDNL,PCMTD1
11	106237000	105877000	106256000	419.391	MSANTD4,KBTBD3,AASDHPPT
13	48798100	48722300	49288100	414.218	ITM2B,RB1,LPAR6,RCBTB2,CYSLTR2
3	19240300	19090800	19424900	408.064	KCNH8
2	194986000	194680000	195299000	404.394	-
12	15962600	15690100	16137200	402.558	PTPRO,EPSS,STRAP,DERA
9	125564000	125484000	126074000	400.096	ZBTB26,RABGAP1,GPR21,STRBP,OR1L4,OR1L6,OR5C1,PDCL,OR1K1,RC3H2,ZBTB6
15	28565300	28324600	28611900	398.519	OCA2,HERC2
8	47631700	42502000	49037700	396.687	CHRN3,CHRNA6,THAP1,RNF170,HOK3,FNTA,POMK,HGSNAT,SPIDR,CEBPD,MCM4,UBE2V2
1	116994000	116808000	117027000	395.221	ATP1A1
7	99338700	98717600	99376500	393.41	ZSCAN25,CYP3A5,CYP3A7,CYP3A4,SMURF1,CPNA7,ARPC1A,ARPC1B,PDAP1,BUD31,PTCD1,ATP5J2
7	30343200	30178800	30485700	391.828	PTCD1,CPSF4,ATP5J2,ZNF789,ZNF394,ZKSCAN5,FAM200A,ZNF655
10	31583000	31430600	31907900	389.863	MTURN,ZNRF2,NOD1
6	10647900	10583800	10778900	387.883	ZEB1
11	123275000	123156000	123313000	386.485	GCNT2,C6orf52,PAK11P1,TMEM14C,TMEM14B,SYCP2L,MAK
15	64642400	64333700	65204100	385.748	-
2	222560000	222523000	222690000	383.336	DAPK2,FAM96A,SNX1,SNX22,PPIB,CSNK1G1,KIAA0101,TRIP4,ZNF609,OA22,RBPM22,PIF1,PLEKHO2
6	43620800	43398400	43687800	378.463	-
14	57643800	57603400	58047900	378.332	ABCC10,DLK2,TJAP1,LRRC73,POLR1C,YIPF3,XPO5,POLH,GTPBP2,MAD2L1BP,RSPH9,MRPS18A
4	33487100	33294500	34347100	377.815	EXOC5,AP5M1,NAA30,C14orf105
3	188699000	188647000	188856000	373.617	-
17	46949100	46821000	47137900	371.886	TPRG1
4	172656000	172565000	172739000	369.949	ATP5G1,UBE2Z,SNF8,GIP,IGF2BP1,TTL6,CALCOCO2
15	34404500	34212600	34413500	369.949	GALNTL6
1	32888000	32445400	33065900	369.725	AVEN,CHRM5,EMC7,PGBD4
22	46820900	46593300	46834700	369.511	KHDRBS1,TMEM39B,CPNA6,TLXNA,CCDC28B,IQCC,DCDC2B,TMEM234,EIF3I,FAM167B,LCK,HDAC1,MARCKSL1,TSSK3,FAM229A,BSDC1,ZBTB8B,ZBTB8A,ZBTB80S
10	93143600	93060500	93324900	368.648	PPARA,CDPF1,PKDREJ,TTC38,GTSE1,TRMU,CELSR1
6	14845800	14753800	14948200	367.9	HECTD2

Table S4. Enriched GO categories in the European, East Asian and Modern Human branches. We tested for ontology enrichment among the regions in the 99.5% quantile of the 3P-CLR scores for each population branch ($P < 0.05$, $FDR < 0.3$). The Eurasian branch did not have any category that passed these cutoffs.

Population Branch	Raw p-value	FDR	GO category
European	0.00002	0.05977	cuticle development
European	0.00007	0.096085	hydrogen peroxide catabolic process
East Asian	0.00001	0.013385	regulation of cell adhesion mediated by integrin
East Asian	0.00001	0.013385	epidermis development
East Asian	0.00014	0.14102	cell-substrate adhesion
East Asian	0.00023	0.185135	nucleosomal DNA binding
East Asian	0.0003	0.185135	nuclear chromosome
East Asian	0.00033	0.185135	RNA polymerase II core promoter proximal region sequence-specific DNA binding
East Asian	0.00048	0.2023525	transcription factor activity involved in negative regulation of transcription
East Asian	0.00048	0.2023525	negative regulation of vitamin metabolic process
East Asian	0.00058	0.219074444	substrate adhesion-dependent cell spreading
East Asian	0.00077	0.258110909	regulation of ERK1 and ERK2 cascade
East Asian	0.00084	0.258110909	retinol binding
East Asian	0.00112	0.296474	primary alcohol catabolic process
East Asian	0.00125	0.296474	D1 dopamine receptor binding
East Asian	0.00127	0.296474	RNA polymerase II transcription regulatory region sequence-specific DNA binding
East Asian	0.0013	0.296474	transcription factor activity involved in negative regulation of transcription
East Asian	0.0013	0.296474	gap junction assembly
Modern Human	0.00002	0.031153333	nuclear division
Modern Human	0.00003	0.031153333	organelle fission
Modern Human	0.00003	0.031153333	mitosis
Modern Human	0.00006	0.0490675	intra-Golgi vesicle-mediated transport
Modern Human	0.00012	0.069241429	regulation of cell cycle
Modern Human	0.00014	0.069241429	retinoic acid-responsive element binding
Modern Human	0.00015	0.069241429	cell cycle process
Modern Human	0.00029	0.12784125	T cell migration
Modern Human	0.00041	0.162306667	chromosomal part
Modern Human	0.00055	0.198124	'de novo' IMP biosynthetic process
Modern Human	0.00072	0.237017273	intracellular organelle
Modern Human	0.00081	0.24451	SNAP receptor activity
Modern Human	0.00113	0.294514286	ATP-dependent protein binding
Modern Human	0.00114	0.294514286	RNA biosynthetic process

Table S5. Top hits for 3P-CLR run on the ancestral branch to Eurasians and Yoruba, using archaic humans as the outgroup and 0.25 cM windows.. We show the windows in the top 99.9% quantile of scores. Windows were merged together if the central SNPs that define them were contiguous. Win max = Location of window with maximum score. Win start = left-most end of left-most window for each region. Win end = right-most end of right-most window for each region. All positions were rounded to the nearest 100 bp. Score max = maximum score within region.

chr	Win max	Win start	Win end	Score max	Genes within region
2	95724900	95561200	96793700	859.783	ZNF514,ZNF2,PROM2,KCNIP3,FAHD2A,TRIM43,GPAT2,ADRA2B,ASTL,MAL,MRPS5
5	87054300	86463700	87101400	852.543	RASA1,CCNH
17	61538200	60910700	61557700	849.335	TANC2,CYB561,ACE
14	72207400	71649200	72283600	849.304	SIPAL1L
18	19089800	15012100	19548600	846.182	ROCK1,GREB1L,ESCO1,SNRPD1,ABHD3,MIB1
3	110675000	110513000	110932000	841.499	PVRL3
2	37990900	37917900	38024200	841.339	CDC42EP3
3	36938000	36836900	37517500	839.211	TRANK1,EPM2AIP1,MLH1,LRRFIP2,GOLGA4,C3orf35,ITGA9
7	107246000	106642000	107310000	838.948	PRKAR2B,HBP1,COG5,GPR22,DUS4L,BCAP29,SLC26A4
12	96986900	96823000	97411500	835	NEDD1
2	201056000	200639000	201340000	832.4	C2orf69,TYW5,C2orf47,SPATS2L
1	66851800	66772600	66952600	832.221	PDE4B
10	37795700	37165100	38978800	831.353	ANKRD30A,MTRNR2L7,ZNF248,ZNF25,ZNF33A,ZNF37A
2	156129000	155639000	156767000	827.839	KCNJ3
17	56516700	56379200	57404800	826.026	BZRAP1,SUPT4H1,RNF43,HSF5,MTMR4,SEPT4,C1orf47,TEX14,RAD51C,PPM1E,TRIM37,SKA2,PRR11,SMG8,GDPD1
5	18755900	18493900	18793500	825.858	-
2	61190300	61050900	61891900	824.962	REL,PUS10,PEX13,KIAA1841,AHSA2,USP34,XPO1
22	40392200	40360300	41213400	824.52	GRAP2,FAM83F,TNRC6B,ADSL,SGSM3,MKL1,MCHR1,SLC25A17
2	99013400	98996400	99383400	821.891	CNGA3,INPP4A,COA5,UNC50,MGAT4A
4	13294400	13137000	13533100	820.222	RAB28
18	32975600	32604100	33002800	819.128	MAPRE2,ZNF397,ZSCAN30,ZNF24,ZNF396
21	35204700	34737300	35222100	818.754	IFNGR2,TMEM50B,DNAJC28,GART,SON,DONSON,CRYZL1,ITSN1
12	73048100	72740100	73160400	816.903	TRHDE
1	213511000	213150000	213563000	814.632	VASH2,ANGEL2,RPS6KC1
1	27500300	26913700	27703900	814.332	ARID1A,PIGV,ZDHC18,SFN,GPN2,GPATCH3,NUDC,NR0B2,C1orf172,TRNP1,FAM46B,SLC9A1,WDTC1,TMEM222,SYTL1,MAP3K6,FCN3
8	79219300	78698200	79558000	813.796	PKIA
12	116455000	116380000	116760000	809.406	MED13L
11	72857900	72416300	72912800	809.274	ARAP1,STARD10,ATG16L2,FCHSD2
4	22941400	22827300	23208900	808.696	-
12	79783400	79748800	80435300	804.117	SYT1,PAWR,PPP1R12A
13	35534800	35429700	36097500	801.815	NBEA,MAB2L1
4	146141000	145514000	146214000	799.686	HHIP,ANAPC10,ABCE1,OTUD4
16	61429300	61124400	61458700	798.318	-
4	46530000	46360000	46881700	797.876	GABRA2,COX7B2
2	133038000	132930000	133117000	796.277	-
17	28980100	28549700	29407200	796.136	SLC6A4,BLMH,TMIGD1,CPD,GOSR1,TBC1D29,CRLF3,ATAD5,TEFM,ADAP2,RNF135
5	127332000	127156000	127607000	789.339	SLC12A2,FBN2
5	27208300	27072700	27352900	788.924	CDH9
7	122294000	121973000	122559000	787.777	CADPS2,RNF133,RNF148
10	38218900	37175000	43224100	786.651	ANKRD30A,MTRNR2L7,ZNF248,ZNF25,ZNF33A,ZNF37A,ZNF33B
7	23100200	22888500	23114300	785.919	FAM126A
1	228050000	227587000	228112000	785.53	SNAP47,JMJD4,PRSS38,WNT9A
4	74891400	74846600	75086500	781.895	PF4,PPBP,CXCL5,CXCL3,CXCL2,MTHFD2L
22	34588400	34516300	34811800	781.522	-
2	36899700	36767900	64395700	778.951	EHBP1,OTX1,WDPKP,MDH1,UGP2,VPS54,PEL1
6	136666000	136257000	136967000	778.233	MTRF2,BCLAF1,MAP7,MAP3K5
16	75738400	75522400	75968000	778.171	CHST6,CHST5,TMEM231,GABARAPL2,ADAT1,KARS,TERF2IP
14	63446800	63288600	63597500	776.567	KCNH5
6	117528000	117080000	117579000	775.402	FAM162B,GPRC6A,RFX6
11	30206400	29986200	30443900	775.051	KCNA4,F5HB,ARL14EP,MPPED2
12	67533400	67436200	67639400	772.731	-
20	35460500	35049400	35710900	772.319	DLGAP4,MYL9,TGIF2,TGIF2-C2orf24,C2orf24,SLA2,NDRG3,DSN1,SOGA1,TLDC2,SAMHD1,RBL1
13	80131900	79801800	80268900	771.976	RBM26,NDFIP2
11	121408000	121310000	121493000	771.669	SORL1
4	105305000	104931000	105454000	770.437	CXXC4
5	93218900	92677500	93647600	769.192	NR2F1,FAM172A,POU5F2,KIAA0825
15	49975000	49247500	50040200	768.997	SECISBP2L,COPS2,GALK2,FAM227B,FGF7,DTWD1,SHC4
1	243669000	243505000	244087000	767.303	SDCCAG8,AKT3
21	36822500	36691000	36883300	762.715	RUNX1
1	154133000	153745000	154280000	762.43	INTS3,SLC27A3,GATAD2B,DENND4B,CRTC2,SLC39A1,CREB3L4,JTB,RAB13,RPS27,NUP210L,TPM3,C1orf189,C1orf43,UBAP2L,HAX1
7	144655000	144465000	144700000	762.429	TPK1
12	69177500	68890300	69290800	762.399	RAP1B,NUP107,SLC35E3,MDM2,CPM
2	145116000	144689000	145219000	757.235	GTDC1,ZEB2
1	176195000	175890000	176437000	755.81	RFWD2,PAPPA2
7	152155000	151699000	152199000	754.754	GALNTL5,GALNT11,KMT2C
7	116575000	116324000	116788000	754.606	MET,CAPZA2,ST7
14	29571400	29264600	29691100	754.435	-
1	226323000	226140000	226575000	754.04	SDE2,H3F3A,ACBD3,MIXL1,LIN9,PARP1
7	73051800	72317200	73134700	752.285	POM121,TRIM7,NSUN5,TRIM50,FKBP6,FZD9,BAZ1B,BCL7B,TBL2,MLXIPL,VPS37D,DNAJC30,WBSCR22,STX1A
5	89578700	89408400	89654700	751.498	-
8	22999100	22926500	23113900	749.992	TNFRSF10B,TNFRSF10C,TNFRSF10D,TNFRSF10A,CHMP7
15	75883900	75462000	76038100	749.953	C15orf39,GOLGA6C,GOLGA6D,COMMD4,NEIL1,MAN2C1,SIN3A,PTPN9,SNUPN,IMP3,SNX33,CSPG4,ODF3L1
7	98978400	98719400	99376100	749.35	ZSCAN25,CYP3A5,CYP3A7,CYP3A4,SMURF1,KPNA7,ARPC1A,ARPC1B,PDAP1,BUD31,PTCD1,ATP5J2-PTCD1,CPSF4,ATP5J2,ZNF789,ZNF394,ZKSCAN5,FAM200A,ZNF655

1	96340100	96155200	96608300	748.253	-
2	73508400	73482800	74054300	745.963	FBXO41,EGR4,ALMS1,NAT8,TPRKB,DUSP11,C2orf78
1	150868000	150224000	151137000	745.222	CA14,APH1A,C1orf54,C1orf51,MRPS21,PRPF3,RPRD2,TARS2,ECM1,ADAMTSL4, MCL1,ENSA,GOLPH3L,HORMAD1,CTSS,CTSK,ARNT,SETDB1,CERS2,ANXA9, FAM63A,PRUNE,BNIP1,C1orf56,CDC42SE1,MLLT11,GABPB2,SEMA6C,TNFAIP8L2, SCNM1,LYSMD1
3	99877600	99374500	100207000	744.933	COL8A1,CMSS1,FILIP1L,TBC1D23,NIT2,TOMM70A,LNP1
12	56244900	56086600	56360700	743.698	PMEL,CDK2,ITGA7,BLOC1S1,RDH5,CD63,GDF11,SARNP,ORMDL2,DNAJC14,MMP19, WIBG,DGKA
3	44843200	44139200	45128900	743.157	TOPAZ1,TCAIM,ZNF445,ZKSCAN7,ZNF660,ZNF197,ZNF35,ZNF502,ZNF501,KIAA1143, KIF15,TMEM42,TGM4,ZDHC3,EXOSC7,CLEC3B,CDCP1
12	102922000	102388000	102964000	741.338	DRAM1,CCDC53,NUP37,PARPBP,PMCH,IGF1
1	21114300	21012100	21636800	740.553	KIF17,SH2D5,HP1BP3,EIF4G3,ECE1
11	108770000	108492000	108830000	740.463	DDX10
3	51678700	50188500	51919700	740.272	SEMA3F,GNAT1,GNAI2,LSMEM2,JFRD2,HYAL3,NAT6,HYAL1,HYAL2,TUSC2,RASSF1, ZMYND10,NPRL2,CYB561D2,TMEM115,CACNA2D2,C3orf18,HEMK1,CISH,MAPKAPK3, DOCK3,MANF,RBM15B,RAD54L2,TEX264,GRM2,IQCF6,IQCF3,IQCF2,IQCF5
11	64581900	64293300	64589300	738.648	RASGRP2,PYGM,SF1,MAP4K2,MEN1,SLC22A11,SLC22A12,NRXN2
9	126023000	125542000	126076000	738.221	ZBTB26,RABGAP1,GPR21,STRBP,OR5C1,PDCL,OR1K1,RC3H2,ZBTB6

Table S6. Top hits for 3P-CLR run on the ancestral branch to Eurasians and Yoruba, using archaic humans as the outgroup and 1 cM windows. We show the windows in the top 99.9% quantile of scores. Windows were merged together if the central SNPs that define them were contiguous. Win max = Location of window with maximum score. Win start = left-most end of left-most window for each region. Win end = right-most end of right-most window for each region. All positions were rounded to the nearest 100 bp. Score max = maximum score within region.

chr	Win max	Win start	Win end	Score max	Genes within region
14	71698500	71349200	72490300	1210.24	PCNX,SIPA1L1,RGS6
4	145534000	145023000	146522000	1157.25	GYPB,GYPA,HHIP,ANAPC10,ABCE1,OTUD4,SMAD1
2	156103000	155391000	156992000	1100.35	KCNJ3
5	93425300	92415600	94128600	1065.66	NR2F1,FAM172A,POU5F2,KIAA0825,ANKRD32,MCTP1
7	106717000	106401000	107461000	1049.82	PIK3CG,PRKAR2B,HBP1,COG5,GPR22,DUS4L,BCAP29,SLC26A4,CBLL1,SLC26A3
7	151831000	151651000	152286000	1028.93	GALNTL5,GALNT11,KMT2C
2	145008000	144393000	145305000	1027.28	ARHGAP15,GTDC1,ZEB2
19	16578500	16387600	16994000	991.083	KLF2,EPS15L1,CALR3,C19orf44,CHERP,SLC35E1,MED26,SMIM7,TMEM38A,NWD1,SIN3B
2	37996300	37730400	38054600	989.901	CDC42EP3
2	63467700	62639800	64698300	989.891	TMEM17,EHBP1,OTX1,WDPCCP,MDH1,UGP2,VPS54,PELI1,LGALS1
10	38074100	36651400	44014800	988.663	ANKRD30A,MTRNR2L7,ZNF248,ZNF25,ZNF33A,ZNF37A,ZNF33B,BMS1,RET,CSGALNACT2,RASGEF1A,FXDYD4,HNRNPF
1	27203100	26703800	27886000	988.598	LIN28A,DHDDS,HMG2N,RPS6KA1,ARID1A,PIGV,ZDHC18,SFN,GPN2,GPATCH3,NUDC,NR0B2,C1orf172,TRNP1,FAM46B,SLC9A1,WDC1,TMEM222,SYTL1,MAP3K6,FCN3,CD164L2,GPR3,WASF2,AHDC1
12	102906000	102308000	103125000	966.591	DRAM1,CCDC53,NUP37,PARBP,PMCH,IGF1
2	133034000	132628000	133270000	941.856	GPR39
15	43507200	42284300	45101400	938.129	PLA2G4E,PLA2G4D,PLA2G4F,VPS39,TMEM87A,GANC,CAPN3,ZNF106,SNAP23,LRR57,HAUS2,STARD9,CDAN1,TBKB2,UBR1,EPB42,TMEM62,CCNDBP1,TGM5,TGM7,LCMT2,ADAL,ZSCAN29,TUBGCP4,TP53BP1,MAP1A,PIIP5K1,CKMT1B,STRC,CATSPER2,CKMT1A,PDIA3,ELL3,SERF2,SERINC4,HYPK,MFAP1,WDR76,FRMD5,CASC4,CTDSP2,EIF3J,SPG11,PATL2,B2M,TRIM69
2	73848400	73178500	74194400	934.997	SFXN5,RAB11FIP5,NOTO,SMYD5,PRADC1,CCT7,FBXO41,EGR4,ALMS1,NAT8,TPRKB,DUSP11,C2orf78,STAMBP,ACTG2,DGUOK
5	54861800	54193000	55422100	927.745	ESM1,GZMK,GZMA,CDC20B,GPX8,MCIDAS,CCNO,DHX29,SKIV2L2,PPAP2A,SLC38A9,DDX4,IL31RA,IL6ST,ANKRD55
3	52356200	50184000	53602300	925.895	SEMA3F,GNAT1,GNAI2,LSMEM2,IFRD2,HYAL3,NAT6,HYAL1,HYAL2,TUSC2,RASSF1,ZMYND10,NPRL2,CYB561D2,TMEM115,CACNA2D2,C3orf18,HEMK1,CISH,MAPKAPK3,DOCK3,MANF,RBM15B,RAD54L2,TEX264,GRM2,IQCF6,IQCF3,IQCF2,IQCF5,IQCF1,RRP9,PARP3,GPR62,PCBP4,ABHD14B,ABHD14A,ACY1,RPL29,DUSP7,POC1A,ALAS1,TLR9,TWFP3,PPM1M,WDR82,GLYCK,DNAH1,BAP1,PHF7,SEMA3G,TNCC1,NISCH,STAB1,NT5DC2,SMIM4,PBRM1,GNL3,GLT8D1,SPCS1,NEK4,ITIH1,ITIH3,ITIH4,MUSTN1,TMEM110,MUSTN1,TMEM110,SFMBT1,RFT1,PRKCD,TKT,CACNA1D,CLDN10,DZIP1,DNAJC3,UGGT2,HS6ST3
13	96364900	96038900	97500100	923.257	POTEC,ANKRD30B,ROCK1,GREB1L,ESCO1,SNRPD1,ABHD3,MIB1,GATA6
18	19248800	14517500	19962400	920.641	MET,CAPZA2,ST7,WNT2,ASZ1,CFTR
7	116587000	116214000	117339000	918.567	FOXG1
14	29544300	29031800	29913200	918.292	COL1A2,CASD1,SGCE,PEG10,PPP1R9A,PON1,PON3,PON2,ASB4
7	94710700	93964000	95170200	910.235	SYT1,PAWR,PPP1R12A
12	79783400	79231600	80435300	906.28	UPF1,CERS1,GDF1,COPE,DDX49,HOMER3,SUGP2,ARMC6,SLC25A42,TMEM161A,MEF2B
19	19290700	18936200	19885600	905.94	MEF2B,MEF2B,MEF2B,RFXANK,NR2C2AP,NCAN,HAPLN4,TM6SF2,SUGP1,MAU2,GATAD2A,TSSK6,NDUFA13,YJEFN3,CILP2,PBX4,LPAR2,GMIP,ATP13A1,ZNF101,ZNF14
11	72551000	72182800	72952400	902.837	PDE2A,ARAP1,STARD10,ATG16L2,FCHSD2,P2RY2
14	31685700	31255700	32384600	895.417	COCH,STRN3,AP4S1,HECTD1,DTD2,NUBPL

Table S7. Overlap between GWAS catalog and catalog of modern human-specific high-frequency changes in the top modern human selected regions (0.25 cM scan). Chr = chromosome. Pos = position (hg19). ID = SNP rs ID. Hum = Present-day human major allele. Anc = Human-Chimpanzee ancestor allele. Arch = Archaic human allele states (Altai Neanderthal, Denisova) where H=human-like allele and A=ancestral allele. Freq = present-day human derived frequency. Cons = consequence. C = C-score. PubMed = PubMed article ID for GWAS study.

Chr	Pos	ID	Hum	Anc	Arch	Freq	Gene	Cons	C	GWAS trait	PubMed
1	27138393	rs12748152	C	T	A/A,A/A	0.95	Metazoa SRP	upstream	4.193	HDL cholesterol	24097068
1	27138393	rs12748152	C	T	A/A,A/A	0.95	Metazoa SRP	upstream	4.193	LDL cholesterol	24097068
1	27138393	rs12748152	C	T	A/A,A/A	0.95	Metazoa SRP	upstream	4.193	Triglycerides	24097068
1	151009719	rs1534059	A	G	A/A,A/A	0.92	BNIP1	intron	7.111	DNA methylation, in blood cell lines	21251332
1	244044810	rs7553354	A	C	A/A,A/A	0.94	NA	intergenic	2.376	Response to taxane treatment (paclitaxel)	23006423
2	64279606	rs10171434	C	T	A/A,A/A	0.92	NA	intergenic	8.324	Suicide attempts in bipolar disorder	21041247
2	64279606	rs10171434	C	T	A/A,A/A	0.92	NA	intergenic	8.324	Urinary metabolites	21572414
2	144783214	rs16823411	T	C	A/A,A/A	0.93	GTDC1	intron	4.096	Body mass index	21701565
2	144783214	rs16823411	T	C	A/A,A/A	0.93	GTDC1	intron	4.096	Body mass index	21701565
2	145213638	rs731108	G	C	A/A,H/H	0.92	ZEB2	intron,nc	12.16	Renal cell carcinoma	23184150
2	156506516	rs4407211	C	T	A/A,A/A	0.92	NA	intergenic	2.077	Alcohol consumption	23953852
3	51142359	rs4286453	T	C	A/A,A/A	0.91	DOCK3	intron	2.344	Multiple complex diseases	17554300
3	51824167	rs6796373	G	C	A/A,A/A	0.94	NA	intergenic	2.285	Response to taxane treatment (paclitaxel)	23006423
4	13325741	rs2867467	G	C	A/A,A/A	0.91	NA	intergenic	0.56	Obesity (extreme)	21935397
4	13328373	rs6842438	T	C	A/A,A/A	0.92	NA	intergenic	3.609	Obesity (extreme)	21935397
4	13330095	rs10019897	C	T	A/A,A/A	0.92	NA	intergenic	0.303	Multiple complex diseases	17554300
4	13330095	rs10019897	C	T	A/A,A/A	0.92	NA	intergenic	0.303	Obesity (extreme)	21935397
4	13333413	rs9996364	A	G	A/A,A/A	0.92	HSP90AB2P	upstream	4.041	Obesity (extreme)	21935397
4	13338465	rs11945340	C	T	A/A,A/A	0.92	HSP90AB2P	intron,nc	10.31	Obesity (extreme)	21935397
4	13340249	rs6839621	T	C	A/A,A/A	0.92	HSP90AB2P	non coding exon,nc	0.873	Obesity (extreme)	21935397
4	13346602	rs11930614	C	T	A/A,A/A	0.92	NA	intergenic	0.22	Obesity (extreme)	21935397
4	13350973	rs10021881	T	C	A/A,A/A	0.92	NA	regulatory	3.346	Obesity (extreme)	21935397
4	13356393	rs16888596	G	A	A/A,A/A	0.94	NA	intergenic	1.347	Obesity (extreme)	21935397
4	13357274	rs11732938	A	G	A/A,A/A	0.94	NA	intergenic	20	Obesity (extreme)	21935397
4	13360622	rs11947529	T	A	A/A,A/A	0.93	RAB28	downstream	4.509	Obesity (extreme)	21935397
4	13363958	rs12331157	A	G	A/A,A/A	0.97	RAB28	intron	1.536	Obesity (extreme)	21935397
4	13363974	rs12332023	C	T	A/A,A/A	0.97	RAB28	intron	0.363	Obesity (extreme)	21935397
4	13366481	rs7673680	C	T	A/A,A/A	0.93	RAB28	intron	3.083	Obesity (extreme)	21935397
4	13370308	rs10003958	T	C	A/A,A/A	0.93	RAB28	intron	14.23	Obesity (extreme)	21935397
4	13373583	rs9998851	C	T	A/A,A/A	0.97	RAB28	intron	0.402	Obesity (extreme)	21935397
4	13374462	rs9291610	G	A	A/A,A/A	0.93	RAB28	intron	0.826	Obesity (extreme)	21935397
4	13393897	rs9998914	A	T	A/A,A/A	0.96	RAB28	intron	2.579	Obesity (extreme)	21935397
4	13403855	rs11943295	G	A	A/A,A/A	0.94	RAB28	intron	0.842	Multiple complex diseases	17554300
4	13403855	rs11943295	G	A	A/A,A/A	0.94	RAB28	intron	0.842	Obesity (extreme)	21935397
4	13403998	rs11943330	G	A	A/A,A/A	0.93	RAB28	intron	1.179	Obesity (extreme)	21935397
4	13404130	rs7677336	G	T	A/A,A/A	0.94	RAB28	intron	0.385	Obesity (extreme)	21935397
4	13404717	rs7673732	A	C	A/A,A/A	0.93	RAB28	intron	1.116	Obesity (extreme)	21935397
4	13440031	rs11737264	C	G	A/A,A/A	0.93	RAB28	intron	0.138	Obesity (extreme)	21935397
4	13440271	rs11737360	C	T	A/A,A/A	0.94	RAB28	intron	0.54	Obesity (extreme)	21935397
4	13449532	rs16888654	A	C	A/A,A/A	0.94	RAB28	intron	0.905	Obesity (extreme)	21935397
4	13452022	rs16888661	C	A	A/A,A/A	0.91	RAB28	intron	3.789	Obesity (extreme)	21935397
4	13463991	rs11933841	T	C	A/A,A/A	0.93	RAB28	intron	3.377	Obesity (extreme)	21935397
4	13465710	rs11947665	T	A	A/A,A/A	0.93	RAB28	intron	1.709	Obesity (extreme)	21935397
4	23095293	rs6825402	C	T	A/A,A/A	0.96	NA	intergenic	0.797	Multiple complex diseases	17554300
5	89540468	rs2935504	C	T	A/A,A/A	0.97	RP11-61G23.1	intron,nc	3.627	Multiple complex diseases	17554300
6	136947540	rs17723608	A	G	A/A,A/A	0.93	MAP3K5	intron	0.586	Blood pressure, CVD RF and other traits	20877124
7	72746648	rs6943090	C	T	A/A,A/A	0.97	TRIM50	upstream	1.88	Immune response to smallpox (secreted IL-12p40)	22610502
7	106720932	rs12154324	G	A	A/A,A/A	0.93	NA	regulatory	3.447	Multiple complex diseases	17554300
7	116668662	rs4730767	C	T	A/A,A/A	0.93	ST7-OT4	intron,nc	8.279	Response to gemcitabine or arabinosylcytosin in blood cell lines	19898621
7	116668662	rs4730767	C	T	A/A,A/A	0.93	ST7-OT4	intron,nc	8.279	Response to gemcitabine or arabinosylcytosin in blood cell lines	19898621
10	37579117	rs7096155	A	C	A/A,A/A	0.94	ATP8A2P1	intron,nc	2.346	Multiple complex diseases	17554300
10	37579117	rs7096155	A	C	A/A,A/A	0.94	ATP8A2P1	intron,nc	2.346	Multiple complex diseases	17554300
12	56308562	rs772464	G	T	A/A,A/A	0.96	NA	regulatory	1.192	Multiple complex diseases	17554300
12	72889122	rs17111252	A	T	A/A,A/A	0.93	TRHDE	intron	4.133	Multiple complex diseases	17554300
13	35811439	rs10129134	C	T	A/A,A/A	0.93	NBEA	intron	3.514	Body mass index	22446040
16	61340362	rs9922966	G	C	A/A,A/A	0.93	NA	intergenic	4.37	Multiple complex diseases	17554300
22	34557399	rs5999230	T	G	A/A,A/A	0.93	LL22NC03-86D4.1	intron,nc	1.126	HIV-1 viral setpoint	22174851

Table S8. Overlap between GWAS catalog and catalog of modern human-specific high-frequency changes in the top modern human selected regions (1 cM scan). Chr = chromosome. Pos = position (hg19). ID = SNP rs ID. Hum = Present-day human major allele. Anc = Human-Chimpanzee ancestor allele. Arch = Archaic human allele states (Altai Neanderthal, Denisova) where H=human-like allele and A=ancestral allele. Freq = present-day human derived frequency. Cons = consequence. C = C-score. PubMed = PubMed article ID for GWAS study.

Chr	Pos	ID	Hum	Anc	Arch	Freq	Gene	Cons	C	GWAS trait	PubMed
1	27138393	rs12748152	C	T	A/A,A/A	0.95	Metazoa SRP	upstream	4.193	HDL cholesterol	24097068
1	27138393	rs12748152	C	T	A/A,A/A	0.95	Metazoa SRP	upstream	4.193	LDL cholesterol	24097068
1	27138393	rs12748152	C	T	A/A,A/A	0.95	Metazoa SRP	upstream	4.193	Triglycerides	24097068
2	64279606	rs10171434	C	T	A/A,A/A	0.92	NA	intergenic	8.324	Suicide attempts in bipolar disorder	21041247
2	64279606	rs10171434	C	T	A/A,A/A	0.92	NA	intergenic	8.324	Urinary metabolites	21572414
2	144783214	rs16823411	T	C	A/A,A/A	0.93	GTDC1	intron	4.096	Body mass index	21701565
2	144783214	rs16823411	T	C	A/A,A/A	0.93	GTDC1	intron	4.096	Body mass index	21701565
2	145213638	rs731108	G	C	A/A,H/H	0.92	ZEB2	intron,nc	12.16	Renal cell carcinoma	23184150
2	156506516	rs4407211	C	T	A/A,A/A	0.92	NA	intergenic	2.077	Alcohol consumption	23953852
3	51142359	rs4286453	T	C	A/A,A/A	0.91	DOCK3	intron	2.344	Multiple complex diseases	17554300
3	51824167	rs6796373	G	C	A/A,A/A	0.94	NA	intergenic	2.285	Response to taxane treatment (paclitaxel)	23006423
3	52506426	rs6784615	T	C	A/A,A/A	0.96	NA	regulatory	0.316	Waist-hip ratio	20935629
5	54558972	rs897669	G	A	A/A,A/A	0.92	DHX29	intron	5.673	Alcohol and nicotine co-dependence	20158304
7	106720932	rs12154324	G	A	A/A,A/A	0.93	NA	regulatory	3.447	Multiple complex diseases	17554300
7	116668662	rs4730767	C	T	A/A,A/A	0.93	ST7-OT4	intron,nc	8.279	Response to gemcitabine or arabinosylcytosin in blood cell lines	19898621
7	116668662	rs4730767	C	T	A/A,A/A	0.93	ST7-OT4	intron,nc	8.279	Response to gemcitabine or arabinosylcytosin in blood cell lines	19898621
10	37579117	rs7096155	A	C	A/A,A/A	0.94	ATPSA2P1	intron,nc	2.346	Multiple complex diseases	17554300
12	79387804	rs17046168	C	T	A/A,A/A	0.92	RP11-390N6.1	intron,nc	2.716	Response to taxane treatment (paclitaxel)	23006423
15	42527218	rs2620387	C	A	A/A,A/A	0.91	TMEM87A	intron	10.12	Multiple complex diseases	17554300

826 **Supplementary Figures**

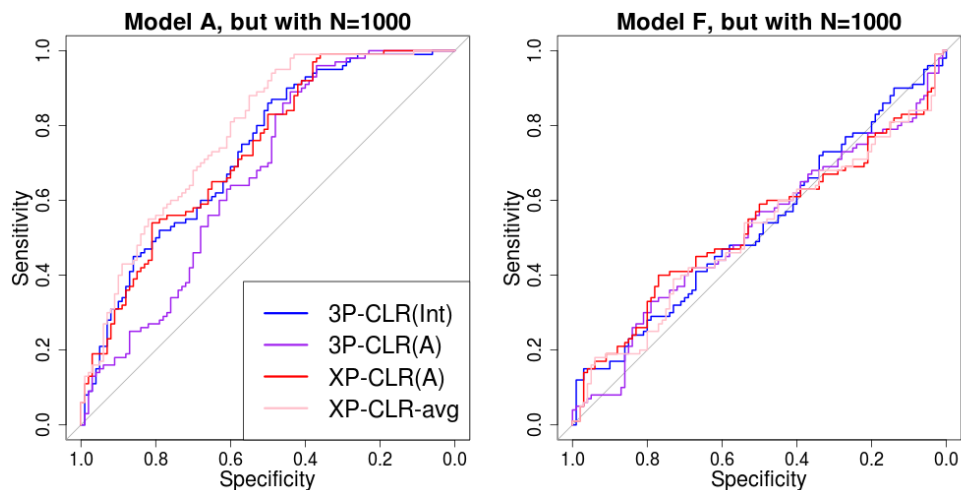


Figure S1. ROC curves for performance of 3P-CLR(Int), 3P-CLR(A) and two variants of XP-CLR in detecting selective sweeps that occurred before the split of two populations a and b , under two demographic models where the population size is extremely small ($N_e = 1,000$).

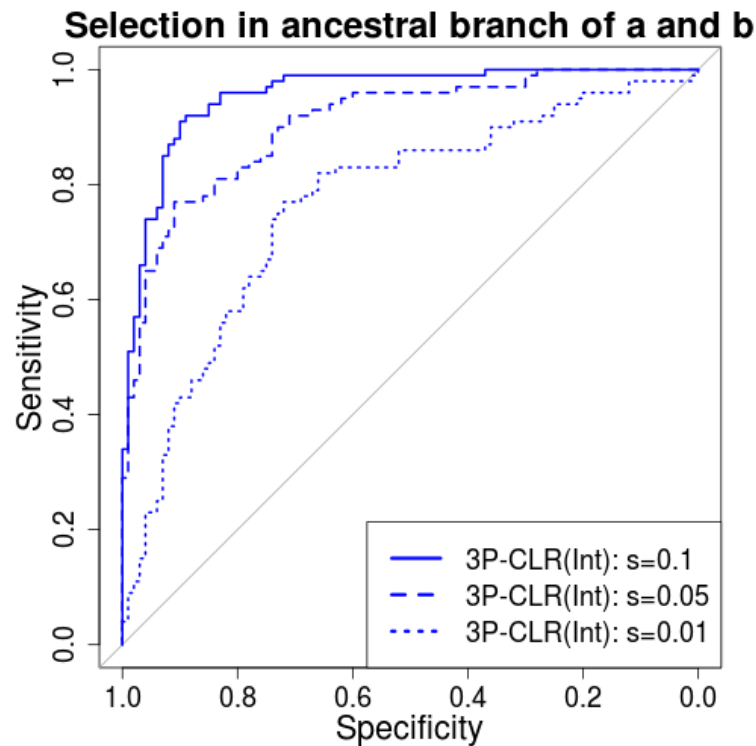


Figure S2. Performance of 3P-CLR(Int) for a range of selection coefficients. We used the demographic history from model B (Table 1) but extended the most ancient split time by 4,000 generations. The reason for this is that we wanted the internal branch to be long enough for it to be easy to sample simulations in which the beneficial allele fixed before the split of populations *a* and *b*, even for weak selection coefficients.

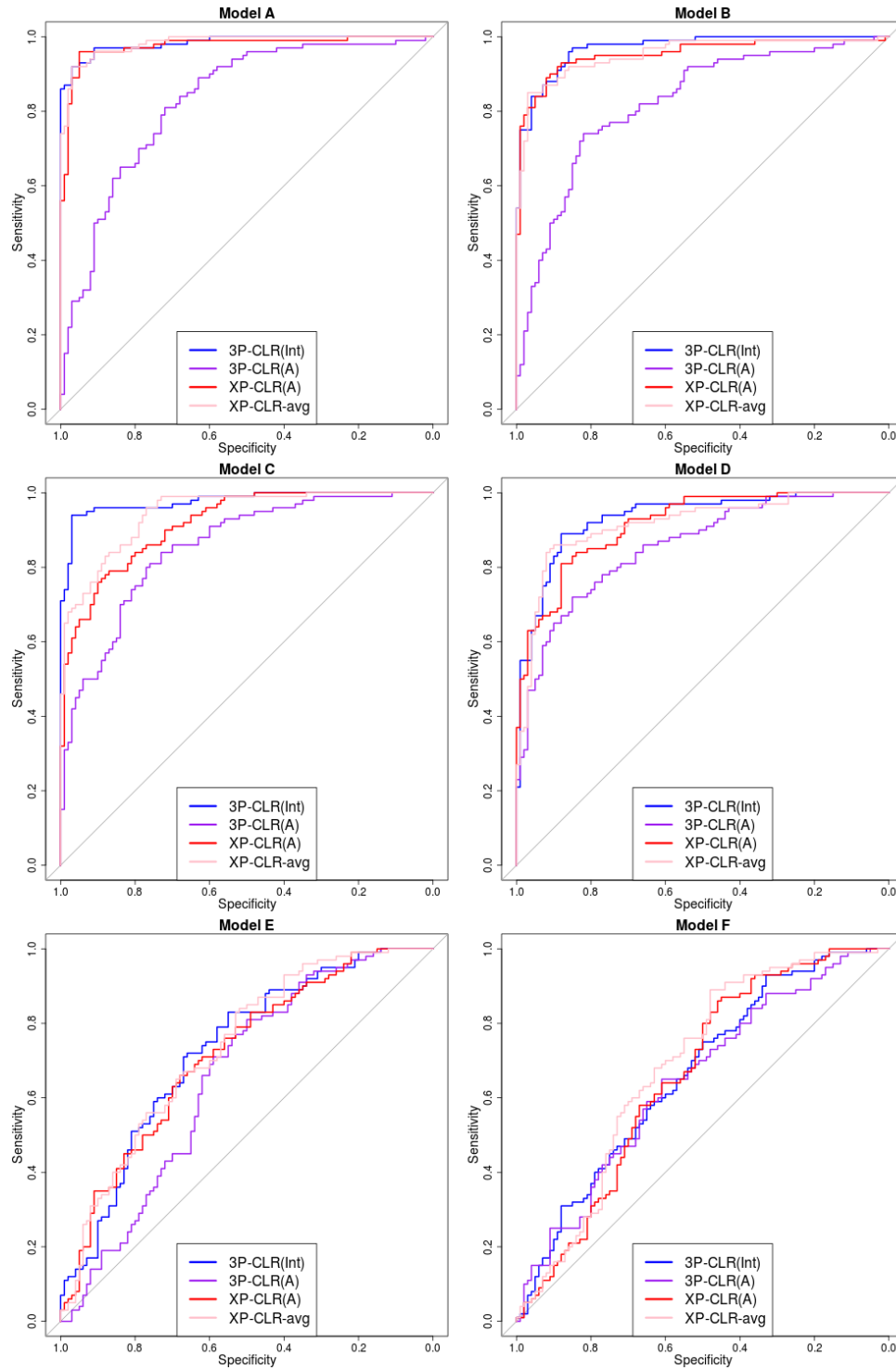


Figure S3. ROC curves for performance of 3P-CLR(Int), 3P-CLR(A) and two variants of XP-CLR in detecting selective sweeps that occurred before the split of two populations *a* and *b*, under different demographic models. In this case, the outgroup panel from population *c* contained 10 haploid genomes. The two sister population panels (from *a* and *b*) have 100 haploid genomes each.

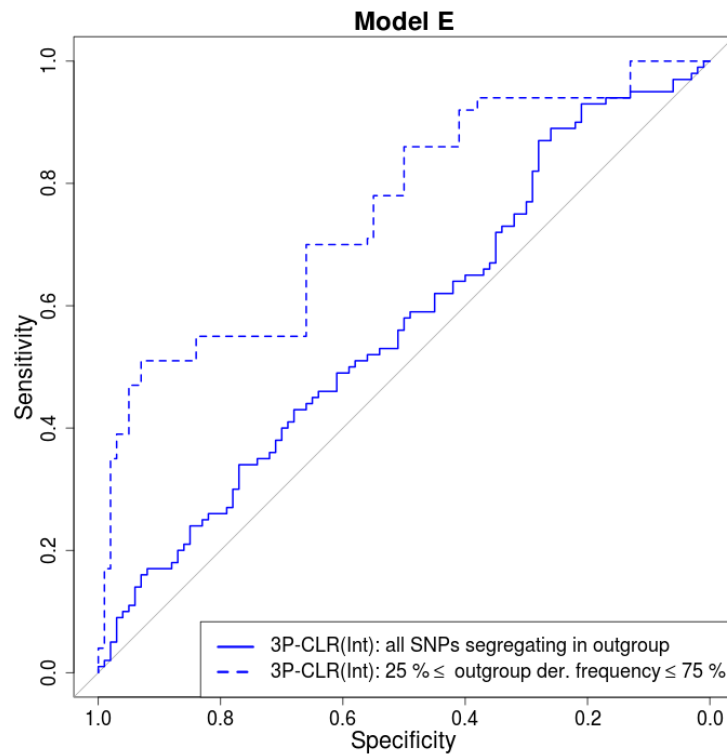


Figure S4. For demographic scenarios with very ancient split times, it is best to use sites segregating at intermediate frequencies in the outgroup. We compared the performance of 3P-CLR(Int) in a demographic scenario with very ancient split times (Model E) under two conditions: including all SNPs that are segregating in the outgroup, and only including SNPs segregating at intermediate frequencies in the outgroup. In both cases, the number of sampled sequences from the outgroup population was 100.

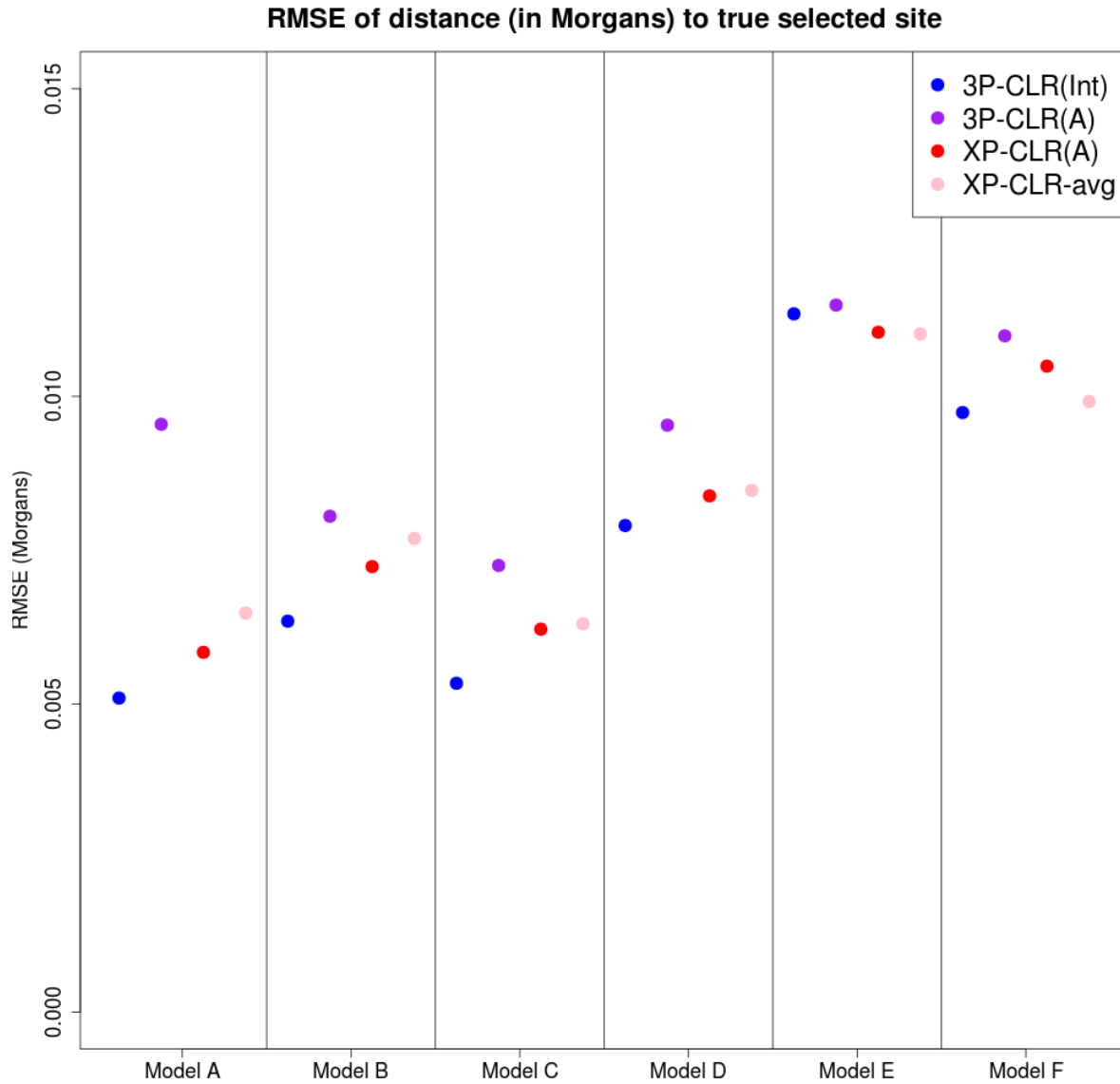


Figure S5. Root-mean squared error for the location of sweeps inferred by 3P-CLR(Int), 3P-CLR(A) and two variants of XP-CLR under different demographic scenarios, when the sweeps occurred before the split of populations *a* and *b*. In this case, the outgroup panel from population *c* contained 100 haploid genomes and the two sister population panels (from *a* and *b*) have 100 haploid genomes each.

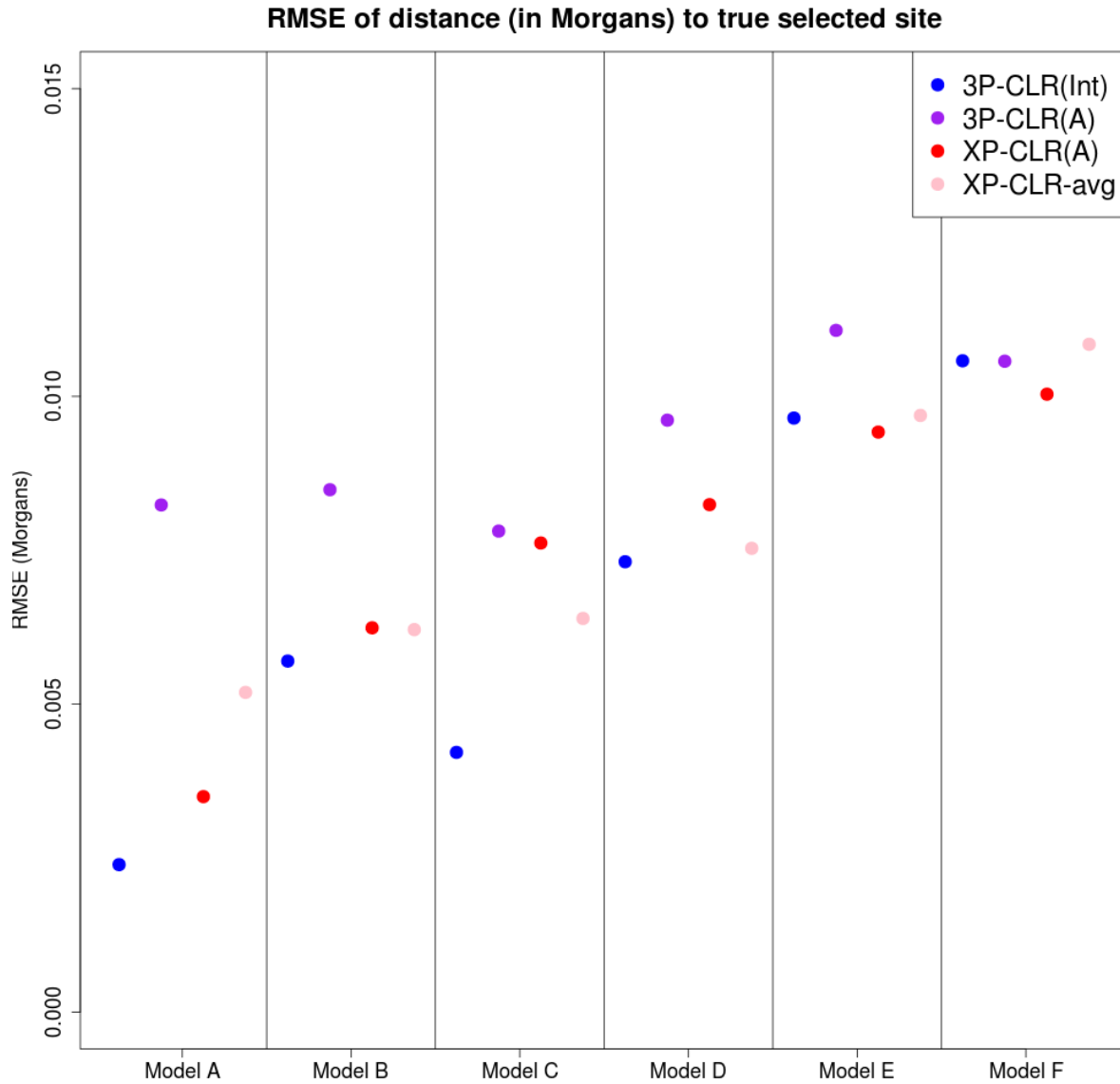


Figure S6. Root-mean squared error for the location of the sweep inferred by 3P-CLR(Int), 3P-CLR(A) and two variants of XP-CLR under different demographic scenarios, when the sweeps occurred before the split of populations *a* and *b*. the outgroup panel from population *c* contained 10 haploid genomes and the two sister population panels (from *a* and *b*) have 100 haploid genomes each.

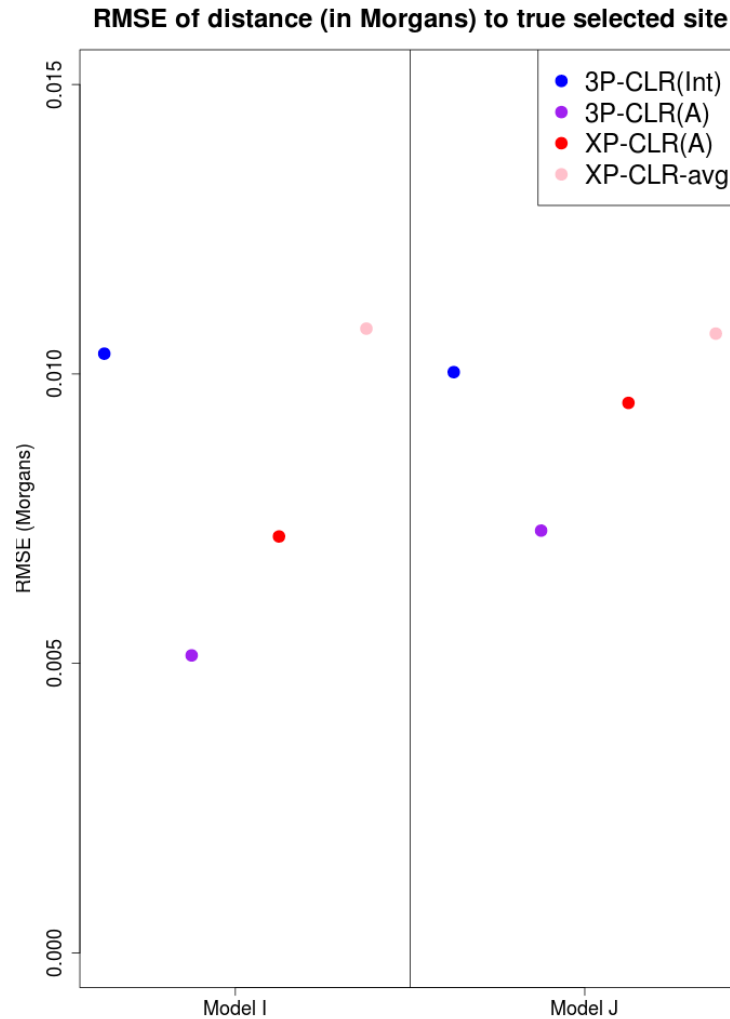


Figure S7. Root-mean squared error for the location of the sweep inferred by 3P-CLR(Int), 3P-CLR(A) and two variants of XP-CLR under different demographic scenarios, when the sweeps occurred in the terminal population branch leading to population *a*, after the split of populations *a* and *b*. In this case, the outgroup panel from population *c* contained 100 haploid genomes and the two sister population panels (from *a* and *b*) have 100 haploid genomes each.

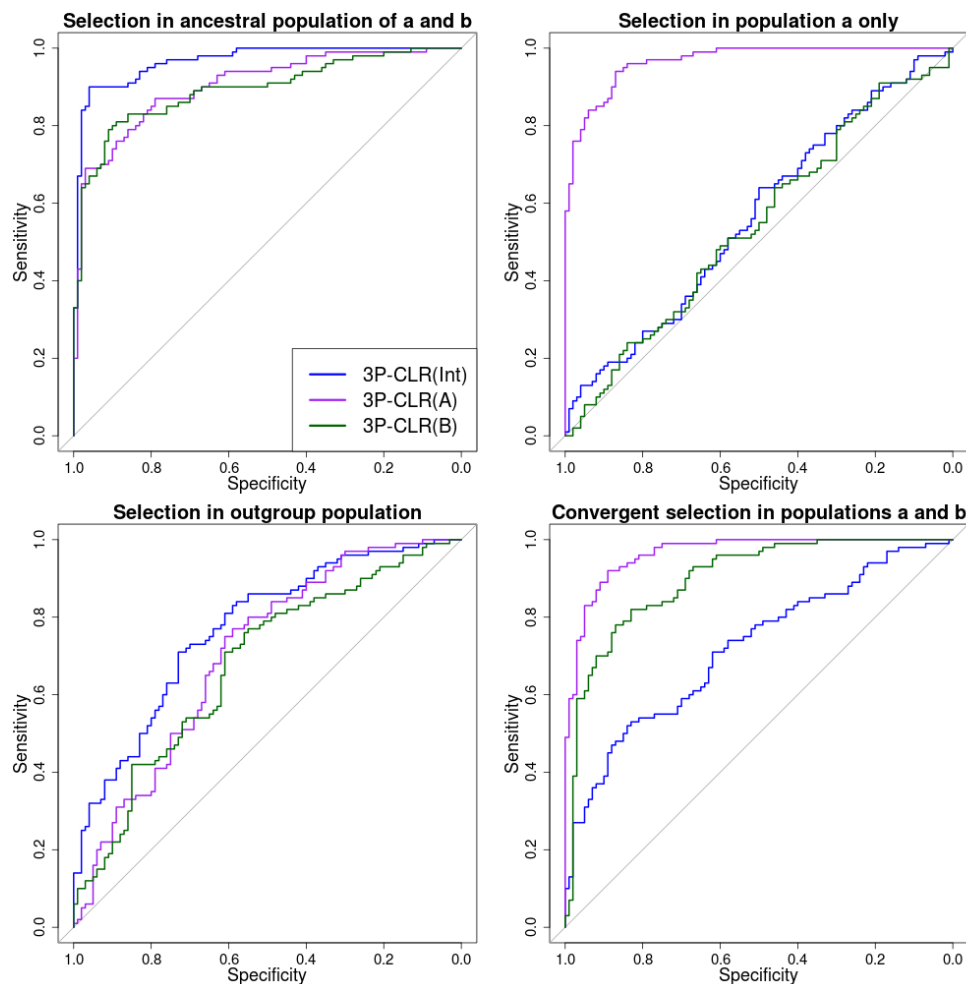


Figure S8. ROC curves for performance of 3P-CLR(Int), 3P-CLR(A) and 3P-CLR(B) when the selective events occur in different branches of the 3-population tree. Upper-left panel: Selection in the ancestral population of populations *a* and *b*. This is the type of events that 3P-CLR(Int) is designed to detect and, therefore, 3P-CLR(Int) is the most sensitive test in this case, though 3P-CLR(A) and 3P-CLR(B) show some sensitivity to these events too. Upper-right panel: Selection exclusive to population *a*. This is the type of events that 3P-CLR(A) is designed to detect, and it is therefore the best-performing statistic in that case, while 3P-CLR(B) and 3P-CLR(Int) are insensitive to selection. Lower-left panel: Selection in the outgroup population. In this case, none of the statistics seem very sensitive to the event, though 3P-CLR(Int) shows better relative sensitivity than the other two statistics. Lower-right panel: Independent selective events in populations *a* and *b* at the same locus. Here, both 3P-CLR(A) and 3P-CLR(B) perform best. In all cases, we used the split times and population sizes specified for Model C.

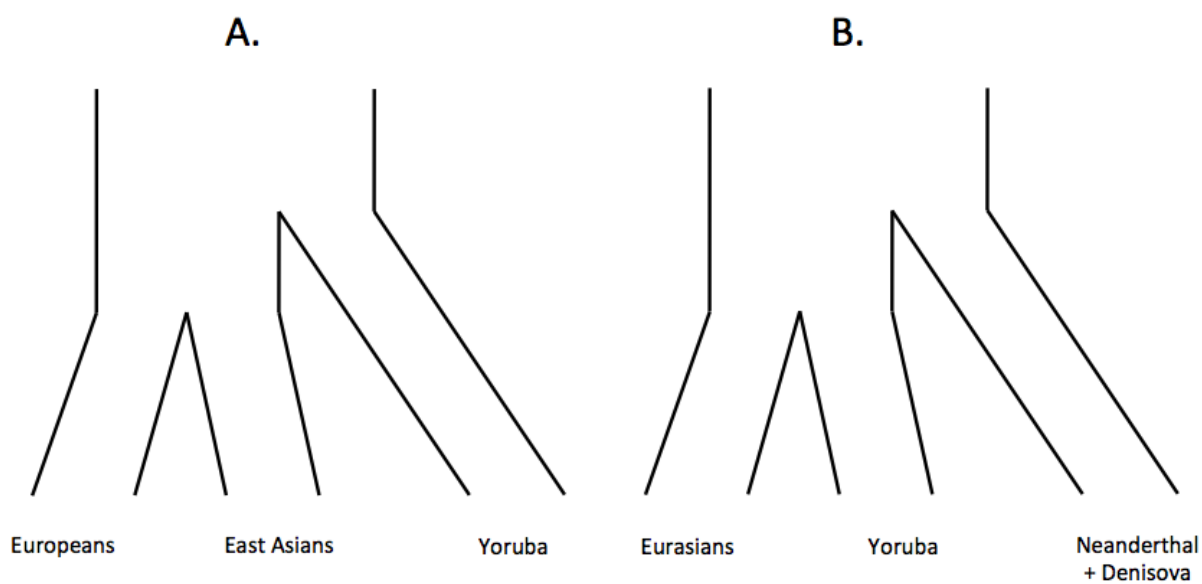


Figure S9. A. Three-population tree separating Europeans, East Asians and Yoruba. B. Three-population tree separating Eurasians, Yoruba and archaic humans (Neanderthal+Denisova).

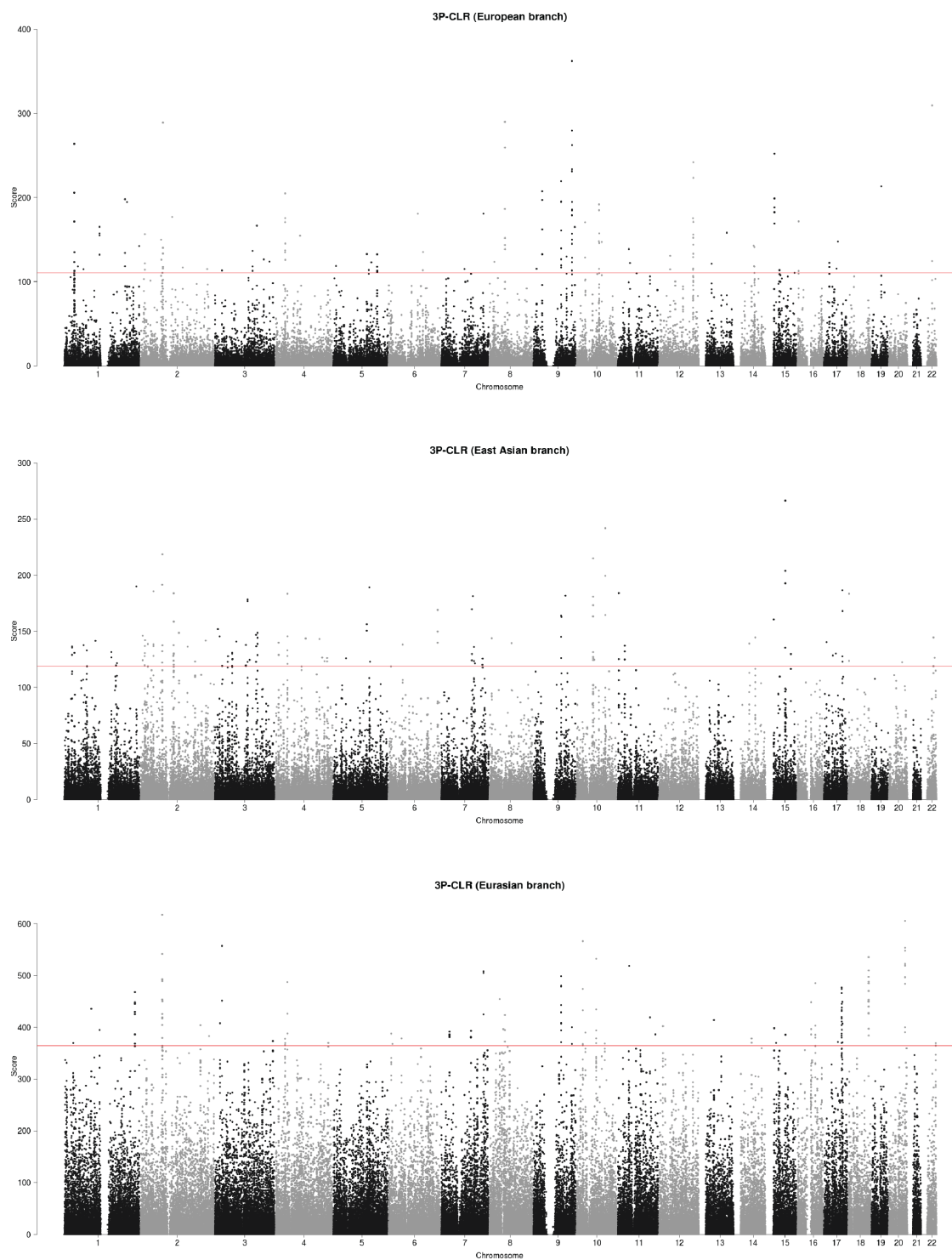


Figure S10. 3P-CLR scan of Europeans (upper panel), East Asians (middle panel) and the ancestral population to Europeans and East Asians (lower panel), using Yoruba as the outgroup in all 3 cases. The red line denotes the 99.9% quantile cutoff.

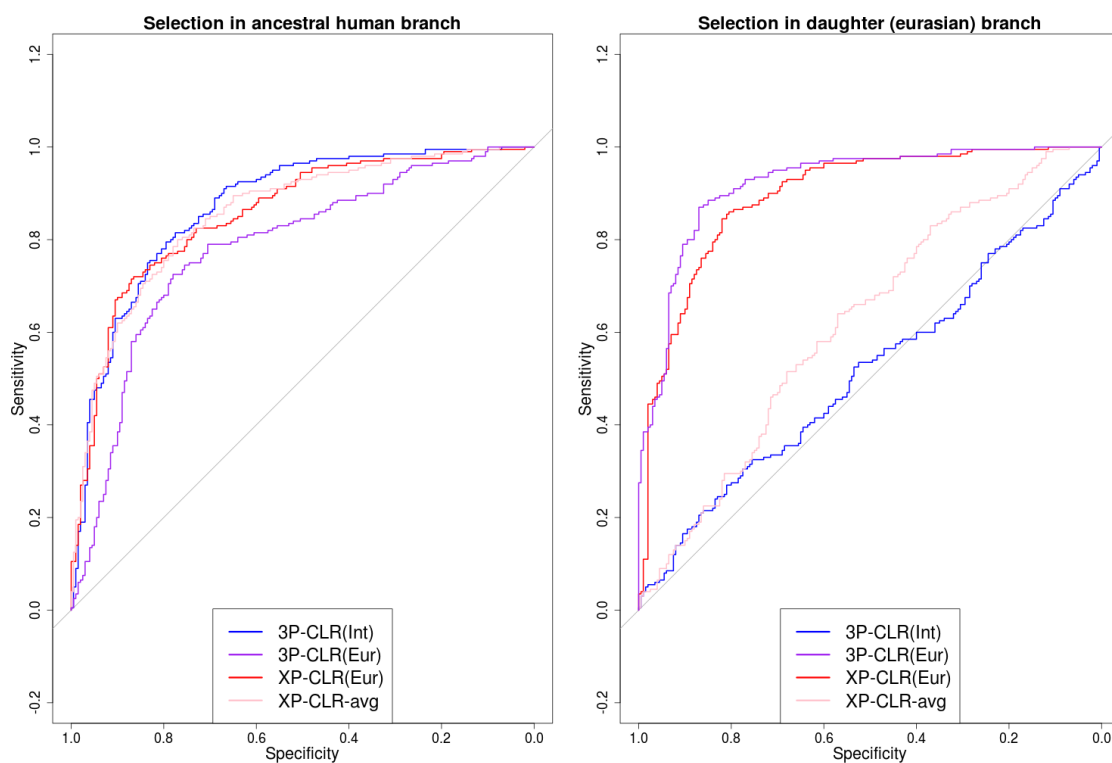


Figure S11. ROC curves for 3P-CLR run to detect selective events in the modern human ancestral branch, using simulations incorporating the history of population size changes and Neanderthal-to-Eurasian admixture inferred in Prüfer et al. (2014).

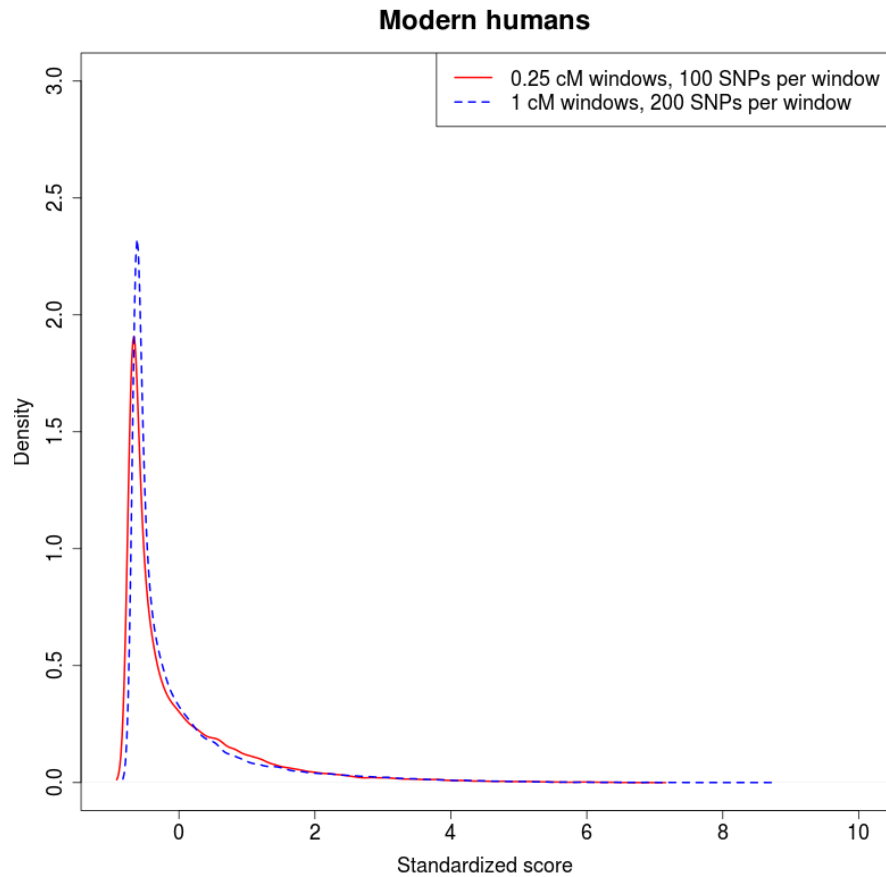


Figure S12. Comparison of 3P-CLR on the modern human ancestral branch under different window sizes and central SNP spacing. The red density is the density of standardized scores for 3P-CLR run using 0.25 cM windows, 100 SNPs per window and a spacing of 10 SNPs between each central SNP. The blue dashed density is the density of standardized scores for 3P-CLR run using 1 cM windows, 200 SNPs per window and a spacing of 40 SNPs between each central SNP.

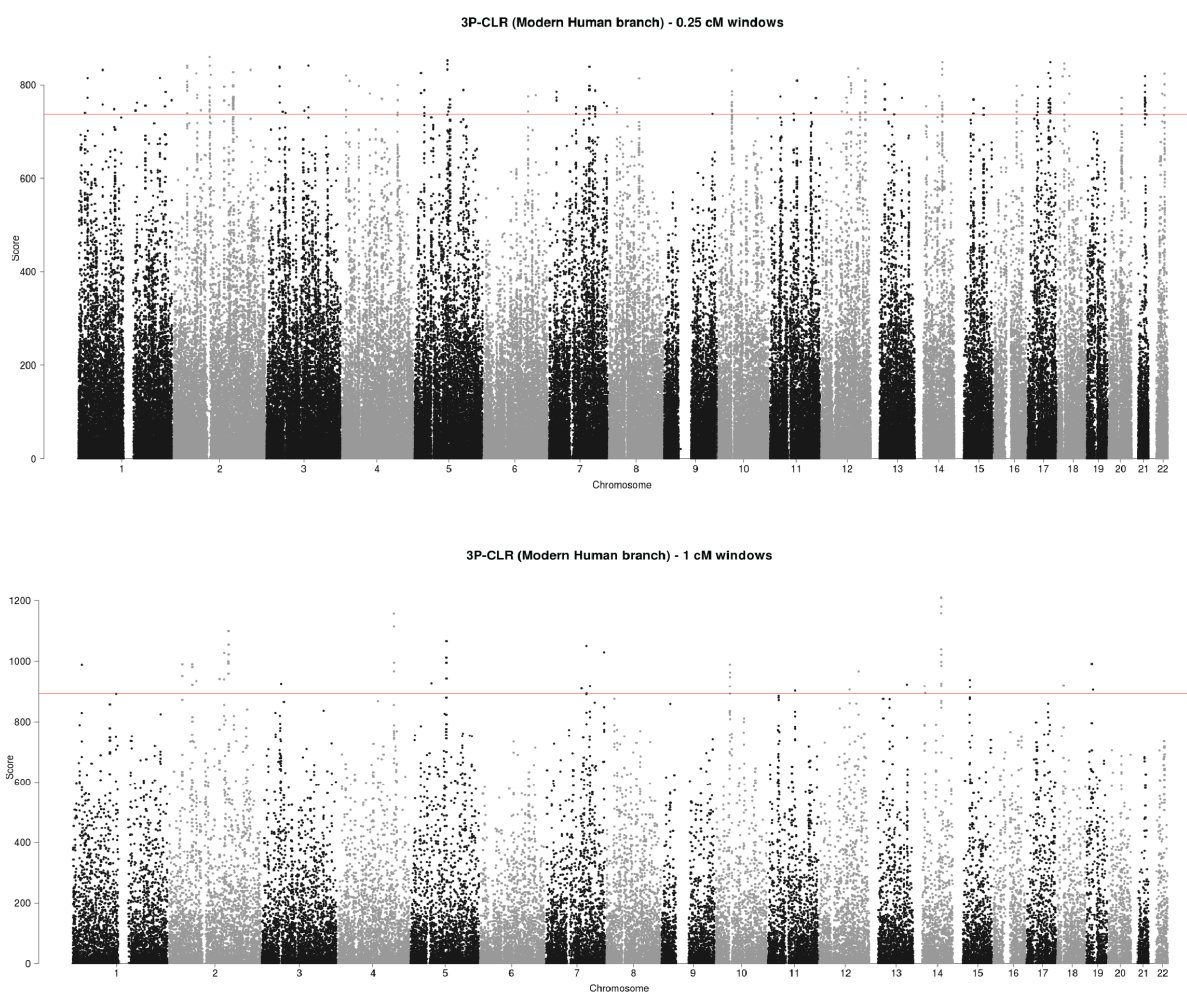


Figure S13. 3P-CLR scan of the ancestral branch to Yoruba and Eurasians, using the Denisovan and Neanderthal genomes as the outgroup. The red line denotes the 99.9% quantile cutoff. The top panel shows a run using 0.25 cM windows, each containing 100 SNPs, and sampling a candidate beneficial SNP every 10 SNPs. The bottom panels shows a run using 1 cM windows, each containing 200 SNPs, and sampling a candidate beneficial SNP every 40 SNPs.

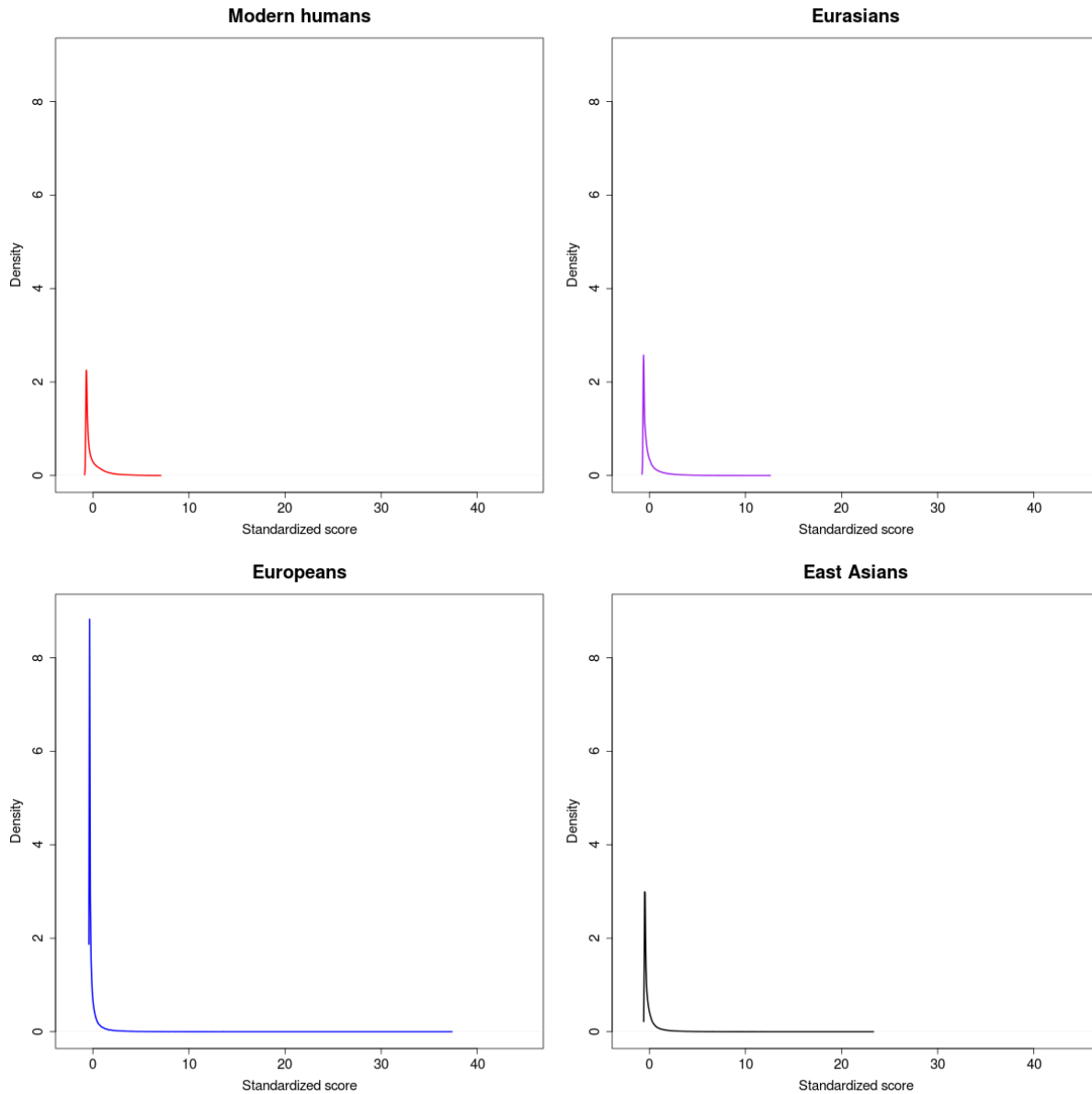


Figure S14. Genome-wide densities of each of the 3P-CLR scores described in this work. The distributions of scores testing for recent selection (Europeans and East Asians) have much longer tails than the distributions of scores testing for more ancient selection (Modern Humans and Eurasians). All scores were computed using 0.25 cM windows and were then standardized using their genome-wide means and standard deviations.

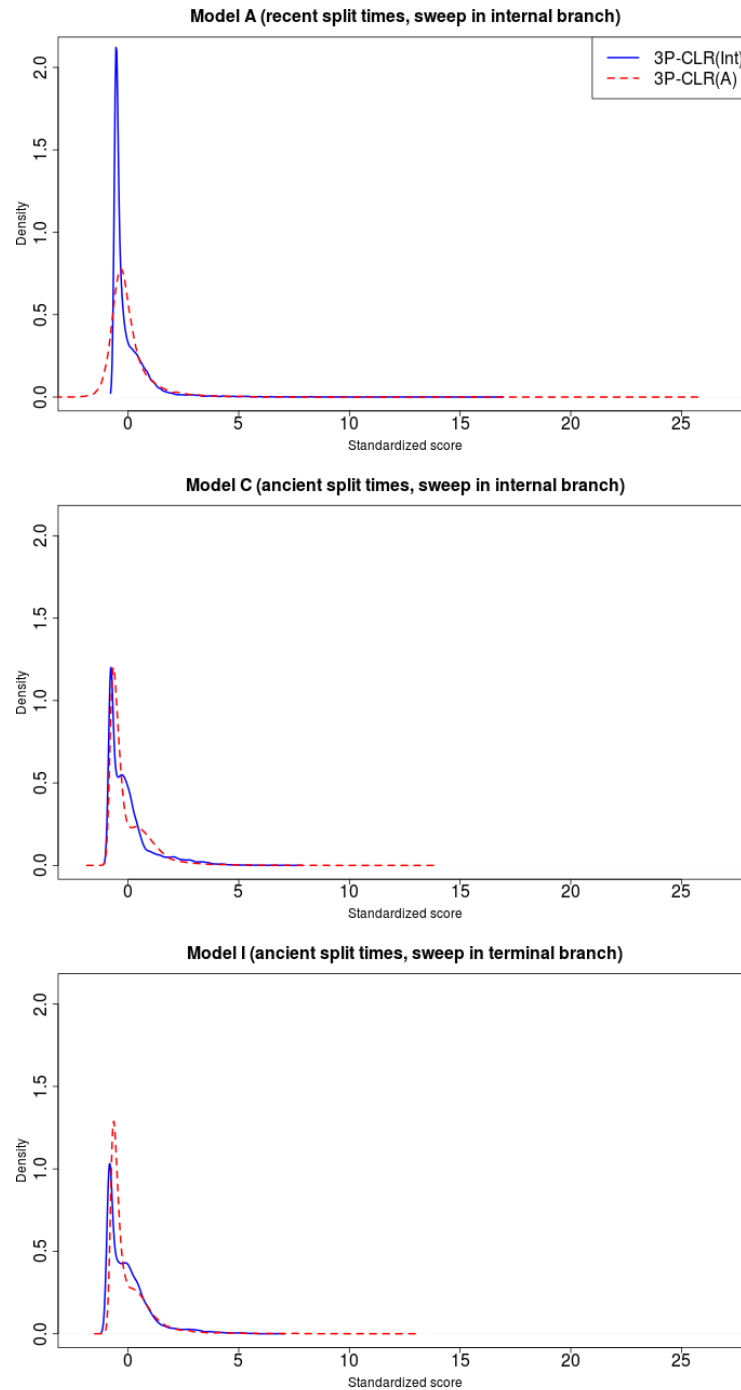


Figure S15. Distribution of 3P-CLR(Int) and 3P-CLR(A) scores under different demographic histories. We combined all scores obtained from 100 neutral simulations and 100 simulations with a selective sweep under different demographic and selection regimes. We then plotted the densities of the resulting scores. Top panel: Model A; Middle panel: Model C; Bottom panel: Model I. See Table 1 for details about each model.